KTH ROYAL INSTITUTE
OF TECHNOLOGY

Degree project in Electric power engineering (TELPM)

Second cycle 30 credits

Lithium-ion battery modeling and SoC estimation

RUOYU XU

Stockholm, Sweden 2023

Lithium-ion battery modeling and SoC estimation

Ruoyu Xu

Master's Programme in Electric Power Engineering
Date: 2023-06-15
Supervisor: Daniel Månsson
Examiner: Nathaniel Taylor
School of Electrical Engineering and Computer Science
KTH Royal Institute of Technology, Stockholm, Sweden

Abstract

The energy crisis and environmental pollution have become increasingly prominent in recent years. Lithium batteries have attracted extensive attention due to their high energy density, safety, and low pollution. To further study how the battery works, it is necessary to establish an accurate model conforming to the battery characteristics. As the core function of a battery management system(BMS), accurate state of charge(SoC) estimation dramatically improves battery life and performance. This thesis selects a ternary lithium battery in the centre for advanced life cycle engineering(CALCE) dataset for a study of cell modeling and SoC estimation.

The second-order Thevenin equivalent circuit model is selected as the cell model due to a trade-off between model complexity and accuracy. The parameters to identify include OCV, internal ohmic resistance, polarized internal resistance and capacitance. They were obtained with the MATLAB toolbox at various SoC state points under different temperatures. The ‘terminal voltage comparison’ method is utilized to verify the identification's accuracy. The simulation results turn out to be satisfactory.

Then cell SoC can be estimated after cell modeling. First, the principles of the Coulomb counting method, OCV method and EKF method are analyzed. The state space equations required in SoC estimation are determined by discretizing the non-linear equivalent circuit model. The simulation results are compared with the experimental results in the HPPC discharge experiment. Furthermore, the robustness of the EKF algorithm is further investigated. The results prove that the EKF algorithm has high precision, fast convergence speed and strong anti-interference capability.

Last but not least, the research on battery pack SoC estimation was continued. How to expand a single cell into a battery pack is analyzed, including aggregating cells into a pack and scaling a cell model to a pack. In addition, battery pack SoC is individually estimated by the 'Big cell' method and 'Short board effect' method. The result is not so good, indicating that further work can be done to improve the SoC estimation accuracy.

Keywords

lithium-ion battery, cell modeling, state of charge, extended Kalman filter, pack modeling

Sammanfattning

Energikrisen och miljöföroreningarna har blivit allt mer framträdande de senaste åren. Litiumbatteri har väckt stor uppmärksamhet på grund av sin höga energitäthet, säkerhet och låga föroreningar. För att ytterligare studera hur batteriet fungerar är det nödvändigt att etablera en exakt modell som överensstämmer med batteriets egenskaper. Som kärnfunktionen hos BMS förbättrar noggrann SoC-uppskattning dramatiskt batteriets livslängd och prestanda. Denna avhandling väljer ett ternärt litiumbatteri i CALCE-datauppsättningen för forskning. Dessutom slutförs cellmodellering och SoC-uppskattning baserat på det.

Den andra ordningens Thevenins ekvivalenta kretsmodell väljs som cellmodell på grund av en avvägning mellan modellens komplexitet och noggrannhet. Parametrarna som måste identifieras inkluderar OCV, intern ohmsk resistans, polariserad intern resistans och kapacitans. De erhölls med MATLAB-verktygslådan vid olika SoC-tillståndspunkter under olika temperaturer. Metoden "terminalspänningsjämförelse" används för att verifiera identifieringens noggrannhet. Simuleringsresultaten visar sig vara tillfredsställande.

Sedan kan cell SoC uppskattas efter cellmodellering. Först analyseras principerna för Coulomb-räknemetoden, OCV-metoden och EKF-metoden. Tillståndsrymdsekvationerna som krävs vid SoC-uppskattning bestäms genom att diskretisera den icke-linjära ekvivalenta kretsmodellen. Simuleringsresultaten jämförs med de experimentella resultaten i HPPC-utsläppsexperimentet. Dessutom, robustheten hos EKF-algoritmen undersöks ytterligare. Resultaten bevisar att EKF-algoritmen har hög precision, snabb konvergenshastighet och stark anti-interferensförmåga.

Sist men inte minst fortsatte forskningen kring SoC-uppskattning av batteripaket. Hur man expanderar ett enskilt batteri till ett batteripaket analyseras, inklusive aggregering av celler till ett paket och skalning av en cellmodell till ett paket. Dessutom uppskattas batteripaketets SoC individuellt med "Big cell"-metoden och "Short board effect"-metoden. Resultatet är inte så bra, vilket indikerar att ytterligare arbete kan göras för att förbättra SoC-uppskattningens noggrannhet.

Nyckelord

litiumjonbatteri, cellmodellering, laddningstillstånd, utökat Kalmanfilter, packmodellering

Acknowledgments

I would like to thank Daniel Månsson for being my supervisor for the last two years, who gave me the warmest encouragement and advice during my darkest time.

I would like to thank Nathaniel Taylor for being my examiner to enable this thesis project and offering professional guidance when I failed to find the correct research direction.

I would like to thank my parents for their listening all the time and forever support whenever I'm not at my best.

I would like to thank KTH for providing such a memorable two years' master program.

Table of contents

List of Figures

List of Tables

List of abbreviations and nomenclatures

Abbreviations

Ah	Ampere hour
BMS	Battery management system
CALCE	Center for Advanced Life Cycle Engineering
ECM	Equivalent circuit model
EKF	Extended Kalman filter
mSnP	m series, n parallel
OCV	Open circuit voltage
SoC	State of charge

Nomenclature

C_1	Concentration polarization capacitance
C_2	Electrochemical polarization capacitance
R_0	Ohmic polarization resistance
R_1	Concentration polarization resistance
R_2	Electrochemical polarization resistance
U_{OC}	Open circuit voltage
U_L	Terminal voltage

1 Introduction

1.1 Background

Renewable energy has proliferated worldwide in recent years, under the influence of the global energy crisis intensifying and the environmental situation worsening. Sweden is actively transitioning to a carbon-free Society and targets to achieve 100% renewable energy power generation in 2040 [1]. It demonstrates Sweden's high-tech capabilities and confidence in making full use of renewable energy. Sweden's draft integrated national energy and climate plan [1] sets out Sweden's climate and energy plans and goals in recent decades.

Table 1- 1: An overview of key climate and energy objectives

Target	Target year	Base year
Reduction of 40 percent of emissions from sectors outside the EU ETS	2020	1990
50 percent share of renewable energy in gross final energy consumption	2020	
Reduction of 63 percent of emissions from sectors outside the EU ETS	2030	1990
Reduction of 70 percent of emissions from domestic transport	2030	2010
Reduction of 75 percent of emissions from sectors outside the EU ETS	2040	1990
100 per cent renewable electricity production	2040	
Sweden will not have any net emissions of greenhouse gases into the atmosphere and should thereafter achieve negative emissions	**2045**	**1990**

Although new energy power generation has been proven to be feasible and practical, it still has the characteristics of instability and discontinuity. Moreover, it is susceptible to interference from the external environment, which in turn affects the quality of power consumption on the user side. Therefore, the microgrid concept was proposed and widely used. One definition of a microgrid is a system composed of loads and renewable power sources [2]. It can ensure reasonable control of the output of new energy power generation systems and ensure the reliability and flexibility of its power supply. Compared with the external large power grid, it is a single controlled unit that can meet the user's requirements for power quality and power supply security.

However, as mentioned above, some microgrids are provided by renewable energy sources, such as solar and wind energy, which are unstable and discontinuous. Hence, supporting energy storage systems must be developed to ensure stable and continuous power generation. The role of the energy storage system is to act as a buffer zone for the microgrid power generation system and enhance the system's inertia [3]. In addition, it can smooth the intermittent characteristics of renewable power generation to ensure the energy quality of the system. As a result, the reliability and flexibility of power consumption for the user can be guaranteed.

A study in [4] briefly introduces different microgrid energy storage methods, including mechanical, electrochemical, electromagnetic, and thermal energy storage. Battery energy storage stands out among the many modes and has become the most popular choice. It has significant advantages in terms of cost, energy density, safety and practicability compared with other methods.

As the core of battery energy storage, different power batteries have different characteristics. Standard energy storage batteries include lead-acid, nickel-metal hydride, nickel–cadmium, and lithium-ion batteries [5]. The report [6] compares lead acid and Li-ion batteries, while the paper [7] reveals the difference between NiMH and Li-ion batteries. A detailed comparison among various batteries is provided in [8].

Table 1- 2: Comparison of the technical parameters of different batteries

Specifications	Lead-acid	NiCd	NiMH	Li-ion
Nominal voltage(V/cell)	2	1.2	1.2	3.3–3.7
Specific energy (Wh/kg)	30–50	45–80	60–120	100–250
Cycle life(80%DoD)	200–300	1000	300–500	1000–2000
Charge time	8–16 h	1–2 h	2–4 h	1–2 h
Charge temperature	-20 to 50℃	0 to 45℃		0 to 45℃
Discharge temperature	-20 to 50℃	-20 to 65℃		-20 to 60℃
Overcharge tolerance	High	Moderate	Low	Low
Cost	Low	Moderate		High

Obviously, Li-ion battery shows clear advantages over other types, such as high specific energy, high efficiency, long cycle life, and low self-discharge rate. Li-ion battery has become the mainstream product despite the high cost and low overcharge tolerance. In extreme cases, lithium batteries may be in danger of explosion and harming personal safety. Therefore, a battery management system (BMS) is indispensable to battery management for safe operation, longer service life, and less maintenance cost.

BMS is the core component of the microgrid energy storage system and the brain of the battery system [9]. The main functions of a BMS can be summarized in the following three aspects:

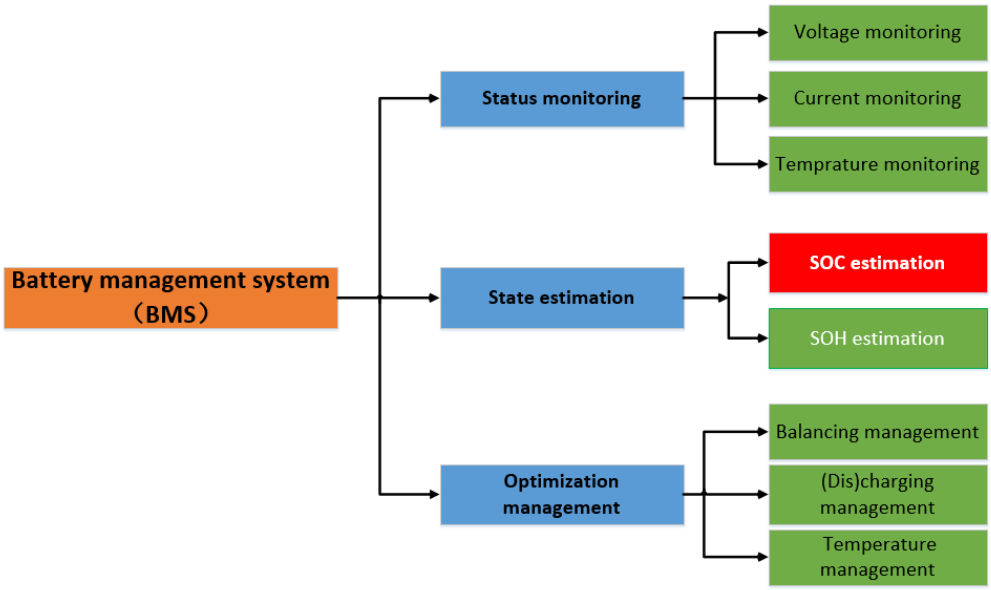

Figure 1- 1: BMS functions

(1) Battery status monitoring: the primary function of BMS. Collecting and monitoring the battery's voltage, current, and temperature in real-time operation is necessary. Other functions of BMS can only be realized based on status monitoring.

(2) Battery state estimation: including state of charge (SoC) and state of health (SoH) estimation. The accuracy of SoC estimation plays a key role in improving battery operating efficiency. Thus, SoC estimation is the core function of BMS.

(3) Battery optimization management includes balancing, temperature, and charge/discharge management.

Among them, SoC estimation is the core of BMS. Cell SoC not only provides the user with the status information of the cells but also plays a crucial role in improving efficiency. It is also the foundation of realizing the subsequent optimization management of BMS. Therefore, the core work of this report is to estimate the SoC of single cells and battery packs reasonably and accurately.

1.2 Objectives

This thesis is for training and demonstrating comprehensive learning skills for the graduation thesis project.

Meanwhile, this thesis aims to strengthen the understanding of Li-ion batteries and BMS to get benefited in future work.

1.3 Thesis outline

This thesis takes lithium-ion batteries as the research object, focusing on the SoC estimation of single cells and battery packs. The lithium-ion cell must first be modeled to carry out SoC estimation. Parameter estimation is also required since the variables cannot be directly obtained from the battery dataset. After the single-cell part is finished, the complicated battery pack must also be modeled. Finally, SoC estimation can be carried out on the battery pack.

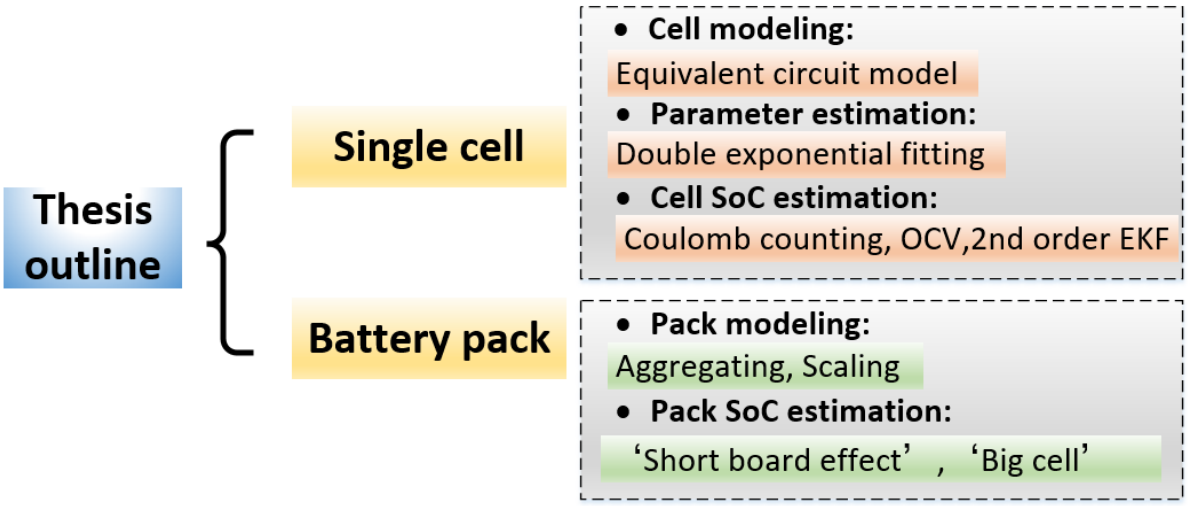

Figure 1- 2: The research framework

The thesis report consists of 6 chapters in all. In Chapter 1, the general thesis background and objectives were introduced. Chapter 2 presents a literature review on cell modeling, parameter identification and SoC estimation. The advantages and disadvantages of various approaches are compared in detail for method selection. Chapter 3 discusses the specific methodologies utilized in the thesis. Chapter 4 describes how the methods are applied in the research in MATLAB/Simulink. Chapter 5 presents the results of Chapter 4 and further discusses the results. Chapter 6 gives the Conclusions and suggests future work.

2 Literature review

As the introduction mentions, the critical part of the thesis is SoC estimation for single cells and battery packs. There are many ways to define the SoC of lithium-ion batteries. The typical definition is shown below:

$$SoC = Q_{remain} / Q_n \tag{2.1}$$

The numerator is the battery's remaining dischargeable capacity, and the denominator is the battery's rated capacity under the same conditions [10].

The SoC of a lithium battery is a physical quantity that cannot be directly measured [10]. Hence it can only be calculated indirectly through other external characteristic parameters of the battery (such as current, terminal voltage, etc.). However, there is a strong non-linear relationship between them. A lithium-ion battery is a highly time-varying, non-linear system. Therefore, it is necessary to establish a suitable model to estimate the SoC.

Many scholars have conducted relevant research on cell modeling, parameter identification and SoC estimation. The following will conduct a literature review to detail the achievements in these fields and the existing challenges.

2.1 Review of cell modeling

The report [10] overviews the typical cell modeling methods.

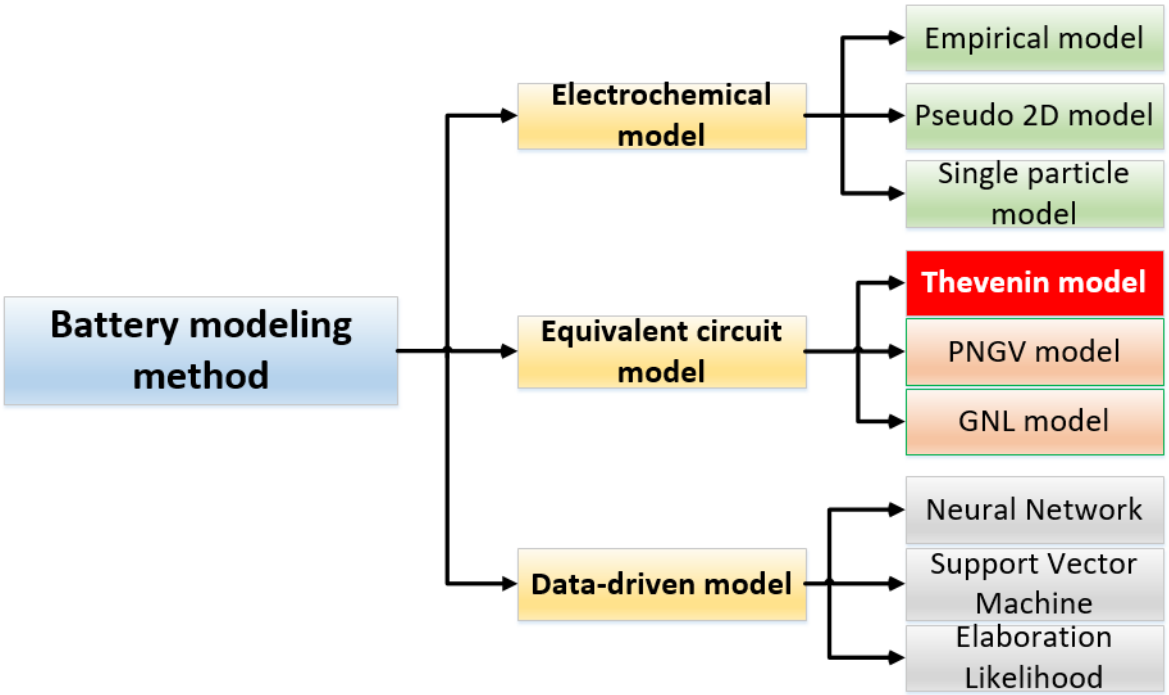

Figure 2- 1: Different battery modeling methods

2.1.1 Research status

At present, there are three types of standard battery models [11]:

i. White box model: Electrochemical model

The electrochemical model is based on the fundamental chemical principles inside the battery. It consists of a series of partial differential equations with boundary conditions, which can simulate the complex reactions inside the battery with the highest accuracy. Gregory L. Plett explains the principle and mechanism of electrochemical models in detail in the book [12]. However, the model is too complicated and has many parameters, so it is unsuitable for the online estimation of SoC.

If the electrochemical model is simplified by further assumptions and repeated practical experience, then it becomes an empirical model. In empirical models, the battery terminal voltage is usually represented as a mathematical function of the SoC and the current [10]. Some typical empirical models are given below:

Table 2- 1: ***Typical empirical models***

Model type	Model equations
Shepherd model	$y_k = E_0 - R \cdot i_k - K_1 / z_k$
Unnewehr universal model	$y_k = E_0 - R \cdot i_k - K_1 \cdot z_k$
Nernst model	$y_k = E_0 - R \cdot i_k - K_2 \cdot \ln(z_k) + K_3 \cdot \ln(1 - z_k)$

ii. Black box model: Data-driven model

Data-driven models are proven to perform well despite non-linearity [13]. It can represent the external characteristics of the battery without establishing a battery model, and the calculation accuracy is high [13]. Nonetheless, the learning process requires a large amount of previous original data, which highly depends on the quantity and quality of training data. Besides, the training cycle is quite long. Moreover, the convergence robustness of the algorithm is difficult to control. If the initial value is not selected correctly, it is easy to fall into a local optimum and different to converge [14].

iii. Grey box model: Equivalent circuit model

ECM consists of a voltage source related to SoC, an internal resistor, and Resistance-Capacitance (RC) networks, which can describe the electrical relationship between the inputs (current, SoC, and temperature) and the terminal voltage [15]. Traditional electronic components (resistors, capacitors, controllable voltage sources, etc.) are selected to simulate the dynamic response. Therefore, it is a model between electrochemical and neural networks. It generally describes the chemical reaction inside the battery and affects the dynamic response outside the battery. There is no doubt that it balances well between accuracy and operational feasibility.

Compared to empirical models, ECMs are much easier to understand the electrical characteristic of the battery. Moreover, ECMs have great convergence and robustness as long as the model is established correctly. Some common ECMs will be introduced in Chapter 3 [16].

The pros and cons of the three battery models are listed below:

Table 2- 2: ***Pros and cons of cell modeling methods***

Modeling methods	Electrochemical	Data-driven	Equivalent circuit
Pros	High accuracy, reflecting the real chemical process	Strong non-linearity, superior adaptability	Easy to understand, Great universality
Cons	Complicated, high computational cost	Training data needed, Prone to diverge	Parameter identification needed

2.1.2 Challenges

As shown in the above table, each battery modeling method has inherent flaws determined by its internal principles. First, the electrochemical model is complicated with a substantial computational cost. It is not adopted due to insufficient data in this project. Second, the data-driven model also requires a lot of training data. In contrast, the principle of ECM is clear to understand with less calculation cost and high reliability. Therefore, the ECM is selected for this project. Single cells and battery packs will be established in the Simulink environment.

2.2 Review of parameter identification

After establishing a suitable battery model, the next step is identifying the battery parameters based on the experimental data in the data set, which is the basis for subsequent SoC estimation. Generally, the parameters that need to be identified include the open circuit voltage OCV, the polarization resistance R and the capacitance C of the cell. A study in [17] introduces various approaches to identify the parameters in a cell, including the Least square method, Fuzzy logic, Genetic Algorithm, etc. Furthermore, these methods can be classified into online and offline identification.

2.2.1 Research status

Online identification is generally based on the battery model, using the recursive least squares method to obtain the parameters of the equivalent circuit model in real-time [18]. Previous experiments are dispensable for online parameter identification. The problem of time-varying battery parameters can also be solved to a large extent since they are detected in real-time [19]. However, the online method has no physical meaning itself, and the online identification process is computationally intensive. Moreover, the pre-set parameters easily affect the final results' accuracy [20].

On the contrary, offline identification is based on battery manufacturers' or laboratories' various charge and discharge experiments on batteries. This identification method is based on a large amount of experimental data [21]. A study in [22] adopts a subspace identification method to identify a lumped parameter model, from which the core idea is curve fitting.

The pros and cons of online/offline methods can be summarized below:

Table 2- 3: Pros and cons of online/offline methods

Modeling Methods	Online	Offline
Pros	Save preliminary experiments, high accuracy, can solve time-varying problems	Obtained from experiments, with physical meaning, do not require real-time measurement
Cons	No physical meaning, high computational cost, easily affected by pre-set parameters	Accuracy lacking, cannot represent time-varying characteristics

2.2.2 Challenges

As shown above, each parameter identification method has its inherent drawbacks. In this project, the public dataset used comes from the Internet, and many experiments have been performed in advance. Hence an offline identification method is used in this thesis to characterize the physical meaning represented by the ECM.

2.3 Review of SoC estimation

SoC estimation is the key to BMS and this thesis project. There are currently many SoC estimation methods [23]. A brief overview of various SoC estimation methods is introduced in [24]. Mainly four methods are summarized in [25]: Ampere-hour integral, looking-up table based, model-based and data-driven approaches. The most common method in looking-up table based methods is the OCV method. It belongs to the direct measurement type and the coulomb counting method [26].

2.3.1 Research status

1) Ampere-hour integral method:

Ampere-hour integral method estimates cell SoC via real-time coulomb counting. It directly uses the measured value current to add the initial SoC estimation value and the cumulative integral of the battery current during charging and discharging [24].

$$SoC = SoC_{o} - 1 / Q_{\text{rated}} \int \eta I dt \tag{2.2}$$

Where SoC_{o} is the initial value, Q_{rated} is the rated capacity under the set temperature and charge-discharge rate, and η is the charge/discharge efficiency.

Coulomb counting has been standardized in the industry as an SoC estimation method [27]. It is the most widely used since it is the most accurate technique for short-term calculations [24]. The advantage is that the principle is easy to understand, and the measurement is convenient and quick.

However, it is greatly affected by the initial value of SoC. If the initial value is inaccurate, this error will always be retained because there is no correction mechanism [25]. Moreover, a sizeable cumulative error will be generated over time due to the existence of the integral link if there exists some error in the current sampling. The coulomb counting method is essentially an open-loop estimation method [24].

2) Open circuit voltage method:

SoC estimation methods commonly impose a characterization of the OCV curve (mainly through a look-up table). A study in [28] proves a certain relationship exists between OCV and SoC (usually high-order polynomial). It can be defined as:

$$SoC = f^{-1}(OCV) \tag{2.3}$$

In the OCV method, the cell's voltage is continuously measured, and the corresponding SoC is obtained from a table. Theoretically, suppose the OCV-SoC relationship curve of a particular cell is known in advance, along with its open circuit voltage value measured at a certain time. In that case, the SoC at that time can be easily calculated.

3) Model-based methods

Among all the SoC estimation methods, the model-based ones seem to be the most practical choice for online SoC estimation at present [29]. There are a great many model-based methods available, including Proportional-Integral Observer, H infinity filter, particle filter, and the most commonly used：Kalman filter based methods [24].

In the study [30], PI observer is applied in the SoC estimation of a cell under the UDDS drive cycle. The estimated SoC is highly consistent with the reference SoC. The report [31] suggests a new method for SoC estimation using an adaptive H∞ filter (AHF). A multiscale dual HIF for battery systems is applied in [32] to estimate battery pack SoC. A study in [33] proposes a particle filter based

robust state and parameter estimation (PF-RSPE) method for estimating SoC and discharge current of lithium batteries. In order to effectively use the cloud data of connected cells, an estimation method based on noise adaptive particle filter (N-APF) is proposed in this paper [34].

Nevertheless, the most widely used now are the SoC estimation methods based on the Kalman filter. The Kalman filter algorithm is a recursive algorithm that can solve the state estimation problem of linear systems [35]. It was proposed by the Hungarian mathematician R.E. Kalman, who introduced the state space model into the filtering theory in 1960. It is suitable for dynamic stochastic processes and can realize recursive calculations by predicting new states and uncertainties and using newly measured values to correct and calibrate predicted values.

However, the standard Kalman filtering algorithm is only suitable for linear systems, and it is more demanding on the conditions of use. For instance, the system (process) noise and measurement noise must be Gaussian white noise and independent of each other. The equivalent circuit model established according to the characteristics of lithium batteries is a typical non-linear system, so EKF (extended Kalman filter) is used. Furthermore, various extensions of EKF arise to increase the accuracy of EKF. The report [35] utilizes a non-linear Dual Extended Kalman Filter (DEKF), allowing simultaneous states and parameter estimation. A study in [36] estimates the SoC of a Li-ion battery pack for an electrical vehicle using an improved extended Kalman filter (IEKF), which benefits from considering the aging phenomenon in the electrical model of cells. An adaptive EKF (AEKF) algorithm is adopted in [37] to increase the reliability and accuracy of SoC estimation. The paper [38] considers the influence of the temperature, and a dual square root unscented Kalman filter based on the unit spherical unscented Kalman filter (UKF) is proposed.

Due to its high accuracy and robustness, EKF will be the primary method in this thesis for cell SoC estimation.

4) Data-driven methods

The data-driven model relies on machine learning. First, the battery model is established based on the black box model. Then a large amount of training data is prepared to obtain the internal parameters that conform to the external characteristics of the battery after training. After that, the SoC can be estimated as well. There are currently two main types of data-driven models: Artificial Neural Network (ANN) and Support Vector Machines (SVM). Based on artificial neural networks and the Thevenin model, this paper uses an improved model predicting the state of charge [39]. The report [40] proposes using a support vector machine with fast learning speed and suitable generalization properties.

The pros and cons of various SoC estimation methods are displayed below.

Table 2- 4: Pros and cons of SoC estimation methods

Method type	Advantages	Disadvantages
Coulomb counting	Direct measurement, low computational cost, easy to understand	Accurate initial SoC needed, Current sensor error accumulated during the process
Open circuit voltage	One-to-one relationship between OCV and SoC, Low computational cost	Long relaxation time needed for OCV measurement, easily affected by temperature, aging
Extended Kalman filter	Insensitive to initial SoC, high accuracy, good robustness	Highly rely on model accuracy, high computational cost
Data-driven	Strong non-linearity, strong adaptability, high precision	Requires a large amount of training data, greatly affected by the training method

2.3.2 Challenges

There are many complicated factors affecting the battery SoC estimation [24]. The main challenge in this field can be summarized as enhancing the SoC estimation accuracy and robustness without increasing the complexity of the models and estimation process. This thesis aims to find a trade-off in the SoC estimation procedures between accuracy and computational complexity in compliance with the motto “simple is better.”

However, in actual SoC estimation, there are many possible sources of error:
(1) In practical cases, Zero-mean sensing noise is inevitable for both current and voltage sensors.

(2) Battery modeling errors or inaccuracies in the models.

(3) Parameters like covariance, noise type and initial SoC in the optimization process.

(4) Other unknown error sources that unknown reasons may have caused.

Favorable assumptions should be adopted, and reasonable estimation methods are supposed to be used to minimize errors.

In addition, the above discussion is aimed at the SoC estimation of the single cell. A battery pack usually consists of hundreds or thousands of single cells, so estimating its SoC will be more difficult. In Chapter 3, different estimation methods for the battery pack SoC will be introduced in detail.

2.4 Summary

In Chapter 2, a comprehensive literature review is presented to understand the achievements made in related fields and be familiar with the basic process of the ongoing project. Understanding the existing theories with their pros and cons is indispensable. Then the specific methods can be selected to continue this project after a comprehensive trade-off between accuracy, complexity, and computational cost.

This project investigates three main fields: cell modeling, parameter identification and SoC estimation. In terms of battery modeling, ECM is adopted as the method after a trade-off between model complexity and accuracy. Then offline parameter identification is used since a great many preliminary experiments have been performed in the CALCE public dataset. Finally, regarding SoC estimation, EKF is utilized due to its superiority in accuracy and robustness. However, the other SoC estimation methods will still be applied for comparison with EKF.

3 Methodology

After the literature review, it is clear to understand different modeling approaches and SoC estimation methods, together with their advantages and disadvantages. In Chapter 3, the most suitable models and techniques will be selected and carried out for further research.

3.1 Cell modeling method

First of all, it is significant to understand the working principle of lithium batteries. After a trade-off between accuracy and complexity, the best ECM will stand out among the common ECMs.

3.1.1 Basic working principle of lithium-ion cell

A lithium-ion battery consists of the following parts: anode, cathode, electrolyte solution, separator, and current collector [12].

（1） Anode: The anode is usually composed of lithium carbon compounds. When the battery is discharged, the negative electrode releases electrons to the external circuit, and an oxidation reaction occurs at this time. When the battery is charged, the negative electrode will absorb electrons from the external circuit, and a reduction reaction will occur at this time.

（2） Cathode: The cathode materials typically consist of transition metal oxides containing lithium ions. When the battery is discharged, the positive electrode absorbs electrons from the external circuit, and a reduction reaction occurs at this time. When the battery is charged, the positive electrode releases electrons to the external circuit, and an oxidation reaction occurs at this time.

（3） Electrolyte: According to the top flow of charge conservation, corresponding compensation ions must enter the battery when electrons move out of the circuit. The electrolyte provides the medium by which ionic charges inside the battery are transferred between the positive and negative electrodes.

（4） Separator: The separator separates the positive and negative terminals of the battery, thereby preventing short circuits and self-discharge inside the battery. They are usually composed of glass mats, fibers, polymers, etc.

（5） Current Collector: Typically, a metal foil to which the positive and negative electrodes are attached to conduct current to the battery terminals.

The figure below shows the basic working principle of a lithium-ion cell.

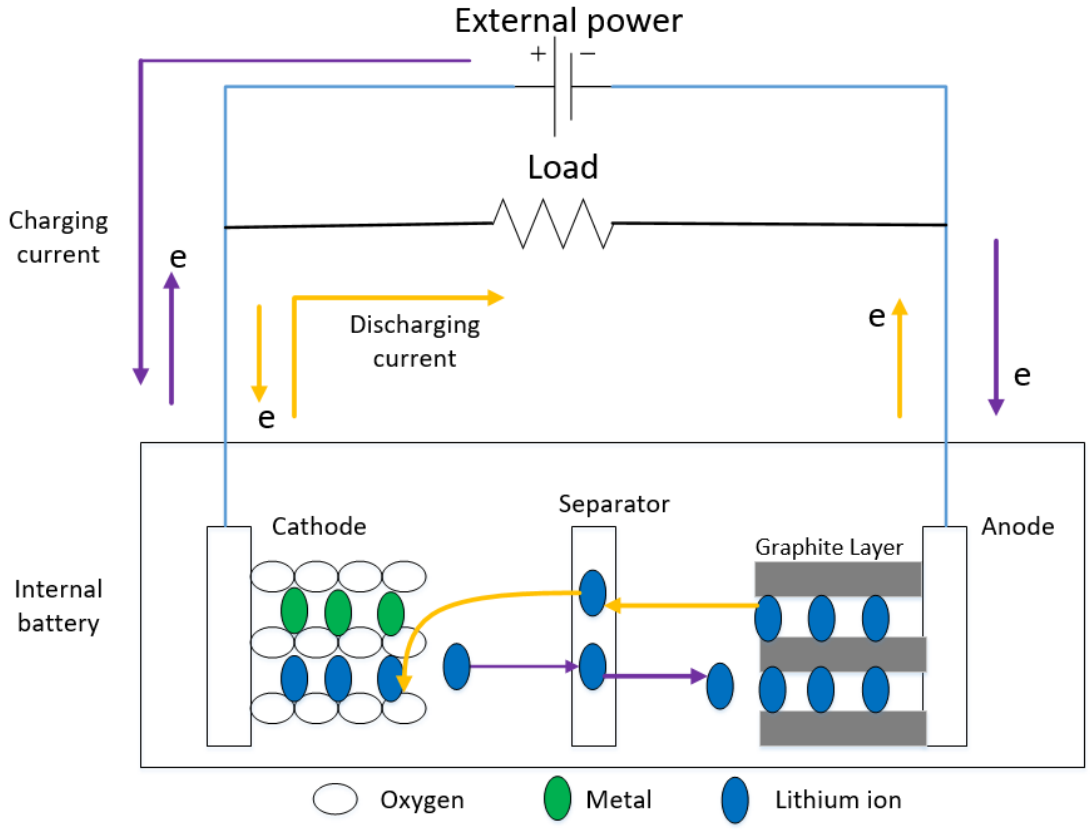

Figure 3- 1: Lithium-ion cell working principle

A lithium-ion battery is essentially a concentration battery. The working principle is shown in the figure above. Lithium ions are detached from the positive plate when the battery charges and inserted into the negative electrode through the electrolyte solution. At this time, the negative electrode is in a lithium-rich state. At the same time, electrons move to the negative pole of the battery through the external circuit, and charge compensation is performed on the negative pole, thereby maintaining the electrical balance of the negative pole. When the battery is discharged, lithium ions fall off the negative electrode plate and are inserted into the positive electrode after passing through the electrolyte solution. At this time, the positive electrode is in a lithium-rich state. From this point of view, when the lithium battery is charging and discharging, lithium ions are continuously intercalated and detached to cause changes in the internal layer spacing of the battery. It is a reversible chemical reaction, like a rocking chair, so it is also called a "rocking chair battery."

During the early charging and discharging process of lithium-ion batteries, the electrochemical reaction equation is as follows [12]:

Cathode: $LiMO_2 \rightarrow Li_{1-x}MO_2 + xLi^+ + xe$

Anode: $nC + xLi^+ \rightarrow Li_xCn$

Overall equation: $LiMO_2 + nC \rightarrow Li_{1-x}MO_2 + Li_xC_n$

Where M refers to iron, nickel, cobalt, manganese, or other metal elements.

3.1.2 Various equivalent circuit models

The modeling method of the equivalent circuit model is to use simple circuit components to form a circuit network. ECM not only has a general description of the internal chemical reaction of the battery but also simulates the dynamic response of the external battery. On one hand, when compared with the electrochemical model, the number of parameters is small, and it is easy to express in the form of state space equations at the mathematical level. The model parameters are easy to identify and facilitate online simulation. On the other, compared with the neural network model, it does not require much historical data for training. The algorithm has good convergence, robustness, and strong universality [10]. Therefore, the equivalent circuit model is selected in this report to model the battery cell.

The equivalent circuit models currently applied include the Rint, RC, Thevenin, PNGV, and GNL models [41].

a. Internal resistance (Rint) model

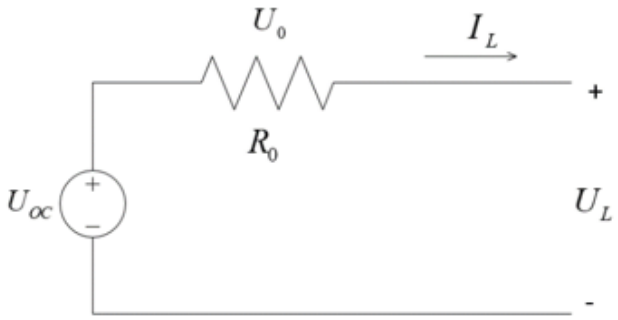

Figure 3- 2: Rint model

It is composed of an ideal voltage source U_{OC} and a battery internal resistance R_0. Only one element R_0 is involved in the internal state change of the cell, considering the complex internal change mechanism of the battery. Thus, it is impossible to simulate the dynamic characteristics of the battery.

According to Kirchhoff's law, the circuit expression is given below.

$$\begin{cases} U_0 = R_0 I_L \\ U_L = U_{OC} - U_0 \end{cases} \tag{3.1}$$

b. Resistance-capacitance (RC) model

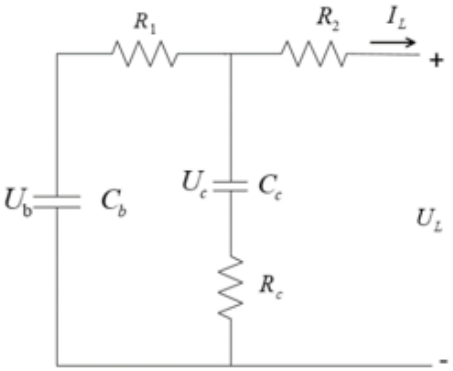

Figure 3- 3: RC model

The RC model only includes capacitance and resistance, where C_b represents the maximum capacity that the battery can store, C_c describes the polarization effect on the battery surface, R_1 is the termination resistance, R_2 is the terminal resistance, and R_C is the surface capacitive resistance. Compared with the internal resistance model, the complexity of the RC model has increased to a certain extent.

According to Kirchhoff's law, the circuit expression is given below.

$$\begin{cases} \dfrac{dU_b}{dt} = -\dfrac{U_b}{(R_1+R_c)C_b} + \dfrac{U_c}{(R_1+R_c)C_b} - \dfrac{R_c I_L}{(R_1+R_c)C_b} \\ \dfrac{dU_c}{dt} = \dfrac{U_b}{(R_1+R_c)C_b} - \dfrac{U_c}{(R_1+R_c)C_b} - \dfrac{R_1 I_L}{(R_1+R_c)C_b} \\ U_L = \dfrac{R_c}{R_1+R_c}U_b + \dfrac{R_c}{R_1+R_c}U_c - R_2 I_L - \dfrac{R_1 R_c}{R_1+R_c}I_L \end{cases} \tag{3.2}$$

c. Thevenin model: (nth order...)

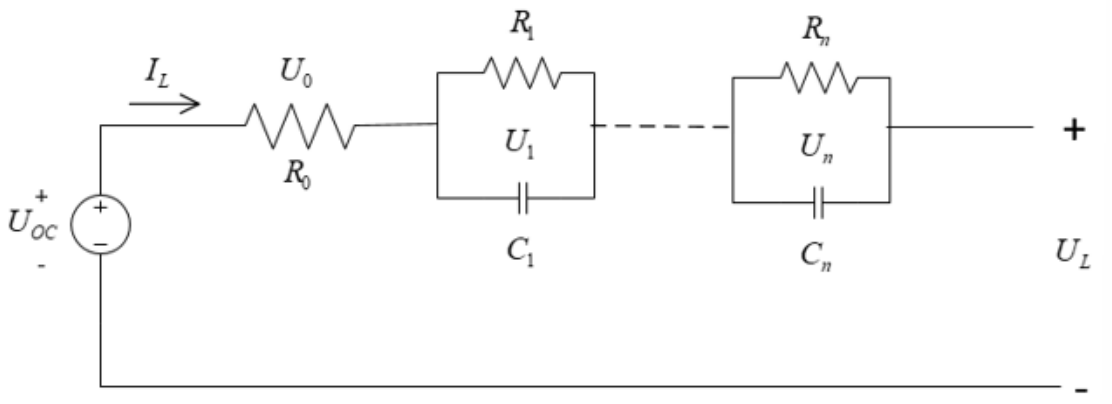

Figure 3- 4: Thevenin model (nth order)

Thevenin equivalent circuit model is currently the most widely used model. It combines the advantages of the Rint model and the RC model. An ideal voltage source U_{OC} is used to represent the open circuit voltage. R_0 is the internal ohmic resistance of the battery, and a parallel RC loop simulates the polarization link inside the battery. Take the most common n=1 as an example, R_1 is the battery polarization resistance, and C_1 is the polarization capacitance [42]. It can well combine the dynamic and static characteristics of the battery for simulation and also considers the non-linearity of the battery.

According to Kirchhoff's law, the circuit expression is given below.

$$\begin{cases} U_0 = R_0 I_L \\ I_L = \dfrac{U_1}{R_1} + C_1 \dfrac{dU_1}{dt} \\ U_L = U_{OC} - U_0 - U_1 \end{cases} \tag{3.3}$$

d. PNGV model

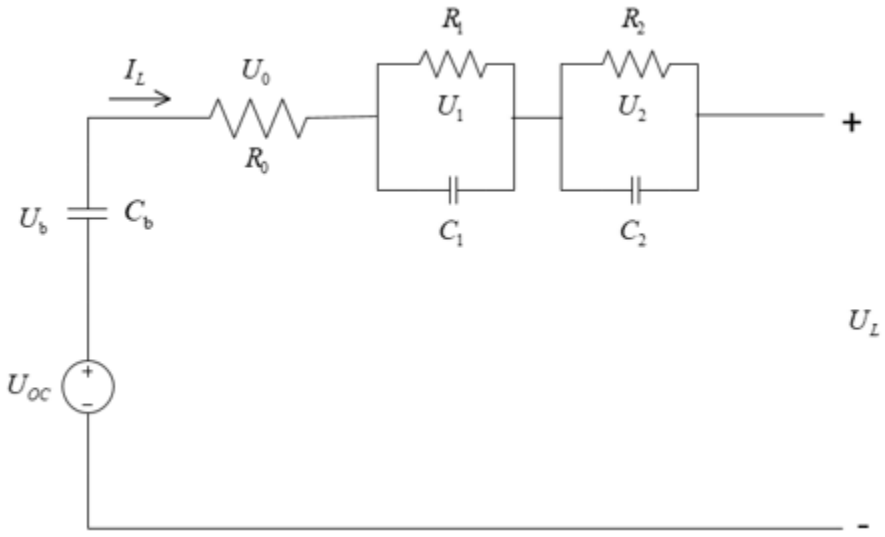

Figure 3- 5: PNGV model

Compared with the Thevenin model, a capacitor C_b is added to the PNGV model, and the voltage U_b across C_b is used to represent the change in the battery's open circuit voltage caused by the accumulated load current over time. This model comprehensively considers the internal resistance of the battery, the polarization effect, and the change of the open circuit voltage caused by the accumulation of load current over time, and the model accuracy is high.

According to Kirchhoff's law, the circuit expression is given below.

$$\begin{cases} U_o = R_o I_L \\ \dfrac{dU_b}{dt} = \dfrac{I_L}{C_b} \\ \dfrac{dU_1}{dt} = -\dfrac{U_1}{R_1 C_1} + \dfrac{I_L}{C_1} \\ U_L = U_{OC} - U_o - U_1 - U_b \end{cases} \tag{3.4}$$

e. GNL model

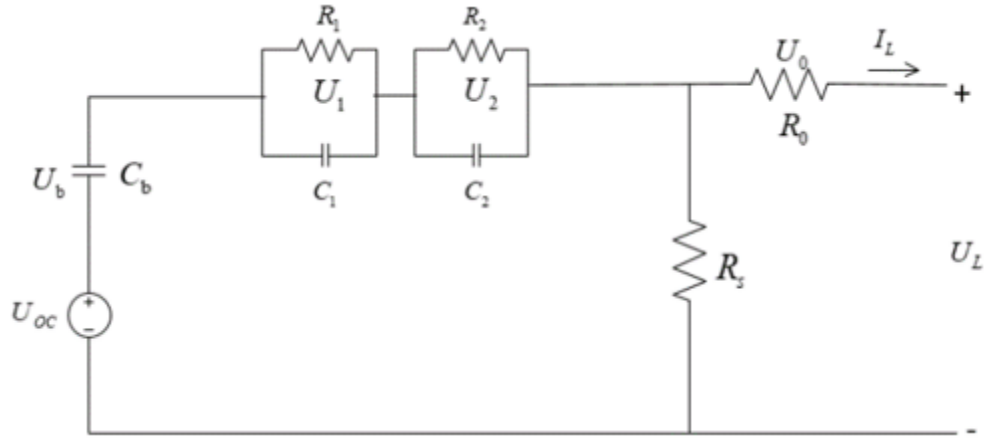

Figure 3- 6: GNL model

The GNL model is an improvement and extension of the PNGV model. Separate modules are established for the ohmic polarization, concentration polarization, and electrochemical polarization inside the battery, taking the battery's self-discharge, overcharge, and over-discharge phenomena into account. It is more complex and has many parameters, but the result is highly accurate. Where R_S is the self-discharge resistor.

According to Kirchhoff's law, the circuit expression is given below.

$$\begin{cases} U_0 = R_0 I_L \\ \dfrac{dU_b}{dt} = -\dfrac{U_b}{C_b R_S} - \dfrac{U_1}{C_b R_S} - \dfrac{U_2}{C_b R_S} + \dfrac{I_L}{C_b} + \dfrac{U_{OC}}{C_b R_S} \\ \dfrac{dU_1}{dt} = -\dfrac{U_b}{C_1 R_S} - \dfrac{U_1}{C_b R_S} - \dfrac{U_1}{C_1 R_1} - \dfrac{U_2}{C_1 R_S} + \dfrac{I_L}{C_1} + \dfrac{U_{OC}}{C_1 R_S} \\ \dfrac{dU_2}{dt} = -\dfrac{U_b}{C_2 R_S} - \dfrac{U_1}{C_2 R_S} - \dfrac{U_1}{C_2 R_S} - \dfrac{U_2}{C_2 R_2} + \dfrac{I_L}{C_2} + \dfrac{U_{OC}}{C_2 R_S} \\ U_L = U_{OC} - U_0 - U_1 - U_2 - U_b \end{cases} \tag{3.5}$$

3.1.3 Model selection

For lithium-ion batteries, the Thevenin circuit has excellent non-linear characteristics and can reasonably simulate the dynamic characteristics of the battery.

First, when compared with the Rint and RC model, based on static characteristics, the Thevenin circuit can well reflect the dynamic characteristics of the cell and consider the non-linear characteristics of the battery to make up for their shortcomings.

Although PNGV and GNL models have higher precision, they involve too many parameter variables, making their working principle more complicated. As a result, the parameter identification is way too tricky. Also, their operability is not as good as the Thevenin circuit. Therefore, this project selects the Thevenin circuit as the cell model.

It should be noted that there is only one RC loop in the primary Thevenin circuit. As the research progresses, the first-order RC can no longer accurately reflect the dynamic response of the battery. At present, the polarization of lithium-ion batteries can be roughly divided into ohmic polarization, electrochemical polarization, and concentration polarization [42]. In this report, in order to analyze the concentration and electrochemical polarization processes inside the battery separately and make up for the lack of an equivalent circuit model for the simulation of the chemical reaction process as much as possible, **the Thevenin circuit with two RC loops is selected.** It is concluded in [42] that the 2nd-order RC can already simulate the terminal voltage well. After upgrading to 3 RC loops, the model's accuracy is improved slightly, but the amount of calculation and the calculation time are significantly increased. Therefore, the 2nd-order RC model is more suitable.

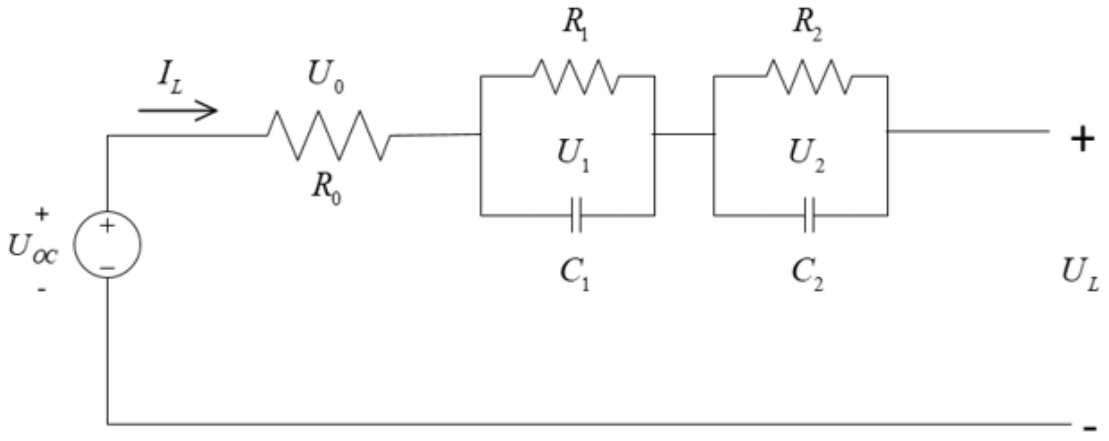

Figure 3- 7: Final cell model: 2nd order Thevenin circuit

According to Kirchhoff's law:

$$\begin{cases} U_0 = R_0 I_L \\ I_L = \dfrac{U_1}{R_1} + C_1 \dfrac{dU_1}{dt} \\ I_L = \dfrac{U_2}{R_2} + C_2 \dfrac{dU_2}{dt} \\ U_L = U_{OC} - U_0 - U_1 - U_2 \end{cases} \tag{3.6}$$

3.2 Parameter identification method

System parameter identification is a mathematical model that describes system behavior according to the input and output functions of the system and is an essential branch of modern control theory [17]. Precise parameter identification can help characterize the system behavior and select a proper model to simulate the actual system behavior. In addition, predict the future evolution of the system output with the current measurable system input and output.

This project selects the public battery dataset from the CALCE website, and many experiments have been performed in advance. Therefore, an offline identification method is used in this thesis to characterize the physical meaning represented by the ECM.

3.2.1 OCV-SoC curve identification

As mentioned above, a specific relationship exists between OCV and SoC (usually high-order polynomial). A polynomial fit considering the temperature effect is given in [43]. In this thesis, the OCV-SoC curves are fitted at three temperatures (0℃, 25℃, 45℃) based on the selected dataset (later introduced in Chapter 4).

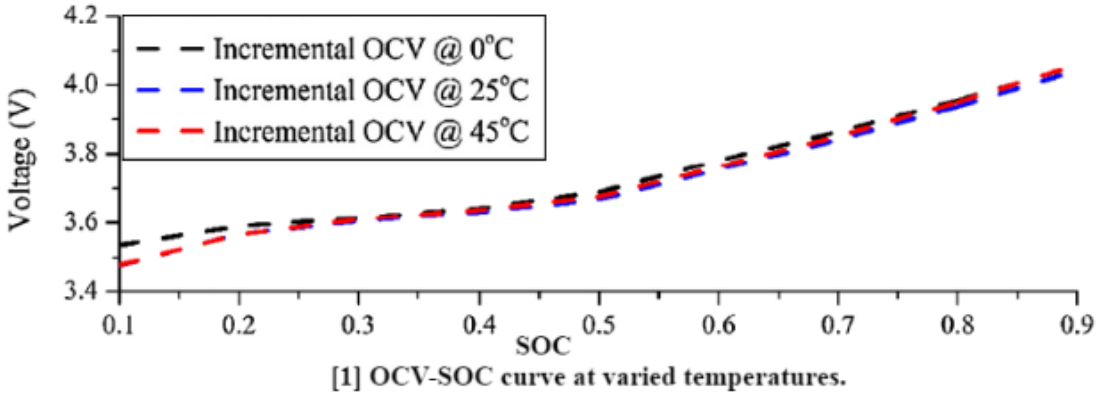

Figure 3- 8: Standard OCV-SoC curve captured from CALCE website [44]

3.2.2 ECM parameter identification

A study in [42] introduces electrochemical and concentration polarization inside the battery. Therefore, 2 RC branches are required to represent them separately. The parameters that need to be identified by the second-order equivalent circuit model include open circuit voltage, internal ohmic resistance R_0, polarization resistance R_1, R_2, and polarization capacitance C_1, C_2.

Freedom CAR Battery Test Manual for Power-Assist Hybrid Electric Vehicles [45] indicates that HPPC (Hybrid pulse power characterization) test is often used for offline parameter identification. Furthermore, a study in [46] gives detailed instructions on how to perform it. Each discharge pulse is utilized to calculate the internal ohmic resistance R_0, polarization resistance R_1, R_2, and polarization capacitance C_1, C_2 during the discharge period. Take one pulse from the Incremental Current OCV profile as an example to illustrate the method.

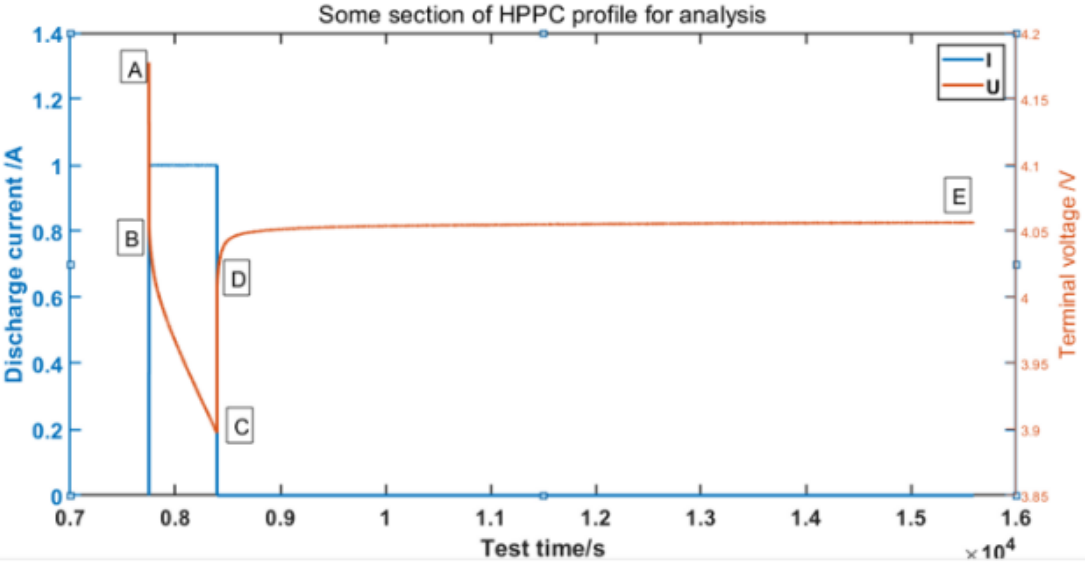

Figure 3- 9: One pulse of the HPPC test profile

It can be seen from the figure that the battery state turns from a discharged state to a static state. And the voltage response curve can be divided into four stages:

Stage 1: AB segment. The battery starts to load and discharge from the initial static no-load state, and the terminal voltage suddenly drops. Since the voltage at both ends of the capacitor cannot change suddenly, this voltage drop is caused by the ohmic internal resistance R_0.

Stage 2: BC segment. The voltage gradually decreases with an exponential trend until it reaches the minimum value, which is affected by the two RC branches R_1C_1, R_2C_2.

Stage 3: CD segment. The pulse excitation disappears, the battery is no longer discharged, and it becomes idle with no load. Also, the voltage across the capacitor cannot change abruptly due to the internal ohmic resistance.

Stage 4: DE segment. The voltage rises slowly to the maximum value with an exponential characteristic.

The voltage change phenomenon described above is called the rebound voltage characteristic of the battery. Due to factors like the electrode material, electrolyte, and battery polarization, a specific voltage drop will occur when the battery is loaded. These factors are combined as the equivalent impedance of the battery. Different parts of the equivalent impedance cause the rebound voltage characteristic.

In this report, the offline parameter identification of ohmic internal ohmic resistance R_0, polarization resistance R_1, R_2, and polarization capacitance C_1, C_2 is carried out by the double exponential fitting method [46].

1. Ohmic internal resistance R_0

Both the AB section and CD section reflect the characteristics of the internal resistance R_0. The ohmic internal resistance R_0 equals the sudden voltage divided by the discharge current. Here, the average value of the two sections is taken:

$$R_0 = \frac{1}{2}\left(\frac{U_A - U_B}{I_L} + \frac{U_D - U_C}{I_L}\right) \tag{3.7}$$

2. Second-order RC parallel link

The slow change of the voltage in the BC segment and the DE segment is due to the action of two RC loops. With the release of the energy of the RC loop, the voltage eventually tends to be stable, and the parameter values of the loop can be obtained by exponential fitting.

From the formula of the second-order RC circuit:

$$\begin{cases} \dfrac{dU_1}{dt} = \dfrac{I_L}{C_1} - \dfrac{U_1}{R_1C_1} \\ \dfrac{dU_2}{dt} = \dfrac{I_L}{C_2} - \dfrac{U_2}{R_2C_2} \end{cases}$$

Solving the ordinary differential equation gives:

$$\begin{cases} U_1(t) = U_1(0)e^{-t/\tau_1} + I_l R_1(1 - e^{-t/\tau_1}) \\ U_2(t) = U_2(0)e^{-t/\tau_2} + I_l R_2(1 - e^{-t/\tau_2}) \end{cases}$$

Where $\tau_1=R_1C_1, \tau_2=R_2C_2$

The pulse current in the DE section no longer exists. Namely, there is no input now. It can be regarded as a zero-input response. Taking point D as the moment t=0, the zero input response of the two RC loops is:

$$\begin{cases} U_1 = U_1(0)e^{-t/\tau_1} \\ U_2 = U_2(0)e^{-t/\tau_2} \end{cases}$$

The output equation:

$$U_L(t) = OCV - U_1(0)e^{-t/\tau_1} - U_2(0)e^{-t/\tau_2}$$

Use the MATLAB cftool tool to fit the DE segment, and the custom exponential function expression is:

$$U_L(t) = b_0 - b_1 e^{-t/\tau_1} - b_2 e^{-t/\tau_2}$$

By comparison, it is evident that:

$$\begin{cases} \tau_1 = 1/\lambda_1 \\ \tau_2 = 1/\lambda_1 \\ U_1(0) = b_1 \\ U_2(0) = b_2 \end{cases} \tag{3.8}$$

Before the AB section, the battery has been left standing for a long time, and the voltage between both ends of C_1, C_2 is approximately 0. Therefore, the BC section can be regarded as a zero-state response. Take point B as the moment t=0, then the zero-state response of the two RC loops can be obtained:

$$\begin{cases} U_1(t) = I_L R_1 (1 - e^{-t/\tau_1}) \\ U_2(t) = I_L R_2 (1 - e^{-t/\tau_2}) \end{cases}$$

The output equation：

$$U_L(t) = OCV - I_L R_0 - I_L R_1 (1 - e^{-t/\tau_1}) - I_L R_2 (1 - e^{-t/\tau_2})$$

The expression for exponential fitting in MATLAB cftool is：

$$U_L(t) = a_0 - a_1 (1 - e^{-t/\tau_1}) - a_2 (1 - e^{-t/\tau_2})$$

It can be concluded that:

$$\begin{cases} R_1 = \dfrac{a_1}{I_L} \\ R_2 = \dfrac{a_2}{I_L} \end{cases} \tag{3.9}$$

Then according to the two time constants: $\tau_1 = R_1 C_1$, $\tau_2 = R_2 C_2$

$$\begin{cases} C_1 = \dfrac{\tau_1}{R_1} \\ C_2 = \dfrac{\tau_2}{R_2} \end{cases} \tag{3.10}$$

The flow chart of the exponential fitting algorithm is given below:

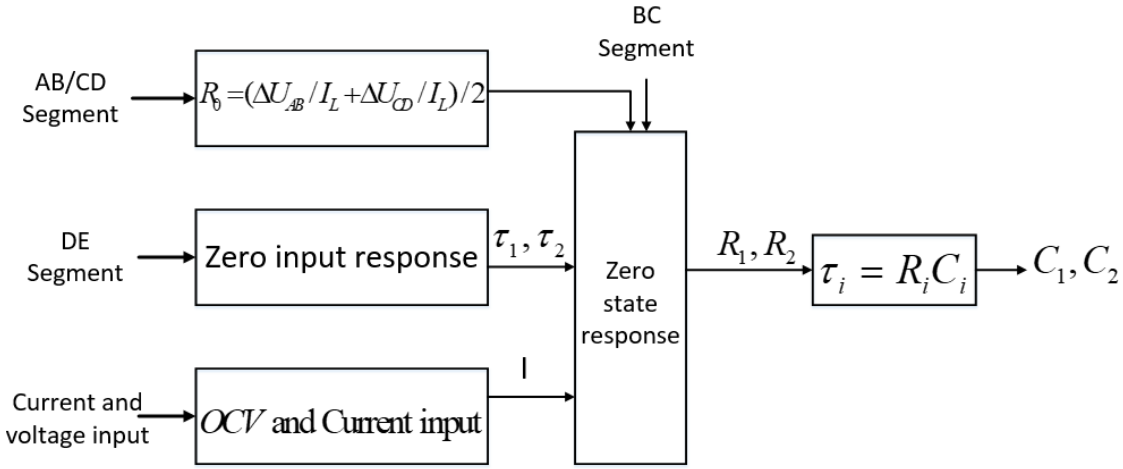

Figure 3- 10: Flow chart of the double exponential fitting algorithm

The detailed implementation will be shown in the next chapter.

3.3 Cell SoC estimation methods

As mentioned in the literature review, the primary cell SoC estimation method is the EKF method. Nevertheless, the other methods will also be applied for comparison and further analysis.

3.3.1 Coulomb counting

The SoC calculation formula via coulomb counting is given in [24]:

$$SoC = SoC_o - 1/Q_{rated}\int \eta I dt \tag{3.11}$$

Where SoC_o is the initial value, Q_{rated} is the rated capacity under the set temperature and charge-discharge rate, and η is the charge-discharge efficiency.

As long as the initial value and the charge and discharge current at each moment are known, the estimated value of SoC at each moment can be obtained.

3.3.2 Looking-up table based

According to equation (2.3), OCV and SoC have a one-to-one relationship with each other. Given the OCV value measured at a specific moment, the SoC value corresponding to that moment can be obtained directly by looking up the table.

The method has inherent difficulties in practical applications: the sensors need high resolution to measure voltage accurately, and sufficient time is required for equilibrium. The OCV method can be very accurate, but as it needs a rest time to estimate the SoC, it cannot be used in real-time. In addition, the OCV–SoC relationship differs from cell to cell. Therefore, unacceptable errors may occur, according to [24].

3.3.3 Extend Kalman filter

Kalman filtering is a filtering algorithm that uses the minimum mean square error as the optimal estimation criterion and adopts the recursive method of "prediction-measurement-correction" to obtain the system state estimation from the noisy measurement [35]. The Kalman filter algorithm is suitable for ordinary linear systems and can solve the problem of state

variable estimation. In practical engineering, it is often necessary to separate the state variables of the system from the observation signals mixed with noise signals. The KF algorithm is a tool that can effectively reduce this noise, especially where the measurement noise and observation noise approximately satisfy the Gaussian distribution characteristics.

Modeling the state space of the system is generally represented by two types of equations, namely, the state equation and the observation equation. The state equation represents the dynamic relationship between the state variables and the output variables of the system. The observation equation describes the relationship between the system's output variables and state variables.

Since the standard KF filtering algorithm is only suitable for linear systems, and the ECM representing characteristics of Li-ion batteries is a typical non-linear system, so EKF is introduced. The first-order Taylor expansion is carried out near the best estimation point, and the higher-order terms are discarded to complete the approximate linearization of the non-linear system. Then the classic KF idea is adopted to achieve the prediction estimation and best estimate in a linearized system.

Assuming that all sampling points are differentiable, the state-space model of the non-linear discrete-time system is established as follows:

$$\begin{cases} x_{k+1} = f(x_k, u_k) + \omega_k \\ y_k = h(x_k, u_k) + v_k \end{cases} \tag{3.12}$$

Where x_k is the state vector at the moment k, y_k is the output vector, u_k is the input vector, f is the non-linear state transfer function, and h is the non-linear observation function. Besides, ω_k is the system noise due to unmodeled parts of the system or unknown inputs, v_k is the measurement noise caused by the inherent precision of the measuring device [36].

The state space of the system is shown in the figure below:

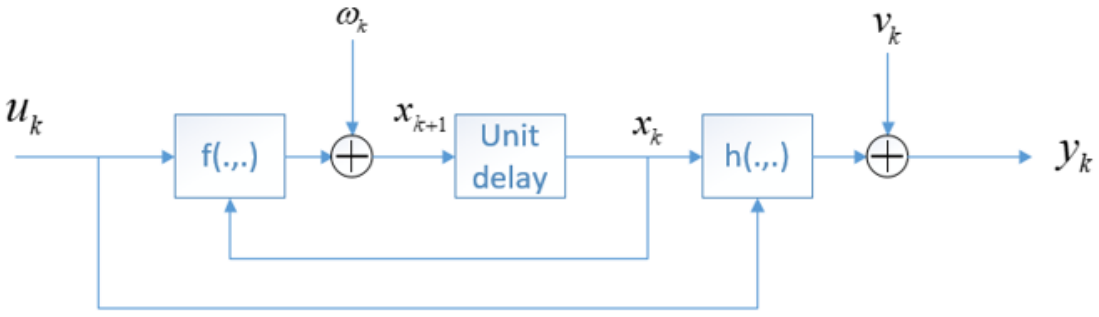

Figure 3- 11: State-space model of a non-linear system

According to the Taylor expansion formula, the first-order Taylor expansion is performed around each recent state estimation moment, such as $\hat{x}_k^+, \hat{x}_k^-$, and the following higher-order items are discarded.

$$\begin{cases} f(x_k, u_k) = f(\hat{x}_k, u_k) + \dfrac{\partial f(x_k, u_k)}{\partial x_k}\Big|_{x_k=\hat{x}_k} (x_k - \hat{x}_k) \\ h(x_k, u_k) = h(\hat{x}_k, u_k) + \dfrac{\partial h(x_k, u_k)}{\partial x_k}\Big|_{x_k=\hat{x}_k} (x_k - \hat{x}_k) \end{cases} \tag{3.13}$$

Define: $\hat{A}_k = \dfrac{\partial f(x_k, u_k)}{\partial x_k}\Big|_{x_k=\hat{x}_k}$, $\hat{C}_k = \dfrac{\partial h(x_k, u_k)}{\partial x_k}\Big|_{x_k=\hat{x}_k}$

The state space equation can be rewritten as:

$$\begin{cases} x_{k+1} \approx \hat{A}_k x_k + f(\hat{x}_k, u_k) - \hat{A}_k \hat{x}_k + \omega_k \\ y_k = \hat{C}_k x_k + h(\hat{x}_k, u_k) - \hat{C}_k \hat{x}_k + \nu_k \end{cases} \tag{3.14}$$

Variable meaning of the EKF algorithm:

$\hat{x}_k^-$: Prior estimate of the state vector at the moment k, before obtaining output value y_k

$\hat{x}_k^+$: Posterior estimate of the state vector at the moment k, after obtaining output value y_k, and $\hat{x}_{k+1}^- = \hat{x}_k^+$

u_k : Input vector at the moment k

f : Non-linear state transfer function

h : Non-linear observation function

Q_k : System covariance noise

R_k : Observation covariance noise

P_k^- : Prior error covariance matrix at the moment k before obtaining measured value y_k, representing the error between the estimated and true state values.

P_k^+ : Posterior error covariance matrix at the moment k, after obtaining measured value y_k

G_k : Kalman gain matrix at the moment k, represents the weight of the actual observed value in correcting the prior estimate of the state vector.

N: Total sampling times

Pseudo-code given:

Output:

1: Initialize parameters:

$$\hat{x}_0^+ = E[x_0]$$

$$P_0^+ = E(x_0 - E[x_0])(x_0 - E[x_0])^T$$

2:

for k=2 to N, **do**

Prior state estimation:

$$\hat{x}_k^- = f(\hat{x}_{k-1}^+, u_{k-1}) + \omega_k$$

Prior error covariance matrix update:

$$P_k^- = A_{k-1} P_{k-1}^+ A_{k-1}^T + Q_k$$

Kalman gain matrix update:

$$G_k = P_k^- C_k^T (C_k P_k^- C_k^T + R_k)^{-1}$$

Posterior state estimation update:

$$\hat{x}_k^+ = \hat{x}_k^- + G_k (y_k - h(\hat{x}_k^-, u_k))$$

Posterior error covariance matrix update

$$P_k^+ = (E - G_k C_k) P_k^-$$

end for

EKF performs Taylor series expansion on the original system and omits the higher-order terms above the second order, which introduces linearization errors. It is only suitable for systems with weak non-linearity, and it is easy to diverge when the non-linearity is strong. Moreover, for a system with a higher model order, the calculation amount of the Jacobian matrix will increase dramatically, so there is still room for improvement [38].

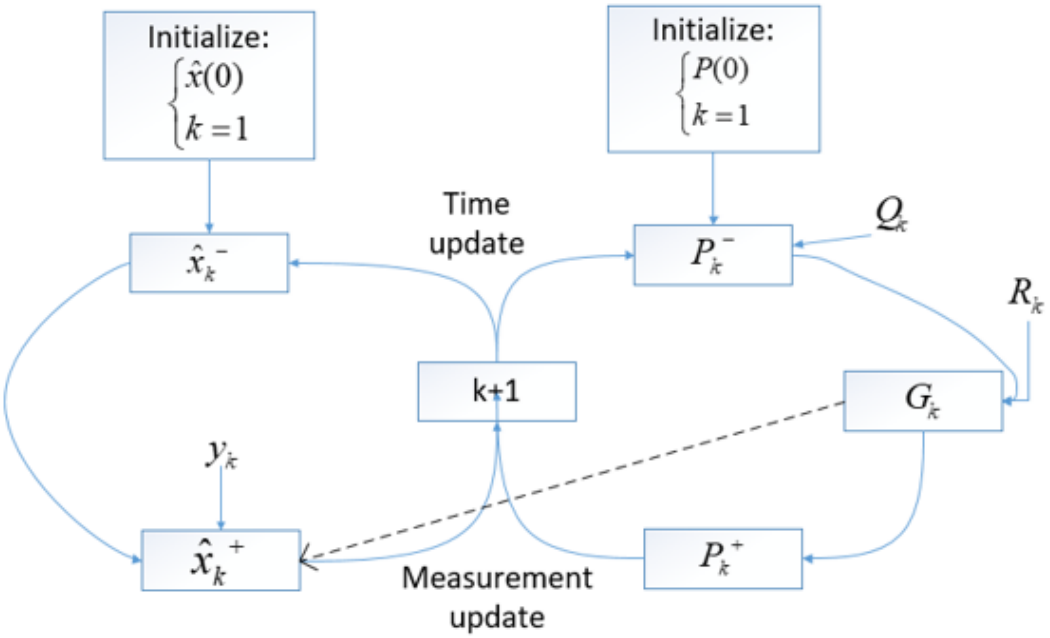

Figure 3- 12: EKF algorithm flowchart

3.3.4 Extension of EKF

Due to the high degree of non-linearity of the power battery in the actual use process, the first-order EKF algorithm ignores the higher-order items above the second-order, resulting in a weaker degree of non-linearity and low estimation accuracy. Therefore, based on the first-order EKF, a second-order EKF algorithm can be proposed to realize the SoC estimation of the battery.

The principle of the second-order EKF is similar to that of the first-order. The difference is that the second-order EKF algorithm is to expand the state space equation of the non-linear discrete system at the state estimation point to the second-order Taylor expansion:

$$\begin{cases} f(x_k,u_k)=f(\hat{x}_k,u_k)+\left.\dfrac{\partial f(x_k,u_k)}{\partial x_k}\right|_{x_k=\hat{x}_k}(x_k-\hat{x}_k)+\dfrac{1}{2}\left.\dfrac{\partial^2 f(x_k,u_k)}{\partial {x_k}^2}\right|_{x_k=\hat{x}_k}(x_k-\hat{x}_k)^2 \\ h(x_k,u_k)=h(\hat{x}_k,u_k)+\left.\dfrac{\partial h(x_k,u_k)}{\partial x_k}\right|_{x_k=\hat{x}_k}(x_k-\hat{x}_k)+\dfrac{1}{2}\left.\dfrac{\partial^2 h(x_k,u_k)}{\partial {x_k}^2}\right|_{x_k=\hat{x}_k}(x_k-\hat{x}_k)^2 \end{cases} \tag{3.15}$$

Define：

$$\begin{cases} A_{\mathrm{k}}=[\dfrac{\partial f(x_k,u_k)}{\partial x_k}-\dfrac{\partial^2 f(x_k,u_k)}{\partial {x_k}^2}\hat{x}_k+\dfrac{1}{2}\dfrac{\partial^2 f(x_k,u_k)}{\partial {x_k}^2}x_k]\Big|_{x_k=\hat{x}_k} \\ C_k=[\dfrac{\partial h(x_k,u_k)}{\partial x_k}-\dfrac{\partial^2 h(x_k,u_k)}{\partial {x_k}^2}\hat{x}_k+\dfrac{1}{2}\dfrac{\partial^2 h(x_k,u_k)}{\partial {x_k}^2}x_k]\Big|_{x_k=\hat{x}_k} \end{cases}$$

After sorting, the linearization equation is obtained:

$$\begin{cases} x_{k+1}=A_k x_k+[f(\hat{x}_k,u_k)-\dfrac{\partial f(x_k,u_k)}{\partial x_k}\hat{x}_k+\dfrac{1}{2}\dfrac{\partial^2 f(x_k,u_k)}{\partial {x_k}^2}\hat{x}_k{}^2]+\omega_k \\ y_k=C_k x_k+[h(\hat{x}_k,u_k)-\dfrac{\partial h(x_k,u_k)}{\partial x_k}\hat{x}_k+\dfrac{1}{2}\dfrac{\partial^2 h(x_k,u_k)}{\partial {x_k}^2}\hat{x}_k{}^2]+\upsilon_k \end{cases} \tag{3.16}$$

The second-order EKF algorithm is similar to the first-order EKF, except that the state space equations of the system are different. Therefore, the expressions of the incidence matrixes are different.

3.4 Pack modeling method

After successfully modeling the cell, the more difficult battery pack modeling is to be solved. In this project, aggregating and scaling are the essential methods to adopt. However, it is indispensable to investigate the influence of different grouping modes on the battery pack performance. A study in [47] reveals that battery configurations significantly influence the battery pack performance. The pack with its modules directly connected in parallel and then assembled in series is more robust against variations of the cell capacity through the battery. In order to prove this point, the following will give explanations from mathematics and circuit principles, respectively.

3.4.1 Circuit design sequence

A battery cell is the most basic unit to form a battery pack. In practice, multiple single cells are generally connected in series or in parallel to form a battery module. Then the modules are connected in series or in parallel to form a battery pack. Significant differences exist in the performance of battery cells, modules, and packs. The overall performance has apparent attenuation in the process of gradually expanding from cells and progressively expanding in scale. The reason is not only the inconsistency between the single cells but also has a lot to do with the connection method between the single cells [12].

From a mathematical point of view, based on probability theory, the battery pack's performance reliability will be analyzed to select the reasonable connection mode between the single batteries in this experiment. Denote the reliable performance of a single cell as an event and the probability of reliable performance $r_i(0\le r_i\le 1)$.

1. First in parallel, then in series

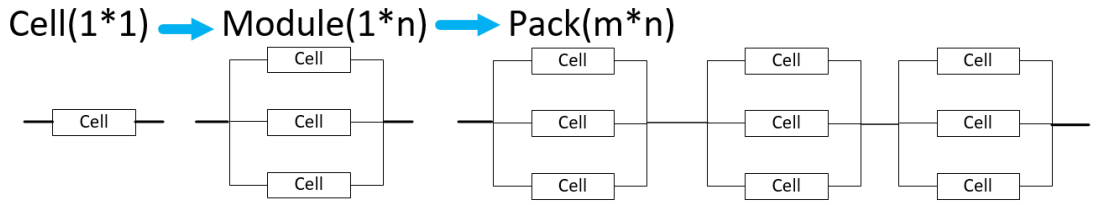

Figure 3- 13: Parallel-series configuration

It can be seen from the basic knowledge of the circuit that when there are multiple branch circuits in parallel in the primary circuit, as long as one of the branch circuits works typically, the entire primary circuit is guaranteed to work as usual. Therefore, record the regular operation of the module formed by connecting n single cells in parallel as an event $B_j = (A_1 \cup A_2 \cup A_3 \cup \ldots \cup A_n)$.

The probability of this happening is:

$$P(B_j) = 1 - \prod_{i=1}^{n} (1 - r_i) \tag{3.17}$$

Then m modules are connected in series to form a battery pack. According to circuit knowledge, when there are multiple series branches in the main road, it is necessary to ensure that each branch usually works to smooth the whole main road. Record the regular operation of the battery pack formed by connecting m modules in series as an event $Pack_1 = (B_1 \cap B_2 \cap B_3 \cap \ldots \cap B_m)$.

The probability of this happening is:

$$P(Pack_1) = \prod_{j=1}^{m} P(B_j) = \prod_{j=1}^{m} [1 - \prod_{i=1}^{n} (1 - r_i)] \tag{3.18}$$

2. First in series, then in parallel

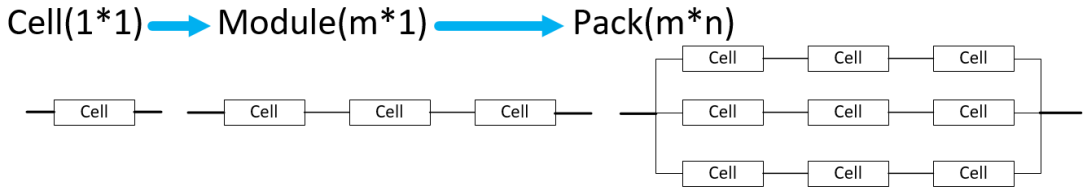

Figure 3- 14: Series-parallel configuration

Similarly, the probability of reliable operation of the battery pack formed by this connection can be obtained. Record the regular operation of the module developed by connecting m single batteries in series as an event $B_j = (A_1 \cap A_2 \cap A_3 \cap \ldots \cap A_m)$

The probability of this happening is:

$$P(B_j) = \prod_{i=1}^{m} r_i \tag{3.19}$$

Record the regular operation of the battery pack formed by connecting n modules in series as an event $Pack_2 = (B_1 \cup B_2 \cup B_3 \cup \ldots \cup B_m)$.

The probability of this happening is:

$$P(Pack_2) = 1 - \prod_{j=1}^{n}[1 - P(B_j)] = 1 - \prod_{j=1}^{n}(1 - \prod_{i=1}^{m} r_i) \tag{3.20}$$

3. Comparison of the reliability of the two connection methods:

First, the reliability of these two connection methods can be analyzed from the perspective of probability theory and mathematics.

In order to simplify the analysis, assuming that every single cell has the same probability of reliable performance r_i , it is more reasonable to compare which connection method is compared through calculation and analysis.

A study in [12] introduces a typical battery pack size of about 12S8P. Therefore, it can be assumed that m=12, n=8. After calculation, the figure below displays the trend of $P(Pack_1)$ and $P(Pack_2)$ changing with r_i .

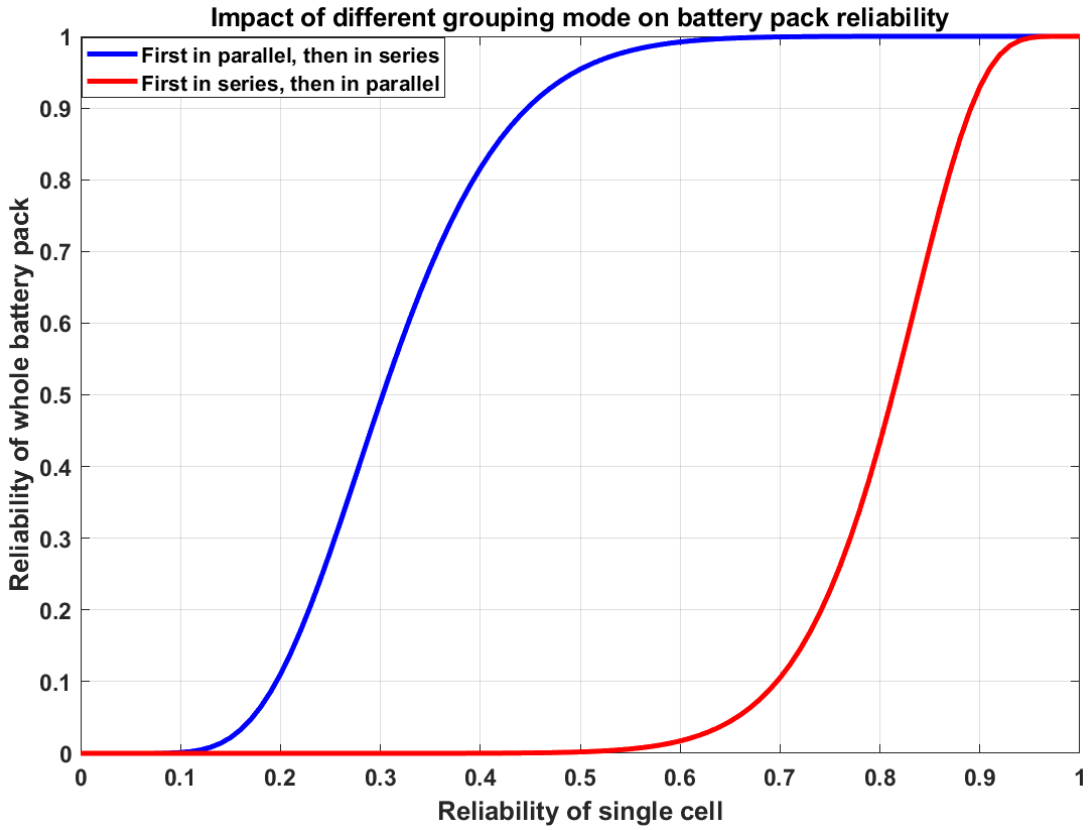

Figure 3- 15: Reliability analysis of Pack 1 and Pack 2

It can be seen from Figure 3-15 that when the probability of reliable work of a single cell r_i is very low $(0 \le r_i \le 0.1)$, the overall reliability of Pack 1 and Pack 2 are both very low, with a slight difference. The final pack's reliability is close to 0, indicating that the battery pack's performance is absolutely unreliable.

When the probability of reliable work of a single cell r_i is high $(0.9 \le r_i \le 1.0)$ the overall reliability of Pack 1 and Pack 2 are both very high, with a tiny gap. The final pack's reliability is close to 1, indicating that the battery pack's performance is absolutely reliable.

When the probability of reliable work of a single cell r_i is $0.1 \le r_i \le 0.9$, the 'parallel-series' connection mode has an obvious advantage over the other mode. Under the same probability of reliable work r_i , the blue curve is much higher than the red curve, which means that the performance of Pack 1 is much better than that of Pack 2. **Therefore, in this project, the battery pack will be designed in parallel first and then in series.**

On the other hand, in terms of the circuit principle, it can also be explained why the connection mode 'parallel first, then series' is superior.

In a series circuit, the current flowing through each cell is equal. If the capacity of a particular battery cell is small, it will reach the charge cut-off voltage first when charging, and it will reach the discharge cut-off voltage first when discharging. Therefore, in a series circuit, the maximum capacity of the battery pack is determined by the single cell with the smallest capacity. It is the so-called short board effect. A battery cell with a small capacity is prone to overcharge or over-discharge, which seriously affects the battery pack's performance.

On the contrary, in a parallel circuit, the energy of every single cell can freely flow between each other. During the charging process, the cell with a small capacity will reach a higher voltage first and charge other batteries. During the discharge process, the cell voltage with a large capacity drops more slowly than others, so its cell voltage is relatively high. Then it will charge another cell with a small capacity.

Based on this analysis, in a ‘series-parallel’ connected battery pack, the voltage difference of the series branches will gradually accumulate due to the inconsistency of different cell voltages. A significant difference in the voltage of each parallel branch will occur accordingly. Therefore, this would cause an extensive range of mutual charging and a sizeable corresponding energy loss in the pack.

Oppositely, in a ’parallel-series connected’ connected battery pack, although the batteries connected in parallel also charge each other, the voltage difference between the single cells is slight. As a result, the power consumption of mutual charging is small, and the influence range is only within the module. This small-scale mutual charging will balance the whole battery pack and supplement the cells with insufficient power [47].

To sum up, from the two perspectives of the mathematical model and circuit principle, it reflects the superiority of the ‘parallel-series’ connection mode.

After determining the circuit sequence, it comes to the pack modeling methods. Three common approaches for battery pack modeling are available in [48]. The first approach is to aggregate cell models in series and parallel to represent the battery pack model. The second approach is to scale the cell model into a battery pack model with one simplified model representing the battery pack. The third approach is building a battery pack model directly on a well-built battery pack with a single battery model capturing the totality of the pack behavior.

Among the three methods, the third is mainly used in commercially available battery packs and seems to be the most promising for system-level designers [49]. The characteristics of the battery cells and thermal effects are naturally included in the pack model as a result of the cumulative impact of cell averaging. In addition, the overall computational cost is relatively low compared to the former two methods [50]. However, it requires a well-built battery pack and preliminary testing data [51]. In this project, the third approach cannot be utilized due to the lack of existing battery pack data. Therefore, the focus will be on aggregating and scaling methods. With no well-built pack in hand, a new battery pack has to be constructed from scratch.

3.4.2 Aggregating method

This approach is easy to understand and requires the least effort going from the cell model to the pack model, as the only information needed is the cell configuration in the battery pack.

However, severe loss of fidelity can occur in the resulting battery pack model due to ignoring the cell variations and thermal unbalancing in the battery pack [52]. At the same time,

not all cells used in battery packs are available to the system designers for battery cell modeling [53]. Therefore, the accuracy of this method needs to be further tested.

3.4.3 Scaling method

Compared with the first approach, the second approach is comprehensive and fast in simulation, which is more suitable for system-level design and simulation [54]. It does not require manual connection of all various cells, thus saving a lot of time.

In order to prove the feasibility of the scaling method, take the first-order RC model as an example for further analysis. The following will demonstrate the feasibility separately from series and parallel connection aspects.

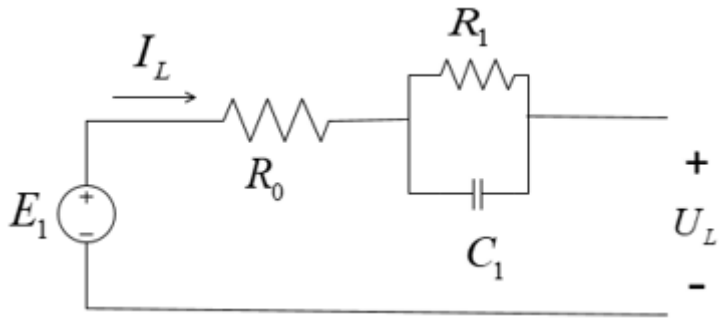

Figure 3- 16: First-order Thevenin model

- **Series connection**

Take two single cells in a series as an example:

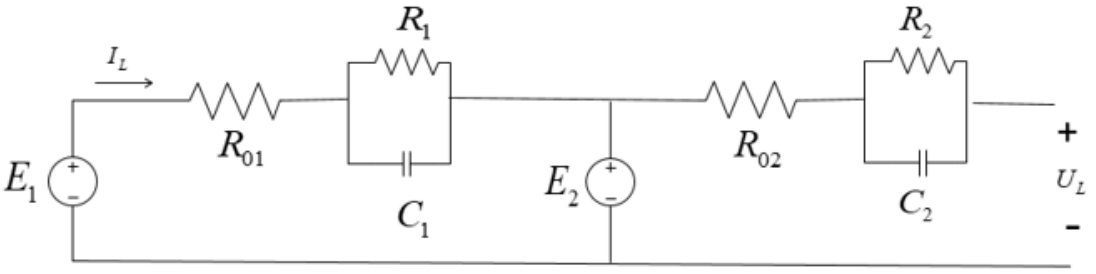

Figure 3- 17: Cell 1 in series with cell 2

According to the basic principles of the electric circuit, internal ohmic resistance R_0 and electromotive force E can be directly combined in a series structure. The feasibility mainly depends on whether the two RC loops (R_1C_1, R_2C_2) can be simplified into another RC loop R_3C_3 with different parameters after being connected in series.

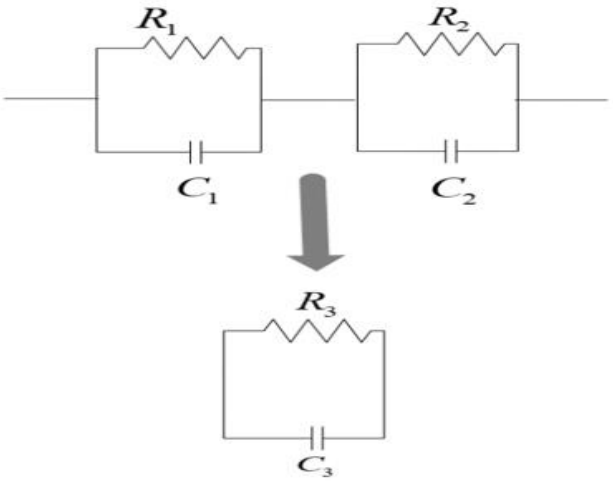

Figure 3- 18: Whether series cell 1&2 can be equal to a single cell 3

The total impedance of the two RC loops (R_1C_1, R_2C_2) in series is:

$$Z_{total1} = \frac{1}{j\omega C_1 + \frac{1}{R_1}} + \frac{1}{j\omega C_2 + \frac{1}{R_2}}$$

The total impedance of the loop R_3C_3 is:

$$Z_{total2} = \frac{1}{j\omega C_3 + \frac{1}{R_3}}$$

If the loop R_3C_3 can be used to equivalent two RC loops, then $Z_{total1} = Z_{total2}$:

$$\frac{1}{j\omega C_1 + \frac{1}{R_1}} + \frac{1}{j\omega C_2 + \frac{1}{R_2}} = \frac{1}{j\omega C_3 + \frac{1}{R_3}}$$

The above formula is deduced and transformed as follows:

$$\frac{1}{1+\omega^2 R_1^{\,2} C_1^{\,2}}(R_1 - j\omega R_1^{\,2} C_1) + \frac{1}{1+\omega^2 R_2^{\,2} C_2^{\,2}}(R_2 - j\omega R_2^{\,2} C_2) = \frac{1}{1+\omega^2 R_3^{\,2} C_3^{\,2}}(R_3 - j\omega R_3^{\,2} C_3)$$

According to the equality of a real number, the real and imaginary parts are correspondingly equal:

$$\begin{cases} \dfrac{R_1}{1+\omega^2 R_1^{\,2} C_1^{\,2}} + \dfrac{R_2}{1+\omega^2 R_2^{\,2} C_2^{\,2}} = \dfrac{R_3}{1+\omega^2 R_3^{\,2} C_3^{\,2}} \\ \dfrac{R_1^{\,2} C_1}{1+\omega^2 R_1^{\,2} C_1^{\,2}} + \dfrac{R_2^{\,2} C_2}{1+\omega^2 R_2^{\,2} C_2^{\,2}} = \dfrac{R_3^{\,2} C_3}{1+\omega^2 R_3^{\,2} C_3^{\,2}} \end{cases}$$

Let

$$\begin{cases} \dfrac{R_1}{1+\omega^2 R_1^{\,2} C_1^{\,2}} + \dfrac{R_2}{1+\omega^2 R_2^{\,2} C_2^{\,2}} = \mathrm{a} \\ \dfrac{R_1^{\,2} C_1}{1+\omega^2 R_1^{\,2} C_1^{\,2}} + \dfrac{R_2^{\,2} C_2}{1+\omega^2 R_2^{\,2} C_2^{\,2}} = b \end{cases}$$

Substituting into the above formula:

$$\begin{cases} R_3 = a(1+\omega^2 \dfrac{b^2}{a^2}) \\ C_3 = \dfrac{b}{a^2(1+\omega^2 \dfrac{b^2}{a^2})} \end{cases} \tag{3.21}$$

Therefore, after multiple single cells are connected in series, the overall structure of the entire series connection can still be represented by a new single cell, and the parameters of the new single cell can be calculated using the parameters of the original single cell.

- **Parallel connection**

Take two single cells in parallel as an example:

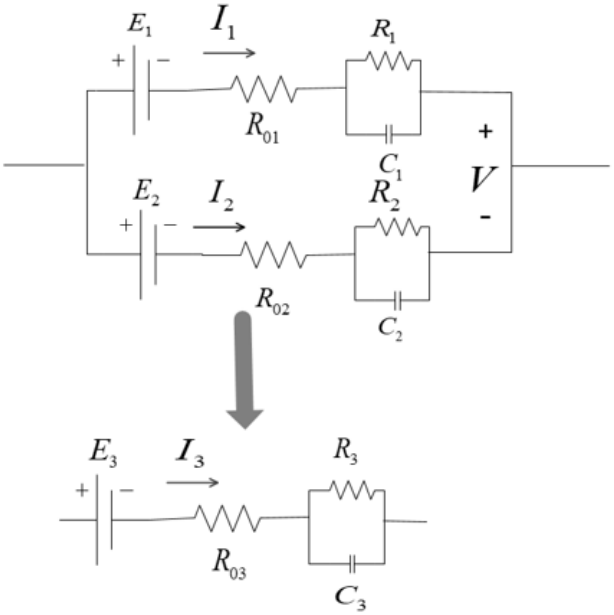

Figure 3- 19: Whether parallel cell 1&2 can be equal to a single cell 3

In this case, the ohmic internal resistance R_0 and the electromotive force E cannot be directly combined and calculated, which is more complicated than the series structure. The derivation process is given below:

Assume that the current of the first branch of the parallel unit is I_1, and the current of the second branch is I_2. In real cases, even if the single cell's consistency is good, each parallel branch's current is still not equal. Suppose $I_1 \neq I_2$ and the voltage at both ends of the parallel unit is V.

Derivation transformation:

$$\begin{cases} I_2E_1 + R_{01}I_1I_2 + Z_1I_1I_2 = VI_2 ① \\ I_1E_2 + R_{02}I_1I_2 + Z_1I_1I_2 = VI_1 ② \end{cases}$$

②-①:

$$V(I_1 - I_2) = I_1V_2 - I_2V_1 + I_1I_2(R_{02} - R_{01}) + I_1I_2(Z_2 - Z_1)$$

V can be expressed below:

$$\begin{aligned} V &= \frac{I_1V_2 - I_2V_1}{I_1 - I_2} + \frac{I_1I_2(R_{02} - R_{01})}{I_1 - I_2} + \frac{I_1I_2(Z_2 - Z_1)}{I_1 - I_2} \\ &= \frac{I_1V_2 - I_2V_1}{I_1 - I_2} + (I_1 + I_2)\frac{I_1I_2(R_{02} - R_{01})}{(I_1 - I_2)(I_1 + I_2)} + (I_1 + I_2)\frac{I_1I_2(Z_2 - Z_1)}{(I_1 - I_2)(I_1 + I_2)} ③ \end{aligned}$$

When two single cells are connected in parallel to form an overall circuit, it is necessary to ensure that the voltage V at both ends of the circuit remains unchanged and the current passing through the overall circuit is the sum $I_1 + I_2$: $\begin{cases} E_1 + R_{01}I_1 + Z_1I_1 = V \\ E_2 + R_{02}I_2 + Z_2I_2 = V \end{cases}$

$$V = V_3 + R_{03}(I_1 + I_2) + Z_3(I_1 + I_2)$$

Comparing with the formula ③:

$$\begin{cases} V_3 = \dfrac{I_1V_2 - I_2V_1}{I_1 - I_2} \\ R_{03} = \dfrac{I_1I_2(R_{02} - R_{01})}{(I_1 - I_2)(I_1 + I_2)} \\ Z_3 = \dfrac{I_1I_2(Z_2 - Z_1)}{(I_1 - I_2)(I_1 + I_2)} \end{cases} \tag{3.22}$$

In practice, V_3, R_{03}, Z_3 should all be positive values, so the expressions of these three parameters need to be further analyzed. When a cell is expanded into a battery pack, since the same type of battery is used, the parameters of each single cell are basically the same. During the cycle life, its electromotive force parameter E only slightly changes, and the internal ohmic resistance R_0 and RC loop impedance Z change in the same trend (increasing). Therefore, it can be considered approximately that: $V_2 \approx V_1$.

Assuming $I_1 > I_2$, due to $V_2 \approx V_1$, it can be concluded that the total impedance of branch 1 is less than the total impedance of branch 2, that is: $R_{01} < R_{02}, Z_1 < Z_2$. Thus, V_3, R_{03}, Z_3 are all positive values. Similarly, it is evident that when $I_1 < I_2$, $R_{01} > R_{02}$, and $Z_1 > Z_2$, the three parameters V_3, R_{03}, Z_3 are also positive.

Therefore, after multiple single cells are connected in parallel, the whole parallel structure can still be represented by a new single cell, and the parameters of the new single can be expressed by equivalent calculations using the parameters of the original cells.

To generalize, in a battery pack, the overall structure can still be represented by the original cell model as the number of single cells increases, no matter in series or in parallel. However, the complexity of the parameters of each part increases as well.

Nonetheless, investigating cell discrepancy and thermal distribution in a battery pack requires extensive effort, and sometimes the battery cells are not readily available to the system designers [55].

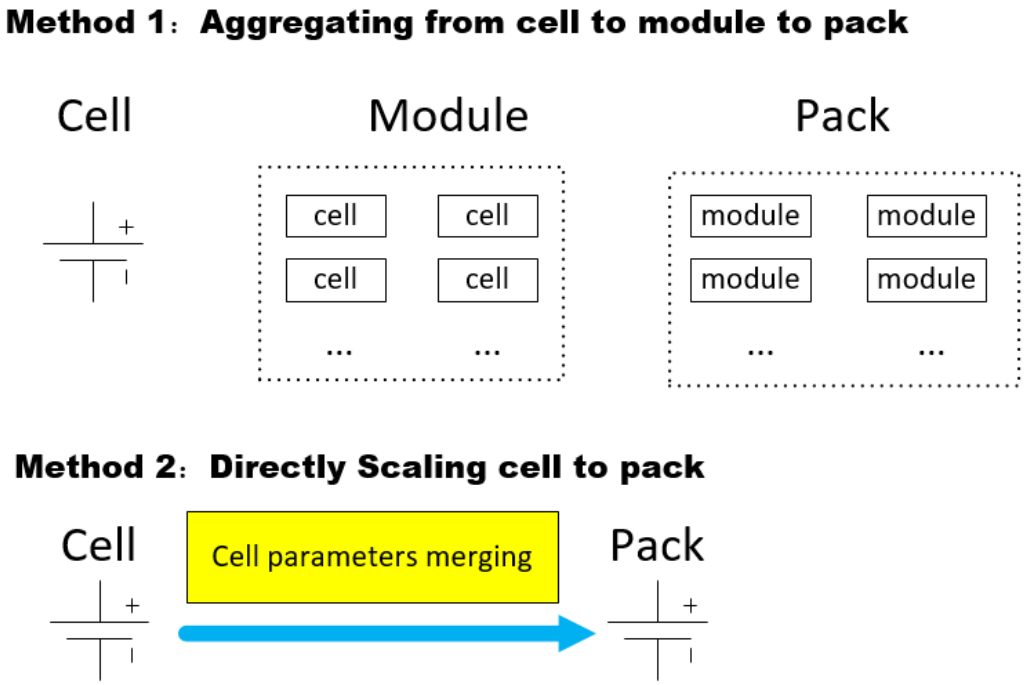

Figure 3- 20: Aggregating and scaling method

3.5 Pack SoC estimation

Cell SoC estimation is the basis of the battery pack SoC estimation. A battery pack usually consists of hundreds or thousands of single cells connected in series and parallel, which adds to the difficulty of pack SoC estimation. A common idea of battery pack SoC estimation is proposed in [56], including cell calculation-based, screening process-based and bias correction methods. Since the latter two ways are too complicated to calculate and require a large amount of experimental data, they are not considered in this project.

The first category, 'Cell calculation,' includes the following three specific methods [23]: 'Big cell' method, 'Short board effect' method and one by one calculation method.

（1） The 'Short board effect' method uses the extreme cell to calculate the pack SoC. Namely, during the discharging process, the cell with the lowest voltage is selected to indicate the whole pack SoC [57].

（2） The 'Big cell' method regards the battery pack as a big cell. The battery pack's voltage and current are used to calculate the pack SoC [58].

（3） One-by-one calculation method estimates the SoC for all cells in a battery pack and then calculates the pack SoC. As expected, this kind of method can obtain the desired estimation accuracy. However, the computational cost is enormous compared to the former two approaches.

This report adopts methods 1 and 2 for battery pack SoC estimation, considering the trade-off between accuracy and computational cost. The computer's computing power is insufficient to afford the simulation amount of the one-by-one calculation method.

3.5.1 'Big cell'

Apparently, this method requires the least computation cost. However, the inconsistent characteristics in cell performance have been ignored. Obviously, it cannot ensure the safety application of the battery pack since the internal cell conditions are neglected [59].

3.5.2 'Short board effect'

This method selects one cell to represent the behavior of the whole battery pack. Therefore, it can improve the safety of the battery pack since the extremely worst cell can be picked whenever testing. However, it will reduce the energy utilization of the battery pack since the effect of other single cells in good condition is not fully considered [60].

In this project, these two methods will both be used for pack SoC estimation.

4 Implementation

The methods and principles used in this project are given in Chapter 3. Next is introducing the specific battery data into the selected model and beginning the research on cell modeling, parameter identification, and SoC estimation individually.

4.1 Single cell research

Due to the lack of experimental data, searching public battery datasets available online is essential. A study in [61] provides battery charge and discharge data published online by different research institutes. This report selects the INR 18650-20R Battery data from CALCE to continue the research.

The battery has many advantages, such as high energy density, long cycle life, low self-discharge rate, stable performance, and meets the requirements of battery energy storage. Moreover, in the public data set, the data of the battery under low current, incremental current and various dynamic working conditions can be obtained, which is convenient for further research. The data can be found at the website: https://calce.umd.edu/battery-data[62].

Figure 4- 1: INR 18650-20R Li-ion cell captured from CALCE website [63]

The lithium-ion battery selected in this project is the INR 18650-20R battery in the public data set of the University of Maryland. Its rated capacity is 2Ah, so 1C=2A.

Here are the battery parameters available on [62]:

Table 4- 1: INR 18650-20R battery parameters

Parameters	Value
Rated capacity	2Ah
Operating voltage	2.5–4.2V
Nominal voltage	3.65V
Weight	45g
Size	18.33mm²
Length	64.85mm

4.1.1 Cell modeling

Simulink BMS development white paper [64] gives detailed cell modeling and desktop simulation instructions. Along with a study in [65], Modeling the single cell in Simulink becomes feasible, including OCV, internal ohmic resistance R_0 , polarization resistance R_1, R_2 , and polarization capacitance C_1, C_2 . The cell model is displayed below:

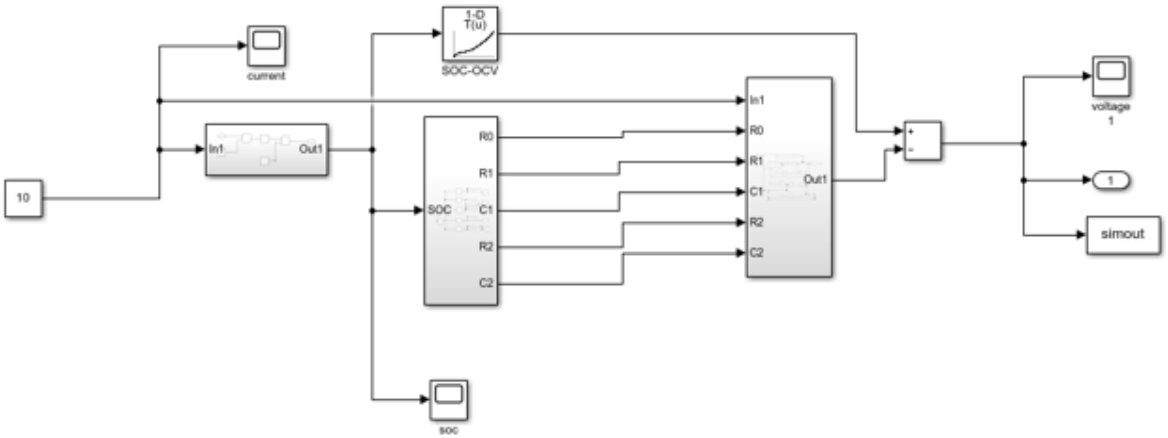

Figure 4- 2: Second order RC Thevenin model built in Simulink

4.1.2 Parameter identification

After obtaining the battery data from the CALCE website, data processing is necessary for further analysis. Among all the profiles, the Incremental OCV profile is the best for parameter identification and the following cell SoC estimation. Two sample cells are tested under three different temperatures, which adds to the complexity of the parameter identification. The test procedures captured from [62] are as follows:

1. Charge the battery fully to 100% SoC.
2. Now discharge using a negative pulse current relaxation duration at every 10% SoC.
3. Charge again following the same routine but with a positive pulse current.
4. Apply Averaging and Linear Interpolation steps to obtain the OCV-SoC curve at 0°C, 25°C and 45°C.

Obviously, it belongs to the HPPC test. Besides that, this charge and discharge experiment is very regular. The pulse charge and discharge are carried out sequentially at intervals of 10% SoC, providing excellent conditions for parameter identification under different SoC. The following implementation is based on this dataset.

Sample 1	Initial Capacity Data	Data for 0°C	Data for 25°C	Data for 45°C
Sample 2	Initial Capacity Data	Data for 0°C	Data for 25°C	Data for 45°C

Figure 4- 3: Two sample datasets for parameter identification captured from [62]

Take sample 1 for example. Extract the current and voltage profile from the dataset [62].

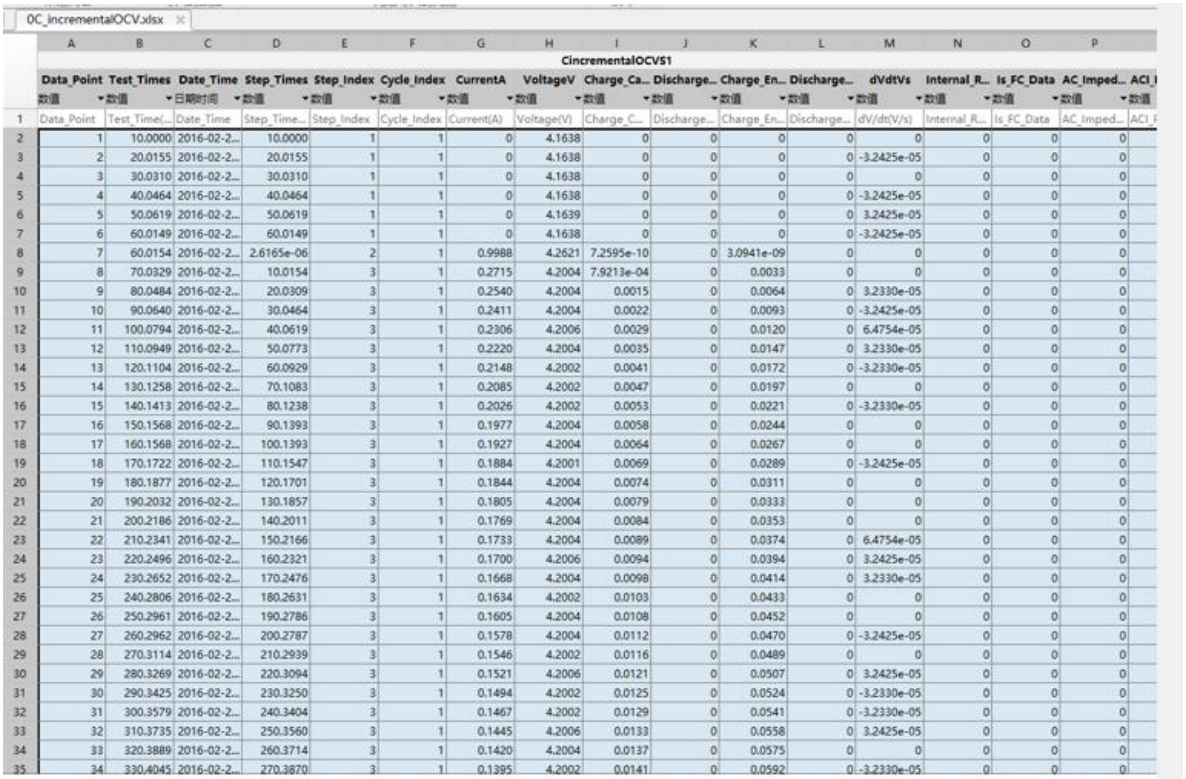

0C_incrementalOCV.xlsx

CincrementalOCVS1

Data_Point	Test_Times	Date_Time	Step_Times	Step_Index	Cycle_Index	CurrentA	VoltageV	Charge_Ca...	Discharge...	Charge_En...	Discharge...	dVdtVs	Internal_R...	Is_FC_Data	AC_Imped...	ACI_I
数值	数值	日期时间	数值	数值	数值	数值	数值	数值	数值	数值	数值	数值	数值	数值	数值	数值
Data_Point	Test_Time(...	Date_Time	Step_Time...	Step_Index	Cycle_Index	Current(A)	Voltage(V)	Charge_C...	Discharge...	Charge_En...	Discharge...	dV/dt(V/s)	Internal_R...	Is_FC_Data	AC_Imped...	ACI_F
1	10.0000	2016-02-2...	10.0000	1	1	0	4.1638	0	0	0	0	0	0	0	0	
2	20.0155	2016-02-2...	20.0155	1	1	0	4.1638	0	0	0	0	-3.2425e-05	0	0	0	
3	30.0310	2016-02-2...	30.0310	1	1	0	4.1638	0	0	0	0	0	0	0	0	
4	40.0464	2016-02-2...	40.0464	1	1	0	4.1638	0	0	0	0	-3.2425e-05	0	0	0	
5	50.0619	2016-02-2...	50.0619	1	1	0	4.1639	0	0	0	0	3.2425e-05	0	0	0	
6	60.0149	2016-02-2...	60.0149	1	1	0	4.1638	0	0	0	0	-3.2425e-05	0	0	0	
7	60.0154	2016-02-2...	2.6165e-06	2	1	0.9988	4.2621	7.2595e-10	0	3.0941e-09	0	0	0	0	0	
8	70.0329	2016-02-2...	10.0154	3	1	0.2715	4.2004	7.9213e-04	0	0.0033	0	0	0	0	0	
9	80.0484	2016-02-2...	20.0309	3	1	0.2540	4.2004	0.0015	0	0.0064	0	3.2330e-05	0	0	0	
10	90.0640	2016-02-2...	30.0464	3	1	0.2411	4.2004	0.0022	0	0.0093	0	-3.2425e-05	0	0	0	
11	100.0794	2016-02-2...	40.0619	3	1	0.2306	4.2006	0.0029	0	0.0120	0	6.4754e-05	0	0	0	
12	110.0949	2016-02-2...	50.0773	3	1	0.2220	4.2004	0.0035	0	0.0147	0	3.2330e-05	0	0	0	
13	120.1104	2016-02-2...	60.0929	3	1	0.2148	4.2002	0.0041	0	0.0172	0	-3.2330e-05	0	0	0	
14	130.1258	2016-02-2...	70.1083	3	1	0.2085	4.2002	0.0047	0	0.0197	0	0	0	0	0	
15	140.1413	2016-02-2...	80.1238	3	1	0.2026	4.2002	0.0053	0	0.0221	0	-3.2330e-05	0	0	0	
16	150.1568	2016-02-2...	90.1393	3	1	0.1977	4.2004	0.0058	0	0.0244	0	0	0	0	0	
17	160.1568	2016-02-2...	100.1393	3	1	0.1927	4.2004	0.0064	0	0.0267	0	0	0	0	0	
18	170.1722	2016-02-2...	110.1547	3	1	0.1884	4.2001	0.0069	0	0.0289	0	-3.2425e-05	0	0	0	
19	180.1877	2016-02-2...	120.1701	3	1	0.1844	4.2004	0.0074	0	0.0311	0	0	0	0	0	
20	190.2032	2016-02-2...	130.1857	3	1	0.1805	4.2004	0.0079	0	0.0333	0	0	0	0	0	
21	200.2186	2016-02-2...	140.2011	3	1	0.1769	4.2004	0.0084	0	0.0353	0	0	0	0	0	
22	210.2341	2016-02-2...	150.2166	3	1	0.1733	4.2004	0.0089	0	0.0374	0	6.4754e-05	0	0	0	
23	220.2496	2016-02-2...	160.2321	3	1	0.1700	4.2006	0.0094	0	0.0394	0	3.2425e-05	0	0	0	
24	230.2652	2016-02-2...	170.2476	3	1	0.1668	4.2004	0.0098	0	0.0414	0	3.2330e-05	0	0	0	
25	240.2806	2016-02-2...	180.2631	3	1	0.1634	4.2002	0.0103	0	0.0433	0	0	0	0	0	
26	250.2961	2016-02-2...	190.2786	3	1	0.1605	4.2004	0.0108	0	0.0452	0	0	0	0	0	
27	260.2962	2016-02-2...	200.2787	3	1	0.1578	4.2004	0.0112	0	0.0470	0	-3.2425e-05	0	0	0	
28	270.3114	2016-02-2...	210.2939	3	1	0.1546	4.2002	0.0116	0	0.0489	0	0	0	0	0	
29	280.3269	2016-02-2...	220.3094	3	1	0.1521	4.2006	0.0121	0	0.0507	0	3.2425e-05	0	0	0	
30	290.3425	2016-02-2...	230.3250	3	1	0.1494	4.2002	0.0125	0	0.0524	0	-3.2330e-05	0	0	0	
31	300.3579	2016-02-2...	240.3404	3	1	0.1467	4.2002	0.0129	0	0.0541	0	-3.2330e-05	0	0	0	
32	310.3735	2016-02-2...	250.3560	3	1	0.1445	4.2006	0.0133	0	0.0558	0	3.2425e-05	0	0	0	
33	320.3889	2016-02-2...	260.3714	3	1	0.1420	4.2004	0.0137	0	0.0575	0	0	0	0	0	
34	330.4045	2016-02-2...	270.3870	3	1	0.1395	4.2002	0.0141	0	0.0592	0	-3.2330e-05	0	0	0	

Figure 4- 4: INR 18650-20R Li-ion cell Sample 1 at **25**℃ extraceted from CALCE dataset [62]

Plot it in MATLAB:

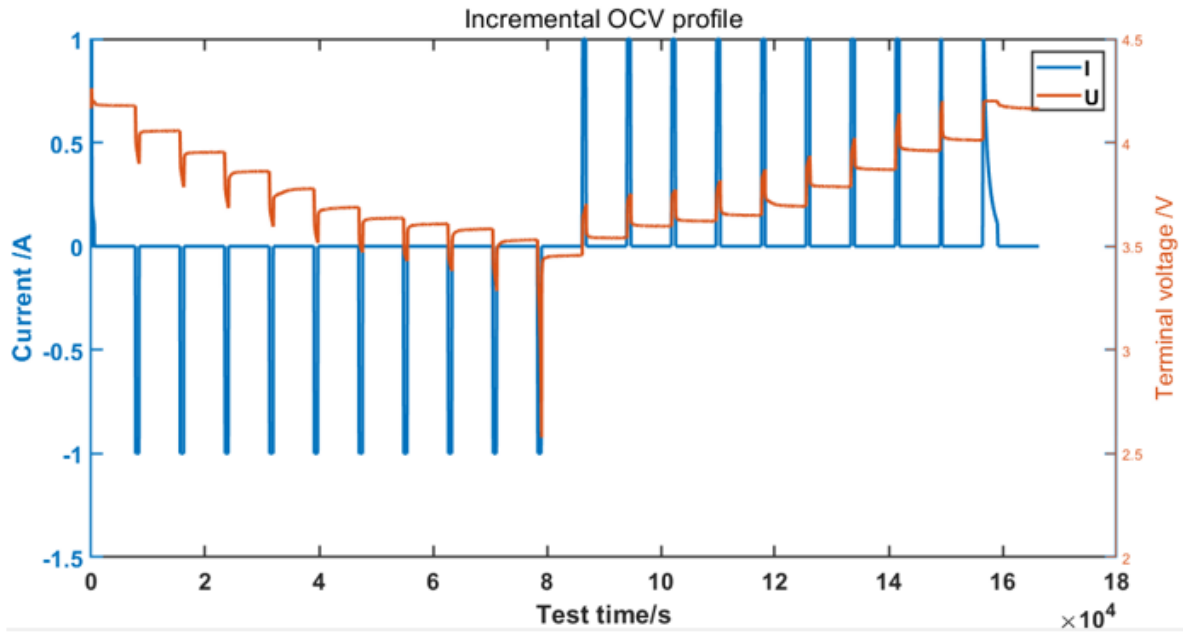

Figure 4- 5: Sample 1 **25**℃ profile

Since the battery discharge process is generally used to verify the accuracy of SoC estimation, the first half of the HPPC pulse discharge process is selected here to verify the accuracy of battery modeling and parameter identification [66].

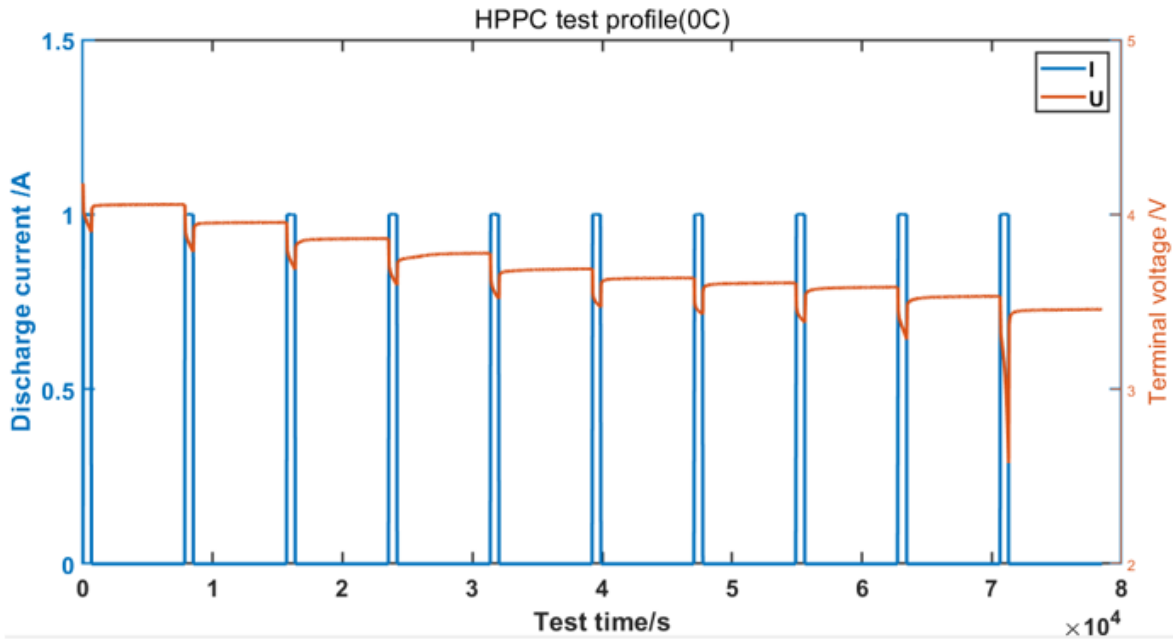

Figure 4- 6: Sample 1 **25**℃ discharging profile

- **OCV-SoC identification**

A study in [28] proves the high-order polynomial relationship between OCV and SoC. Two main methods for obtaining OCV-SoC curves are fast and static. The fast method uses two different discharge rates to discharge the battery at a constant current, from the fully charged state to 0, and perform a specific mathematical transformation process through the two obtained discharge curves to obtain the OCV-SoC mapping relationship. Its advantages are convenient, quick, and time-consuming, but the accuracy of the result is relatively poor.

In this thesis, the static method is selected for the test. The battery is discharged at constant current several times, and the same amount of electricity is released each time. After the battery stops discharging each time, the battery is allowed to stand for a long enough time to measure the battery terminal voltage in a stable state, which can be used as the open circuit voltage (OCV) value corresponding to the SoC value. It is a test method with high precision and requires a long enough rest time. The OCV-SoC correspondence can be obtained by fitting the scattered state points from the experiment to the data.

The principle of the static test is as follows:

(1) Determination of SoC value: Since the value of SoC cannot be directly measured, it is theoretically approximated by the principle of the coulomb counting method. The battery capacity is similar to the amount of electricity released by discharging with a current of 1C rate for 1 hour. The change in battery electricity can be calculated through the constant current and discharge time results, and then the current SoC value can be obtained. Combined with the accuracy of the data collected by the experimental equipment, a current of 1A (0.5C) was used for discharge, a total of 10 constant pulse discharges, each time about 650s, and the SoC change each time was about $0.5\times650/3600\approx0.0902$.

(2) Determination of U_{OC} : After each constant current pulse discharge ends, after a long rest time(1-2 hours), U_0 , U_1 , U_2 all become 0, and the value of the terminal voltage U_L at this time is the open circuit voltage U_{OC} .

In the public data set, the discharge data of SoC and U_{OC} are as follows:

Table 4- 2: SoC-OCV relationship

SoC	OCV/V
1.0000	4.1777
0.9097	4.0565
0.8195	3.9537
0.7292	3.8614
0.6389	3.7778
0.5486	3.6878
0.4584	3.6356
0.3681	3.6077
0.2778	3.5836
0.1875	3.5309
0.0972	3.4561

The cftool toolbox of Matlab is a useful tool for system identification. The toolbox fits the experimental data and obtains the functional relationship between OCV and SoC.

$$OCV = -105.6\times SoC^8 + 373\times SoC^7 - 482\times SoC^6 + 243\times SoC^5 + 9.657\times SoC^4 - 53.59\times SoC^3 + 17.53\times SoC^2 - 1.326\times SoC + 3.466$$

Similarly, the corresponding relationship between OCV-SoC at the other two temperatures can be obtained and plotted together. The results will be shown in Chapter 5.

- **RC identification** (internal ohmic resistance R_0, polarization resistance R_1, R_2, and polarization capacitance C_1, C_2.)

As introduced above, the double exponential fitting can be applied following the flow chart (Figure 3-10).

Take Sample 1 at 0℃ as an example, and the estimated internal ohmic resistance R_0, polarization resistance R_1, R_2, and polarization capacitance C_1, C_2 are displayed below:

Table 4- 3: RC parameter identification result

SoC/%	R_0/Ω	R_1/Ω	C_1/F	R_2/Ω	C_2/F	OCV/V	τ_1/s	τ_2/s
100	0.1117	0.03232	3.7377×10^3	0.4363	2.9957×10^3	4.1777	54.615	1307.0
90	0.1102	0.03885	2.0592×10^3	0.4284	3.5357×10^3	4.0565	80.00	1514.7
80	0.1079	0.04033	4.7868×10^3	0.3066	4.1820×10^3	3.9537	193.05	1282.2
70	0.1084	0.04895	806.19	0.2361	7.8421×10^3	3.8614	39.493	1851.5
60	0.1160	0.04838	1.3616×10^3	0.1514	1.3638×10^4	3.7778	65.876	2071.7

50	0.1180	0.03299	1.9088×10^{3}	0.08976	1.4661×10^{4}	3.6878	62.972	1316.0
40	0.1224	0.03659	2.0958×10^{3}	0.1077	1.2275×10^{4}	3.6356	76.687	1322.1
30	0.1290	0.03849	2.8585×10^{3}	0.2770	4.7533×10^{3}	3.6077	110.02	1316.7
20	0.1569	0.03365	2.3363×10^{3}	0.3775	2.7850×10^{3}	3.5836	78.616	1051.5
10	0.1967	0.01703	3.0847×10^{3}	0.1898	7.0510×10^{3}	3.5309	52.687	1338.3

From the table above, it is explicit that two different types of polarization exist. The two RC branches have different time constants τ_1, τ_2 , proving the correctness of [42]. The identification accuracy can be verified by bringing the identified RC parameters into the established battery model to simulate the analog terminal voltage output. Then the simulated voltage is compared with the measured terminal voltage in CALCE to verify the accuracy of parameter identification. This method is called the terminal voltage comparison method.

The result figures will be shown in the next chapter.

4.1.3 Cell SoC estimation

A. Coulomb counting

The coulomb counting method can easily be applied using the dataset since the discharged capacity is tested and recorded during the test.

From Figure 4-4, the discharged capacity is recorded at each sampling time. Then it is easy to calculate the SoC value at the moment k via the following equation:

$$SoC(k) = SoC_0 - Discharged\ \text{capacity(k)}/\ \text{Nominal capacity} \tag{4.1}$$

B. OCV-SoC

Given the OCV-SoC relationship curve, the SoC value at the moment k can be easily estimated by measuring the OCV at the moment k. However, the OCV data is not directly given in the public data set. Only the terminal voltage is recorded, so it is necessary to approximate the value of OCV.

It can be obtained from Figure 3-7 that:

$$U_L = U_{OC} - U_0 - U_1 - U_2$$

So:

$$U_{OC} = U_L + U_0 + U_1 + U_2 \tag{4.2}$$

U_1, U_2 cannot be obtained directly, but their values are pretty tiny compared to the terminal voltage U_L. So the approximation below is used for SoC estimation.

$$U_{OC} \approx U_L + U_0 \tag{4.3}$$

C. EKF

The report [68] offers guidance on using the EKF algorithm for cell SoC estimation. In order to apply EKF to estimate SoC, the state space equation must be established first. Select the SoC of the battery and the voltages U_1, U_2 at both ends of C_1, C_2 as state variables, and pick the terminal voltage U_L of the battery as the output variable. Then the load current I_L is chosen as the input variable.

Rewrite the equations (3.6) in the following differential format:

$$\begin{cases} SoC(t) = SoC(0) - \int_0^t I_L(t)dt / Q_{rated} \\ \dot{U}_1 = \dfrac{dU_1}{dt} = -\dfrac{U_1}{R_1 C_1} + \dfrac{I_L}{C_1} \\ \dot{U}_2 = \dfrac{dU_2}{dt} = -\dfrac{U_2}{R_2 C_2} + \dfrac{I_L}{C_2} \\ U_L = U_{OC} - R_0 I_L - U_1 - U_2 \end{cases} \tag{4.4}$$

It should be noted that the equations contain the time variable, so it is a non-linear continuous system. Some preparations need to be done before applying EKF here, which is to discretize the state-space equations. The report [69] gives the following conclusion:

Given a non-linear system expressed by the state-space equations:

$$\begin{cases} \dot{x}(t) = Ax(t) + Bu(t) + \omega(t) \\ \omega(t) \sim (0, W) \end{cases}$$

After discretization, the state-space equations will transform into:

$$\begin{cases} x_{k+1} = e^{AT} x_k + [A^{-1}(e^{AT} - E)B]u_k + \omega_k \\ \omega_k \sim (0, Q) \end{cases} \tag{4.5}$$

Applying the conclusion in equations (4.4):

$$\begin{cases} SoC(k) = SoC(k-1) - \dfrac{T}{3600 Q_{rated}} I_L(k-1) \\ U_1(k) = e^{-T/\tau_1} U_1(k-1) + (1 - e^{-T/\tau_1}) R_1 I_L(k-1) \\ U_2(k) = e^{-T/\tau_2} U_2(k-1) + (1 - e^{-T/\tau_2}) R_2 I_L(k-1) \\ U_L(k) = U_{OC}(SoC(k)) - R_0 I_L(k) - U_1(k) - U_2(k) \end{cases} \tag{4.6}$$

where T is the sampling interval.

State equations:

$$\begin{bmatrix} SoC(k) \\ U_1(k) \\ U_2(k) \end{bmatrix} = \begin{bmatrix} 1 & 0 & 0 \\ 0 & e^{-T/\tau_1} & 0 \\ 0 & 0 & e^{-T/\tau_2} \end{bmatrix} \begin{bmatrix} SoC(k-1) \\ U_1(k-1) \\ U_2(k-1) \end{bmatrix} + \begin{bmatrix} -\dfrac{T}{3600Q_{rated}} \\ (1-e^{-T/\tau_1})R_1 \\ (1-e^{-T/\tau_2})R_2 \end{bmatrix} I_L(k) + \omega(k) \tag{4.7}$$

Output equation:

$$U_L(k) = U_{OC}(SoC(k)) - R_0(SoC(k))I_L(k) - U_1(k) - U_2(k) + v(k) \tag{4.8}$$

Let:

$$x_k = \begin{bmatrix} SoC(k) \\ U_1(k) \\ U_2(k) \end{bmatrix}, \ y_k = U_L(k), \ u_k = I_L(k)$$

Define:

$$\hat{A}_k = \frac{\partial f(x_k, u_k)}{\partial x_k}\Big|_{x_k=\hat{x}_k} = \begin{bmatrix} 1 & 0 & 0 \\ 0 & e^{-T/\tau_1} & 0 \\ 0 & 0 & e^{-T/\tau_2} \end{bmatrix}, \ \hat{B}_k = \begin{bmatrix} -\dfrac{T}{3600Q_{rated}} \\ (1-e^{-T/\tau_1})R_1 \\ (1-e^{-T/\tau_2})R_2 \end{bmatrix}$$

$$\hat{C}_k = \frac{\partial h(x_k, u_k)}{\partial x_k}\Big|_{x_k=\hat{x}_k} = \begin{bmatrix} \dfrac{\partial [U_{OC}(SoC) - R_0(SoC)I_L(k)]}{\partial SoC} \\ -1 \\ -1 \end{bmatrix}, \ \hat{D}_k = -R_0$$

Where A is the transfer matrix of the system, B is the input matrix, which describes the input of the system, C is the observation matrix, and D is the feedforward matrix of the system.

It should be noted that U_{OC} and R_0 are both functions of SoC, so that their partial derivatives $\frac{\partial U_{OC}(SoC)}{\partial SoC}$ and $\frac{\partial R_0(SoC)}{\partial SoC}$ are both related to the SoC. Therefore, the results can be obtained by cftool fitting.

The initial conditions for filtering include the initial state of charge of the battery SOC_0, the initial value of the polarization voltage $U_1(0), U_2(0)$, the initial error covariance matrix P(0), the initial process noise variance matrix Q, and the initial measurement noise variance matrix R.

In the experiment, the discharge is usually started from the fully charged state, so SOC_0 is 1. The two RC parallel links are open initially, and no current passes through. Therefore, the initial value of the polarization voltage can be set to 0, so the state variable $\hat{x}_0 = [1.0 \ 0 \ 0]^T$.

According to the voltage, current, and test time test recorded in the Maryland dataset, the accuracy of the experimental equipment used can be inferred, and the error covariance of the process

noise can be set $Q_k = \begin{bmatrix} 10^{-8} & 0 & 0 \\ 0 & 10^{-8} & 0 \\ 0 & 0 & 10^{-8} \end{bmatrix}$ (determined by the system noise of the model and the error in the model establishment). The error covariance of the measurement noise can be set as $R_k = 10^{-4}$ (determined by the accuracy of the load stage measuring voltage sensor) [66]. P(0) is determined by the variance of the initial value $\hat{x}_0$ of the system state, and an appropriate value can be selected according to engineering practice.

The SoC estimation results will be displayed in Chapter 5.

D. 2nd order EKF

For the 2nd-order EKF algorithm, the state space equation of the system is the same as EKF. The difference lies in the Observation matrix C_k.

Since the second derivative of the system transfer function f to the state variable (SoC, U1, U2) is 0, the second derivative of the observation function h to the state variable (SoC) is not 0, and the second derivative to U1, U2 is also 0. Therefore, among the four matrices A, B, C, and D, only the output matrix C differs from the first-order EKF, and the rest of A, C, and D are the same as the first-order EKF algorithm.

$$\hat{A}_k = \frac{\partial f(x_k, u_k)}{\partial x_k}\Big|_{x_k=\hat{x}_k} = \begin{bmatrix} 1 & 0 & 0 \\ 0 & e^{-T/\tau_1} & 0 \\ 0 & 0 & e^{-T/\tau_2} \end{bmatrix}, \hat{B}_k = \begin{bmatrix} -\frac{T}{3600 Q_{rated}} \\ (1-e^{-T/\tau_1})R_1 \\ (1-e^{-T/\tau_2})R_2 \end{bmatrix}, \hat{D}_k = -R_0$$

$$\hat{C}_k = [\frac{\partial h(x_k, u_k)}{\partial x_k} - \frac{\partial^2 h(x_k, u_k)}{\partial x_k^{\,2}}\hat{x}_k + \frac{1}{2}\frac{\partial^2 h(x_k, u_k)}{\partial x_k^{\,2}}x_k]\Big|_{x_k=\hat{x}_k} = \begin{bmatrix} \frac{\partial U_{OC}}{\partial SOC} + \frac{1}{2}\frac{\partial^2 U_{OC}}{\partial SOC^2} \times SOC - \frac{\partial R_0}{\partial SOC} - \frac{1}{2}\frac{\partial^2 R_0}{\partial SOC^2} \times R_0 \\ -1 \\ -1 \end{bmatrix}$$

The remaining steps are similar to the first-order EKF.

4.2 Battery pack

Given the topology of the battery pack, aggregating and scaling methods can be used to build a battery pack. According to the supervisor's guidance, three single cells are first expanded parallelly into a string; then, a module consists of 8 strings connected in series. Finally, 12 modules are connected in series to make a battery pack.

Aggregating method and scaling method will be utilized to complete the task. Since the pack configuration is provided, it takes 3 × 8 × 12 = 288 cells to aggregate into a large battery pack. As for scaling one cell into a pack, the feasibility has been proved in Chapter 3. A study in [70] gives some instructions on the scaling process. It reveals that the RC parameters can be obtained directly by multiplying specific numbers on the original cell in an ideal case.

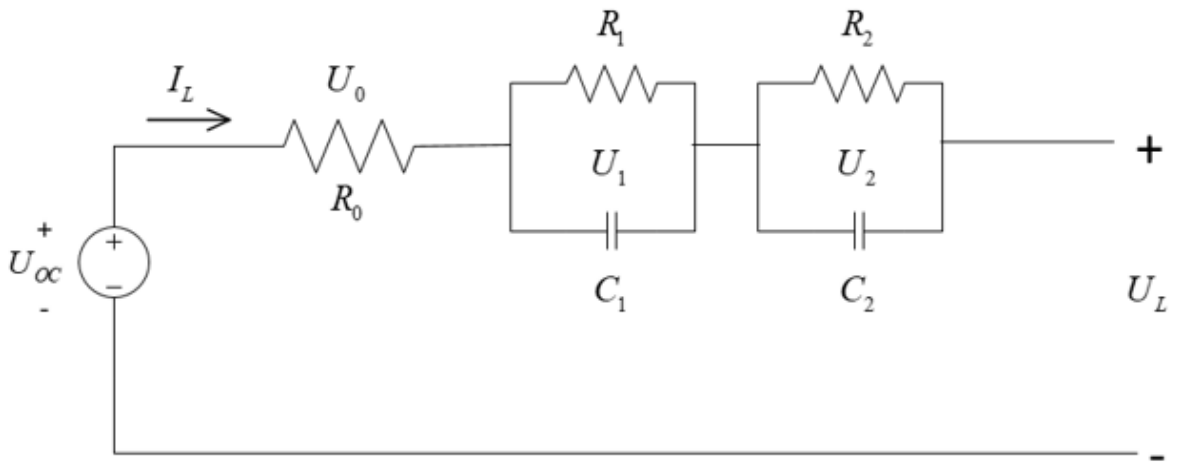

Figure 4- 7: Single cell

Battery pack model in ideal case(n-series and m-parallel)

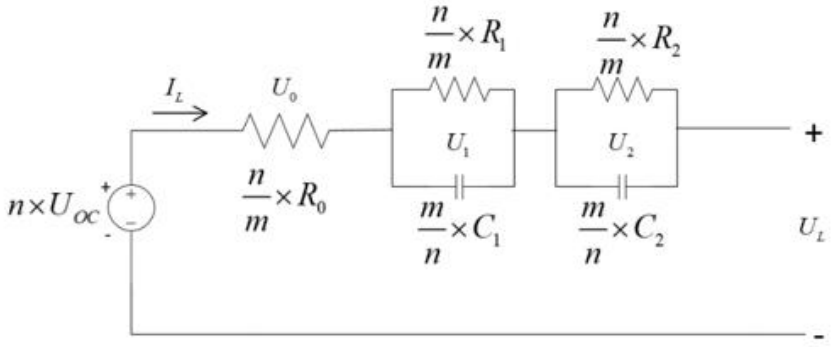

Figure 4- 8: Scaling method in an ideal case

In this case, m=3, n=12 × 8 . This solution does save a lot of time and effort, but the cell discrepancy may be ignored. Sometimes the battery cells are not readily available to the system designers in reality [54]. Therefore, the accuracy of this method needs to be verified.

4.2.1 Pack modeling

- **Aggregating method:**

Follow the cell---string---module---pack sequence:

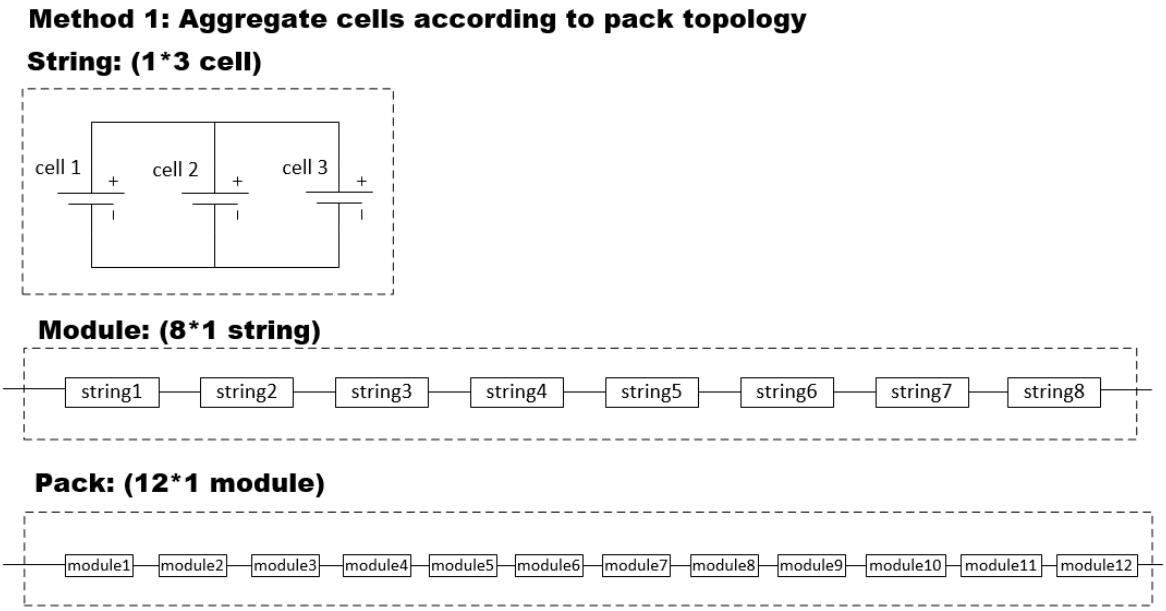

Figure 4- 9: Aggregating method

- **Scaling method:**

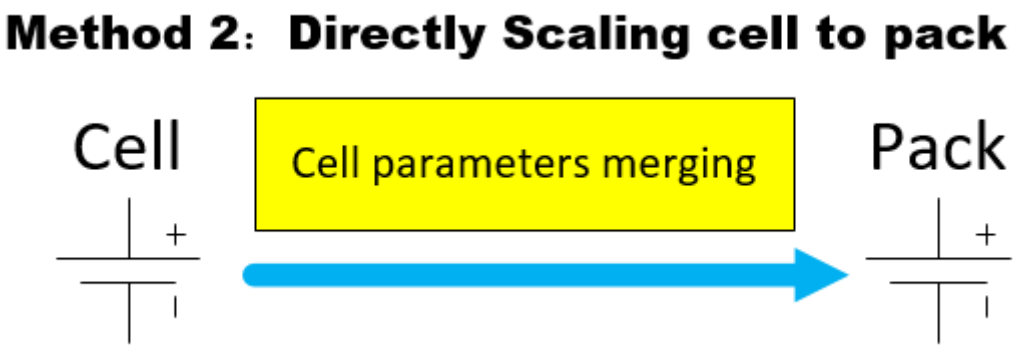

Figure 4- 10: Scaling method

Apply the solution in [67] to scale the cell into a pack.

4.2.2 Pack SoC estimation

After successfully modeling the battery pack, pack SoC can be estimated via the 'Big cell' or 'Short board effect' methods. Two types of sample cells on the CALCE website [62] will both be used in the case study from Figure 4-3.

Before implementing the pack SoC estimation, setting a reference SoC curve for further comparison is essential. Since this project lacks experimental data, an ideal case is used as the reference. Assuming the battery pack is discharged at 1C for one hour, then the pack SoC will drop from 1 to 0 linearly.

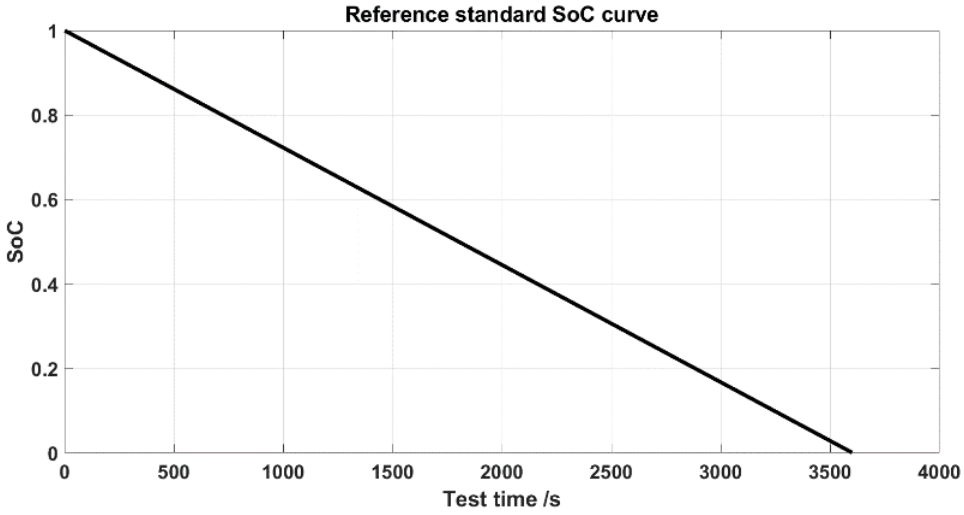

Figure 4- 11: Reference SoC curve

In Simulink, both SoC estimation methods are applied. The interfaces are displayed below:

- **'Big cell' method**

A single cell is expanded to a battery pack by modifying the internal parameters.

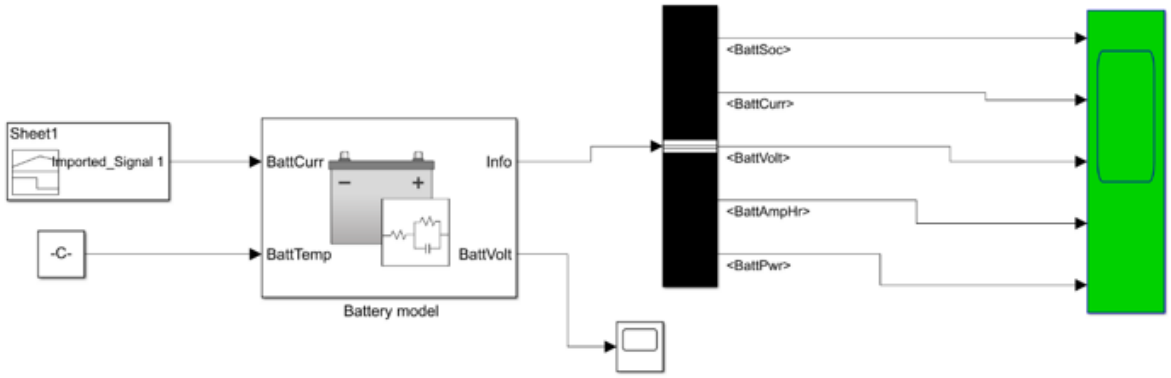

Figure 4- 12: 'Big cell method'

- **'Short board effect' method**

1. String SoC estimation

String: 1 × 3 cells

Rated voltage: 3.65V

Rated Capacity: 3 × 2Ah

Rated current: 3 × 2A

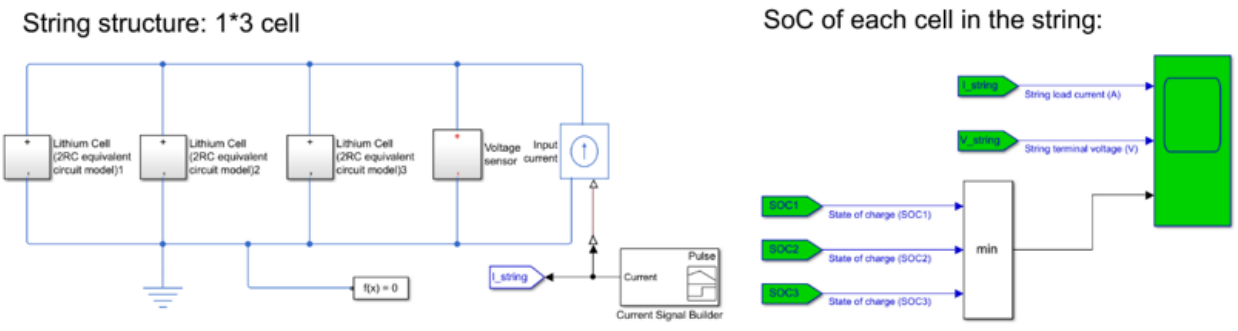

Figure 4- 13: String SoC estimation

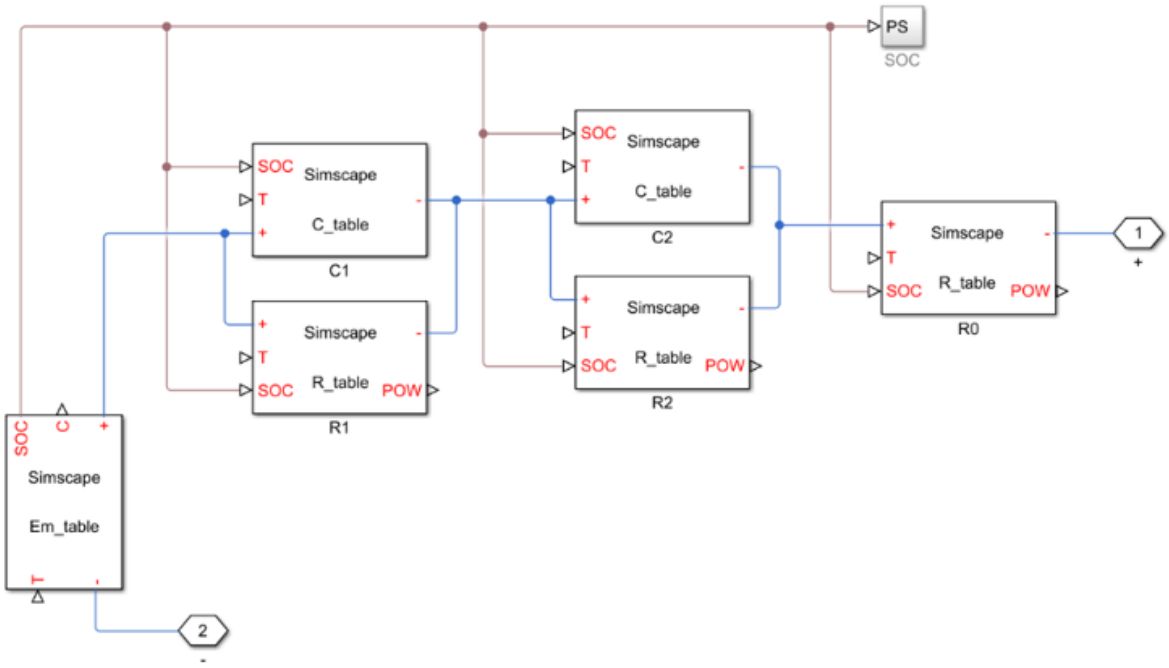

Figure 4- 14: Internal structure of the Simulink model

2. Module SoC estimation

Module： 8 × 1 strings

Rated voltage： 8 × 3.65V

Rated Capacity： 3 × 2Ah

Rated current： 3 × 2A

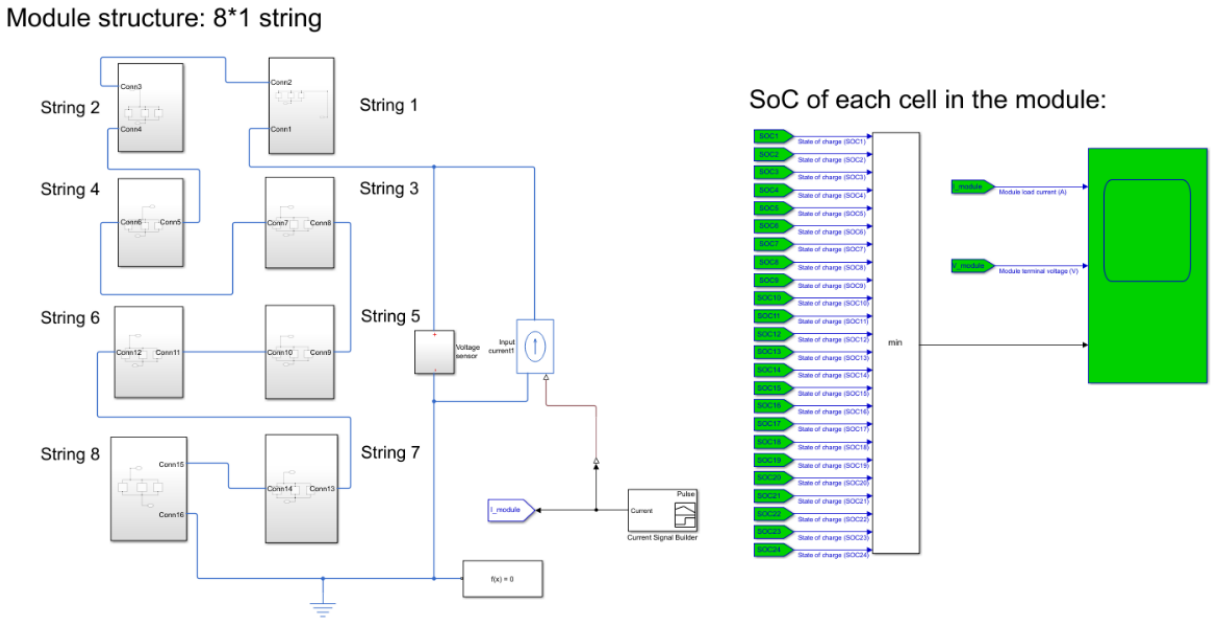

Figure 4- 15: Module SoC estimation

3. Pack SoC estimation

Pack： 12 × 1 modules

Rated voltage： 12 × 8 × 3.65V

Rated Capacity：3 × 2Ah

Rated current： 3 × 2A

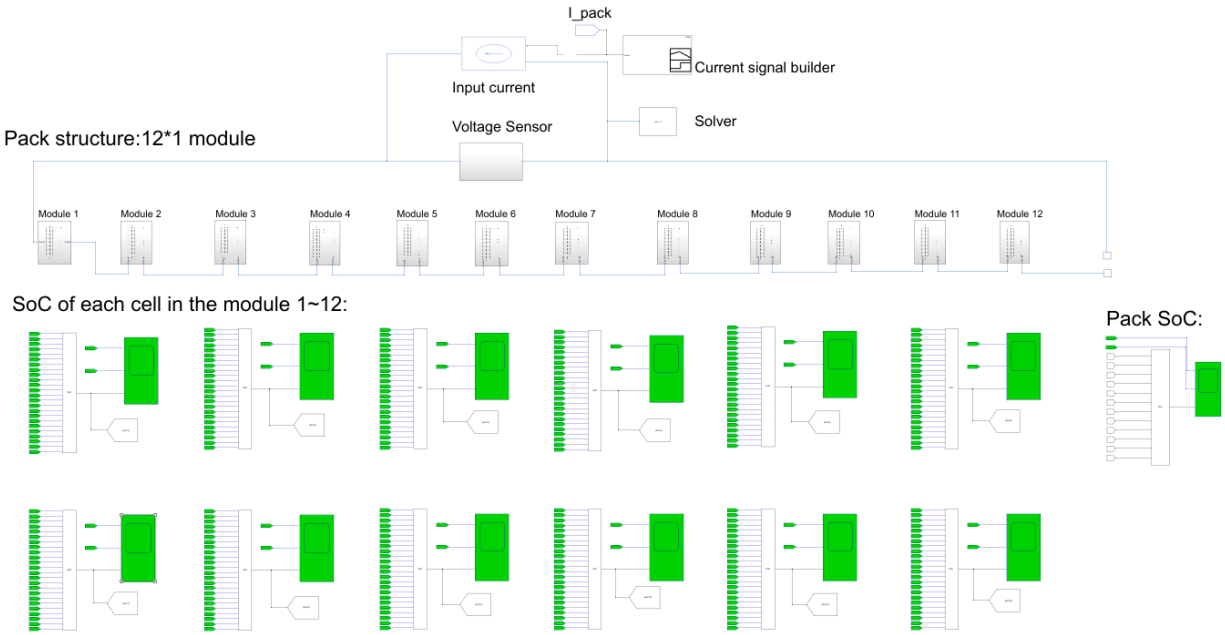

Figure 4- 16: Pack SoC estimation

5 Results and Analysis

This chapter presents the results of the 'Implementation' chapter and further analysis.

5.1 Cell modeling

Cell modeling accuracy can be verified via the terminal voltage comparison method.

The simulated terminal and real measured voltage are compared below under three temperatures. The blue one is the measured value in reality, and the red is the simulated value in Simulink.

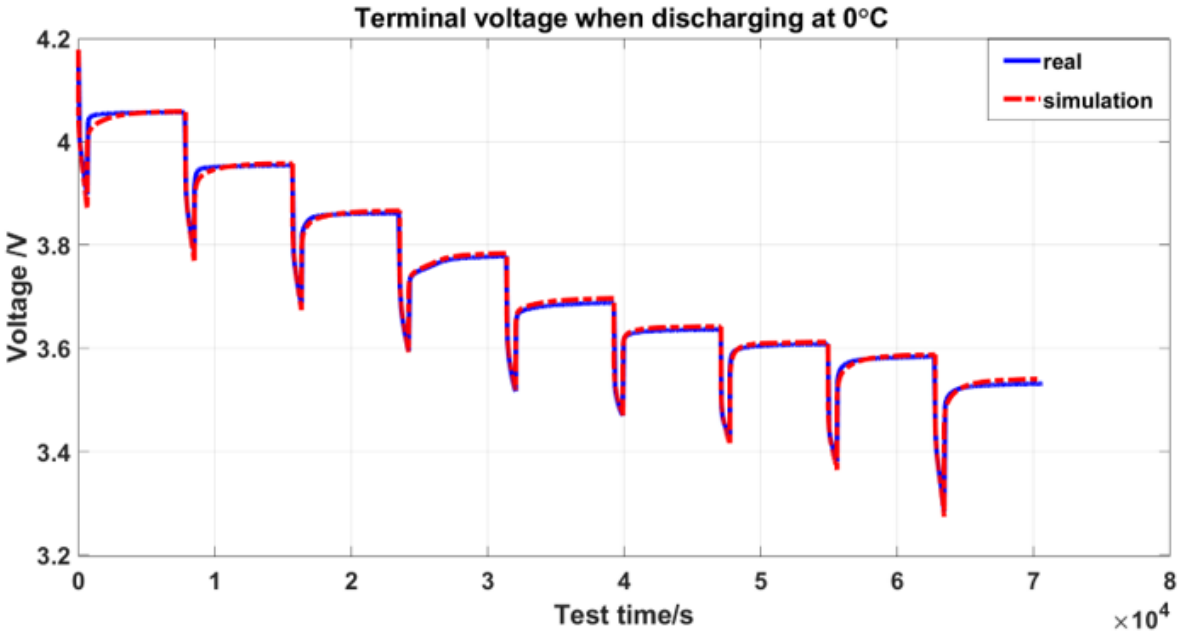

Figure 5- 1: Terminal voltage compared at **0**℃

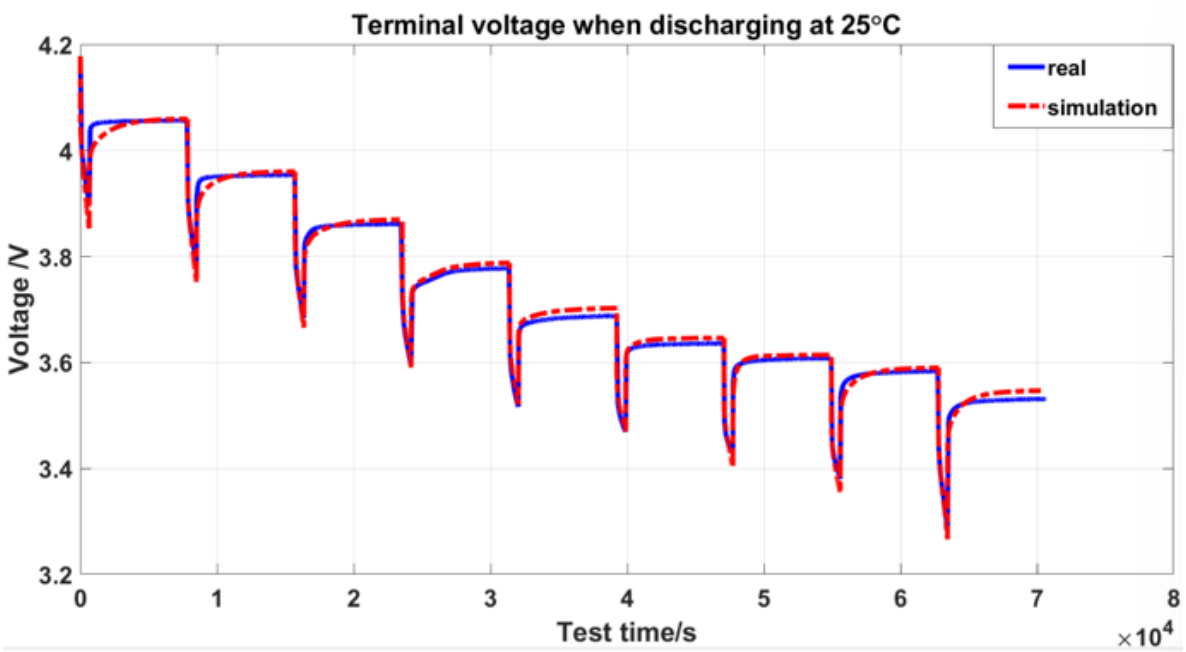

Figure 5- 2: Terminal voltage compared at **25**℃

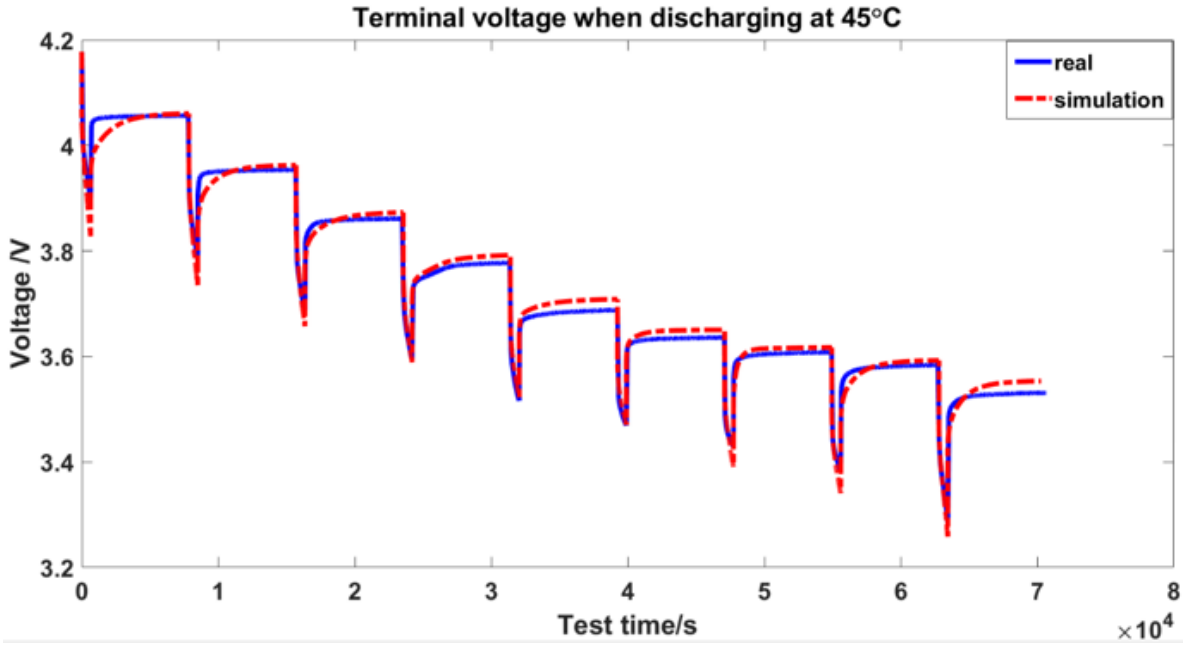

Figure 5- 3: Terminal voltage compared at **45**℃

The error between the real and simulated values is slight under all three temperatures, especially at 0℃. As the temperature rises, the error accumulates as well. The report [28] draws a conclusion that the operating temperature of the battery influences the OCV-SoC characteristic significantly. The varying temperature may also affect the internal reaction, leading to different errors under different temperatures.

5.2 Parameter identification

The RC parameter identification is verified together with the cell modeling part. Here the OCV-SoC estimation accuracy is validated.

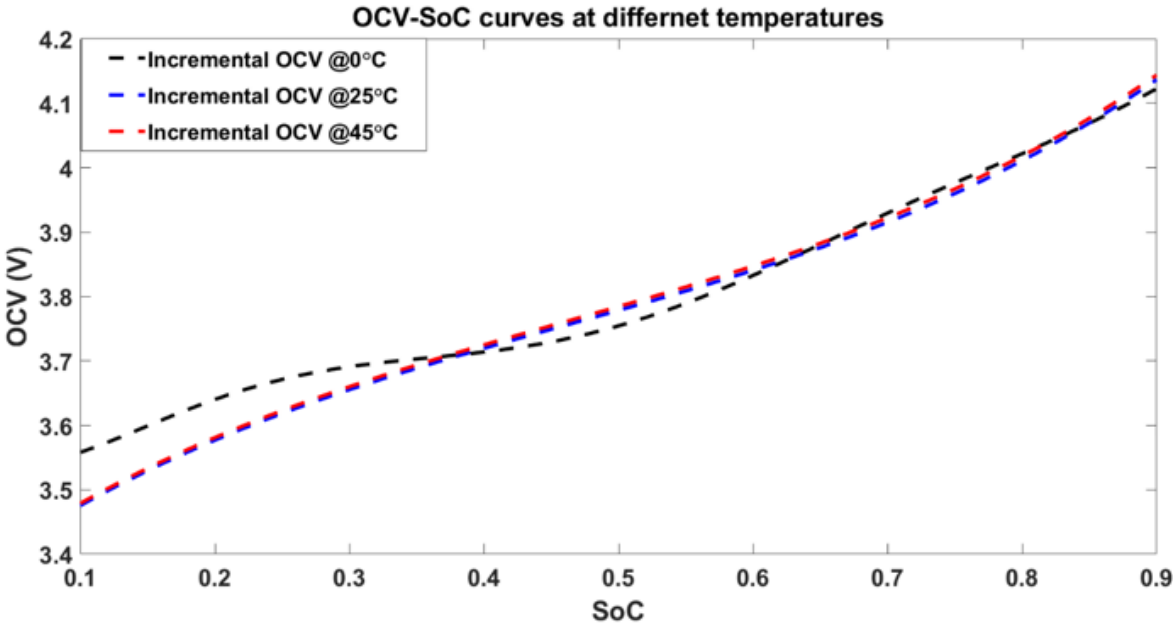

Figure 5- 4: Estimated OCV-SoC curves at three different temperatures

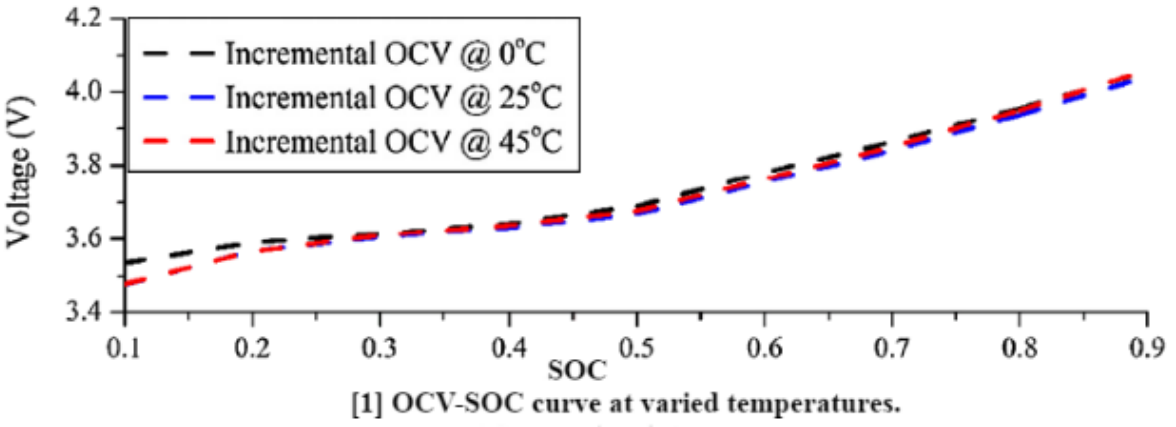

Figure 5- 5: Standard OCV-SoC curve captured from CALCE website [44]

From the two figures above, it is clear that the estimated OCV-SoC curves have great accuracy since it is very similar to the original one captured from the CALCE website.

5.3 Cell SoC estimation

- SoC estimation result

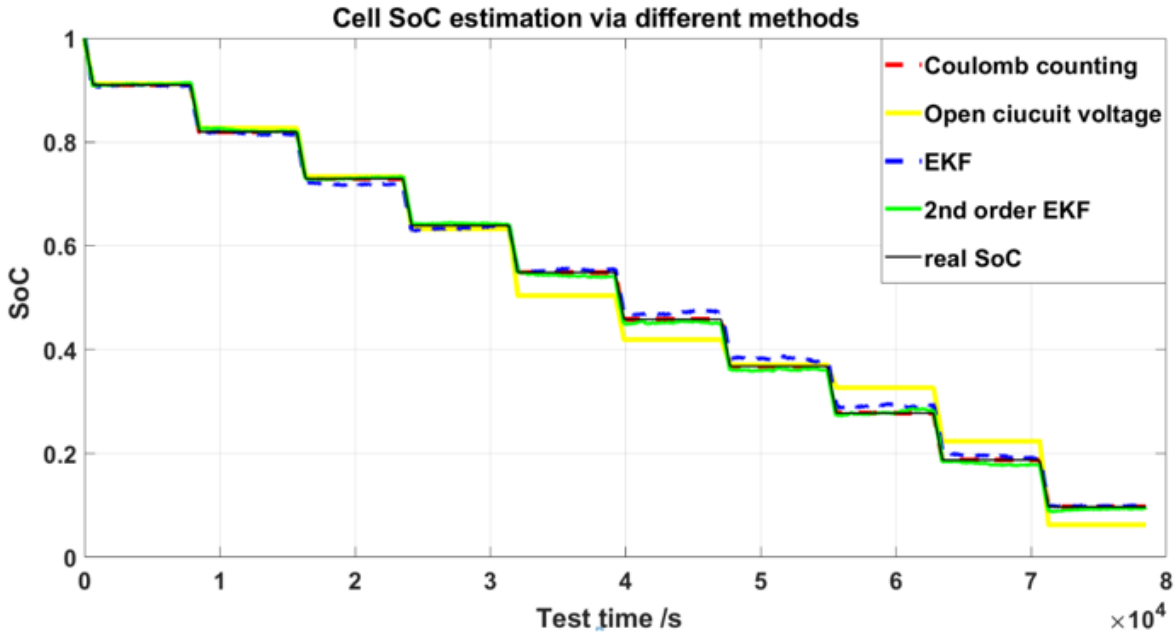

Figure 5- 6: Cell SoC estimation results

Coulomb counting:

In this project, the SoC obtained by using the coulomb counting method (red) is almost the same as the real SoC value. First, the initial SoC is very accurate. Moreover, the experimental procedure is scientific, and the next round of pulse discharge is carried out after each discharge is fully allowed to stand for about 2 hours (7200s). The data of each sampling is fully recorded, including test time, data time, step time, current, terminal voltage, etc. So it almost completely follows the actual value.

OCV:

It is evident that there is a significant error in the prediction of SoC by the OCV method (yellow). Analyzing the reasons, one may be that no matter how many high-order polynomials are used to fit the non-linear relationship between OCV-SoC, the internal non-linear characteristics cannot be represented entirely. The second is that only terminal voltage data is available in the data set. During the discharge pulse, the terminal voltage changes drastically, and the open circuit voltage OCV value is more difficult to obtain, which can only be approximated by mathematical expressions. Therefore, there are significant limitations in estimating SoC via the OCV method.

EKF:

EKF algorithm proves to work well (blue and green), tracking the real SoC curve constantly.

The difference between the second-order EKF and the original EKF is slight.

- Error Analysis

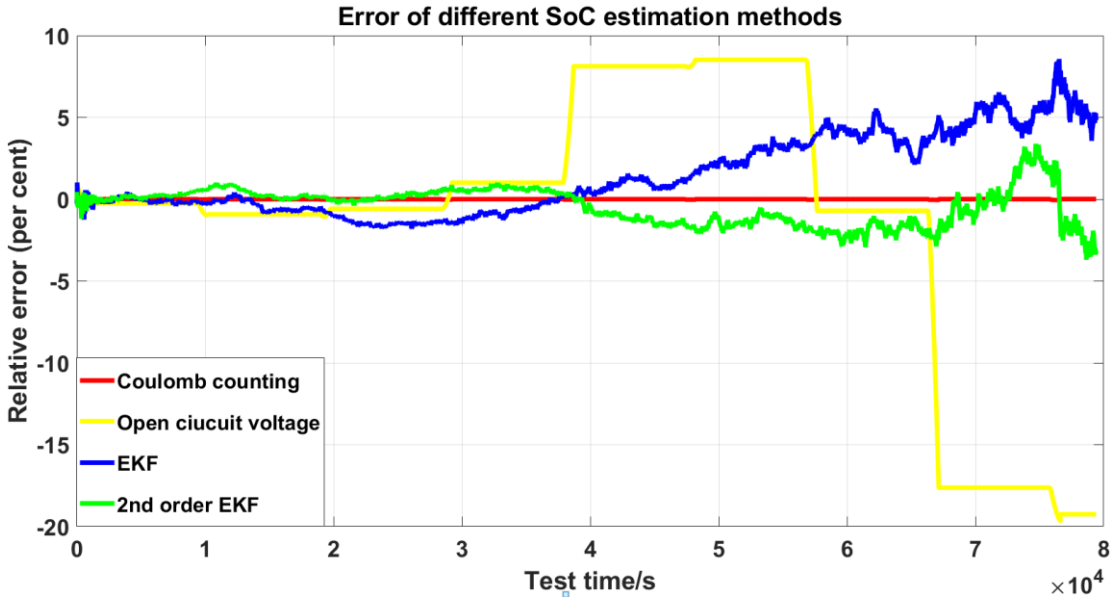

Figure 5- 7: Cell SoC estimation relative errors

The relative error can be calculated by:

$$Error(\%) = (SoC_{estimation} - SoC_{real}) / SoC_{real} \times 100 \tag{5.1}$$

Table 5- 1: Cell SoC estimation error

SoC estimation methods	Peak error (per cent)
Coulomb counting	0.06657
OCV	19.6482
EKF	8.5215
2nd order EKF	3.7030

It is clear that the measurement accuracy of the coulomb counting method is quite high, and the accuracy of EKF is also acceptable, which meets the requirements. But the OCV method is not ideal. This is because there is only terminal voltage in the experimental data set without the needy OCV value, which has to be approximated somehow. Due to the non-linear relationship between OCV and SoC, even high-order polynomials cannot accurately represent the relationship only through the polynomial fitting.

- Robustness analysis

EKF has been widely used due to its robustness to noise and interference. Robustness analysis is done from 2 different angles.

（1） Anti-interference

A slight disturbance noise (I_{noise}) can be added to the input current(I) for simulation to see whether the SoC estimation diverges or deviates significantly from the original trajectory.

$$I_{new} = I + I_{noise} (Interference\ noise\ with\ mean\ value\ 0.01\ and\ variance\ 0.01) \tag{5.2}$$

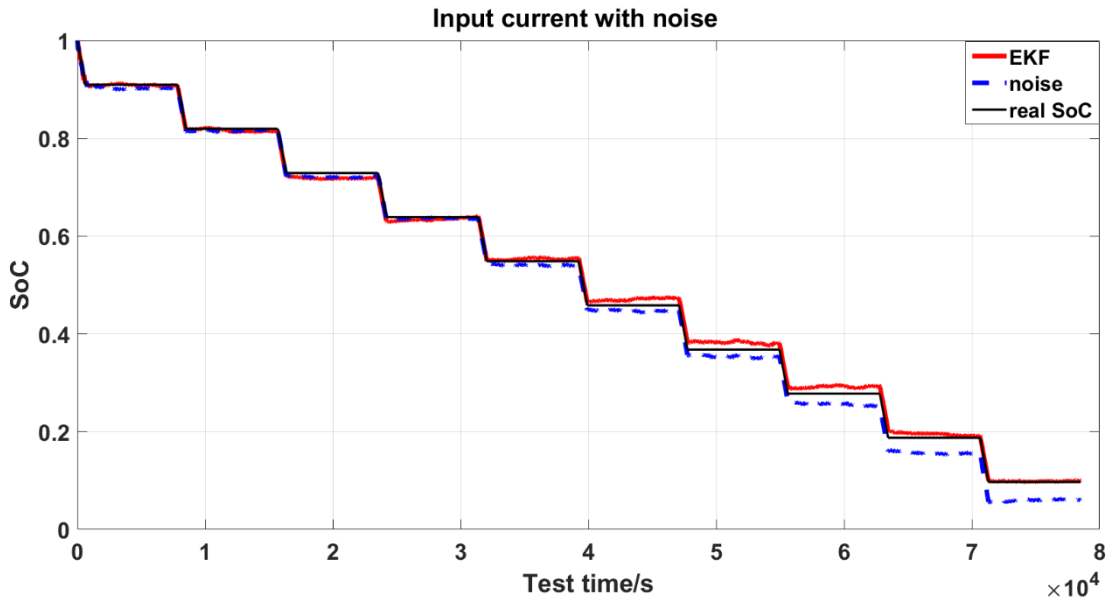

Figure 5- 8: Anti-interference test

Apparently, after adding interference noise to the input current, the SoC estimation result worsens in the second half, and the deviation from the real value is quite large. However, the SoC estimation results did not diverge and did not seriously deviate from the real value. It shows that EKF has a certain degree of anti-interference ability.

（2） Convergence speed

First, keep the initial mean square error matrix P_0 constant, then change the initial value of SoC from 1.0 to some other values(for example, 0.8, 0.5, 0.3) for comparative analysis.

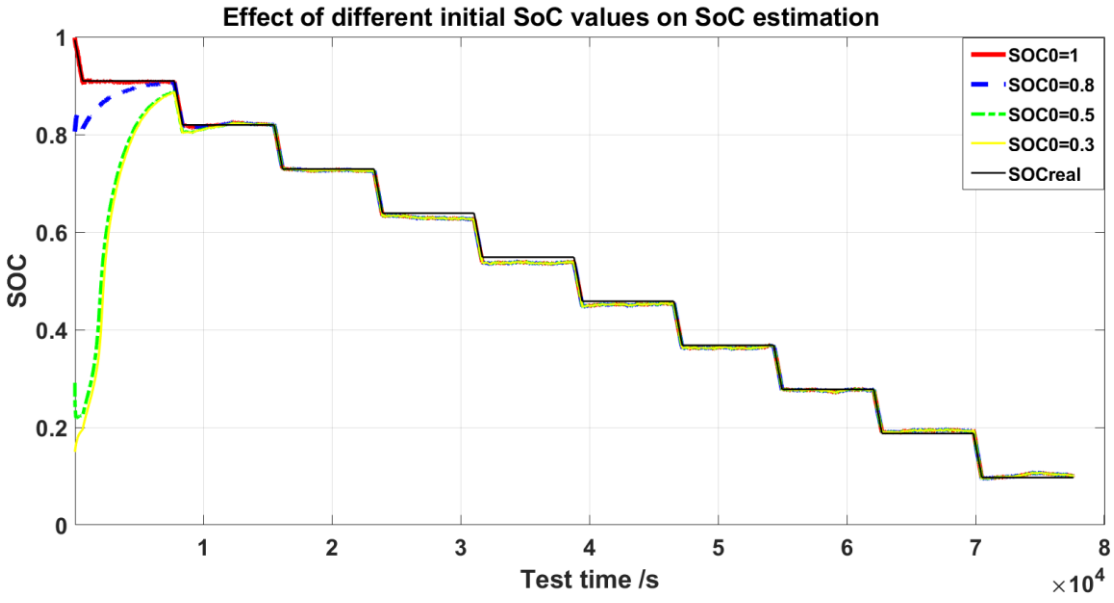

Figure 5- 9: Robustness test on different initial SoC

It can be seen from the figure that under different initial values of SoC, after the first pulse discharge and standing for a long time, the EKF algorithm can make the SoC converge to near the real value. For example, the initial SoC value of the yellow curve is 0.3. The initial gap is huge, but the SoC value can still quickly converge to 0.9 in the first sub-pulse discharge. Apparently, the iterative update process of the SoC value of different curves highly overlaps.

Then let the initial value of SoC = 1.0 stay the same and change the initial mean square error matrix P_0 (for example $0.1\times E_{3,3}$,$1\times E_{3,3}$,$10\times E_{3,3}$) for comparative analysis.

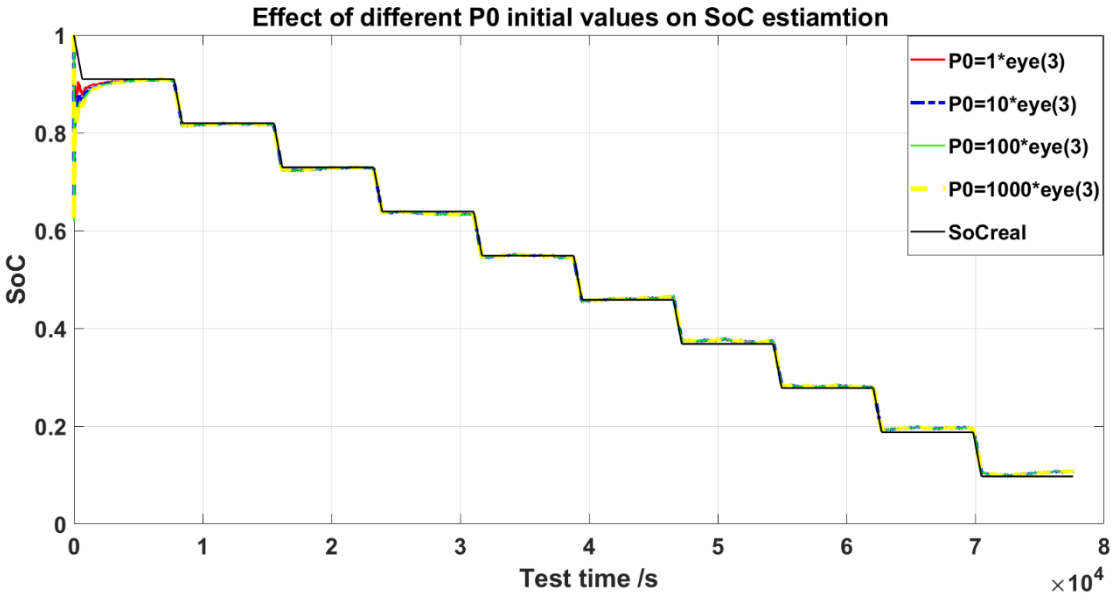

Figure 5- 10: Robustness test on different noise (1)

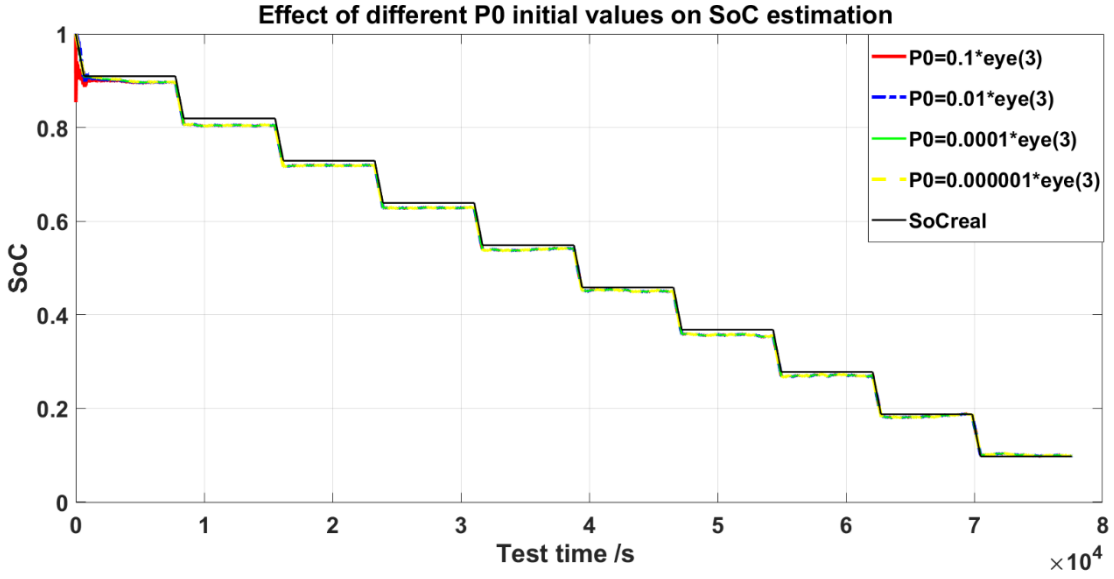

Figure 5- 11: Robustness test on different noise (2)

It can be seen that under different values of the initial mean square error matrix P_o, the EKF curve can always quickly converge to a reasonable range, which proves that the EKF algorithm is very robust. When the initial error value is larger, the deviation of the initial estimated value of SoC from the actual value of SoC is more significant as well. For example, when $P_o = 1000 \times eye(3)$, the initial estimated value of SoC was about 0.6, which is far from 1.0. But as time passes, the gap becomes smaller and smaller, and the EKF tracking speed gradually becomes faster. It is because the larger the pre-set P_o is, the larger the Kalman gain matrix will be.

It can be explained via:

$$G_k = P_k^- C_k^T (C_k P_k^- C_k^T + R_k)^{-1} \tag{5.3}$$

Assuming the correction function for the prior estimate $\hat{x}_k^-$ is large. After the correction, the posterior estimated value $\hat{x}_k^+$ will be closer to the actual value. Therefore, the robustness of the EKF algorithm is extremely strong.

5.4 Pack SoC estimation

Aggregating and scaling methods are applied to pack SoC estimation in this project. Since the reference SoC curves are stipulated in advance, the two approaches can be compared with the reference. The relative error can be calculated via equation (5.1).

The two methods are compared during the entire aggregating process, from string to module to the final pack.

Errors turn out to differ from each other on three different scales.

- String SoC & error:

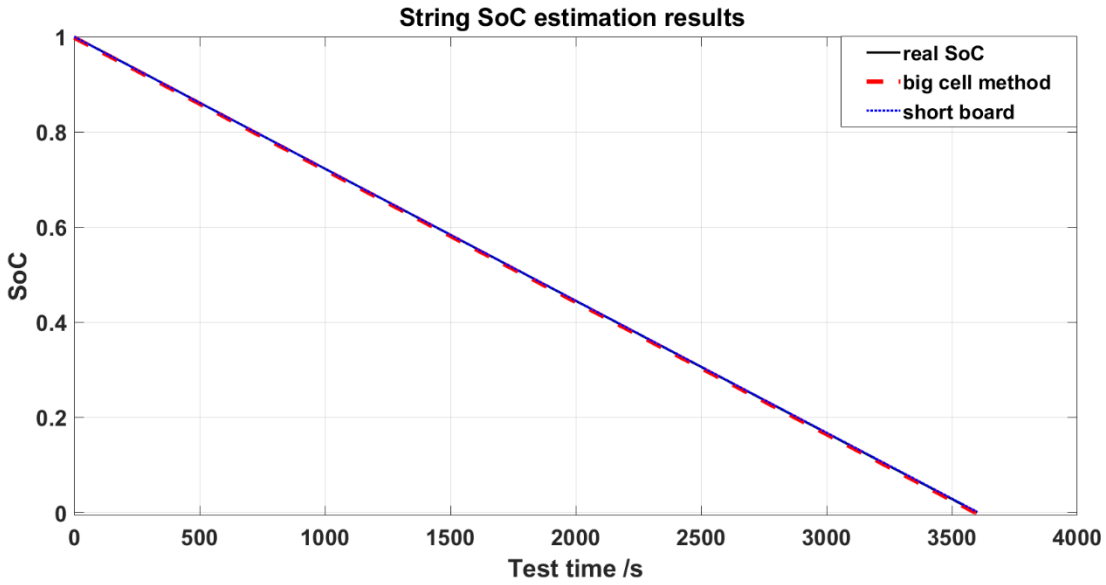

Figure 5- 12: String SoC estimation results

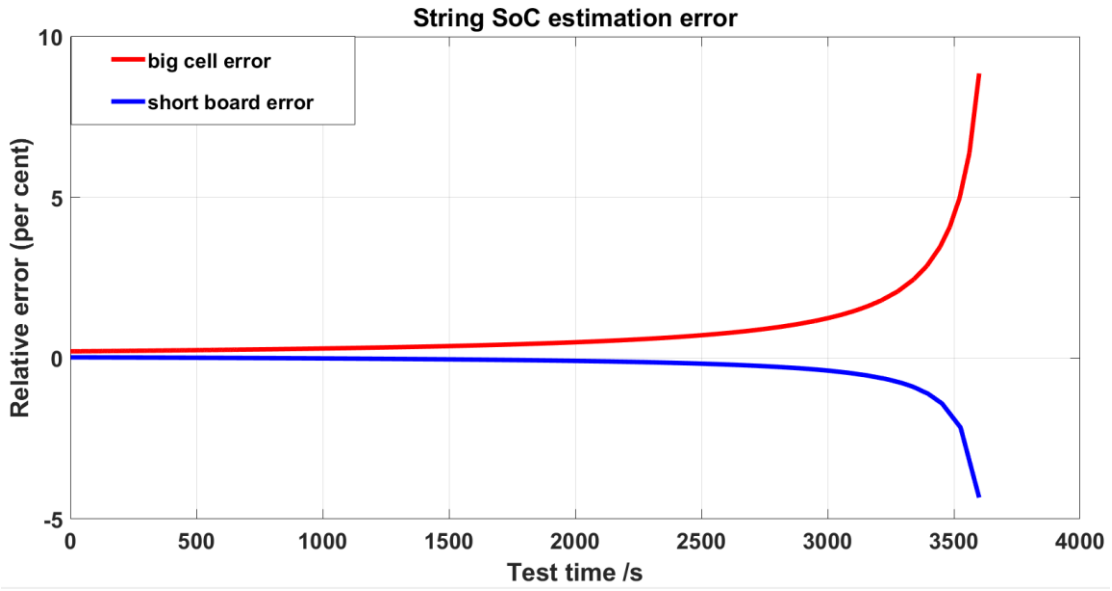

Figure 5- 13: String SoC estimation errors

- Module SoC & error:

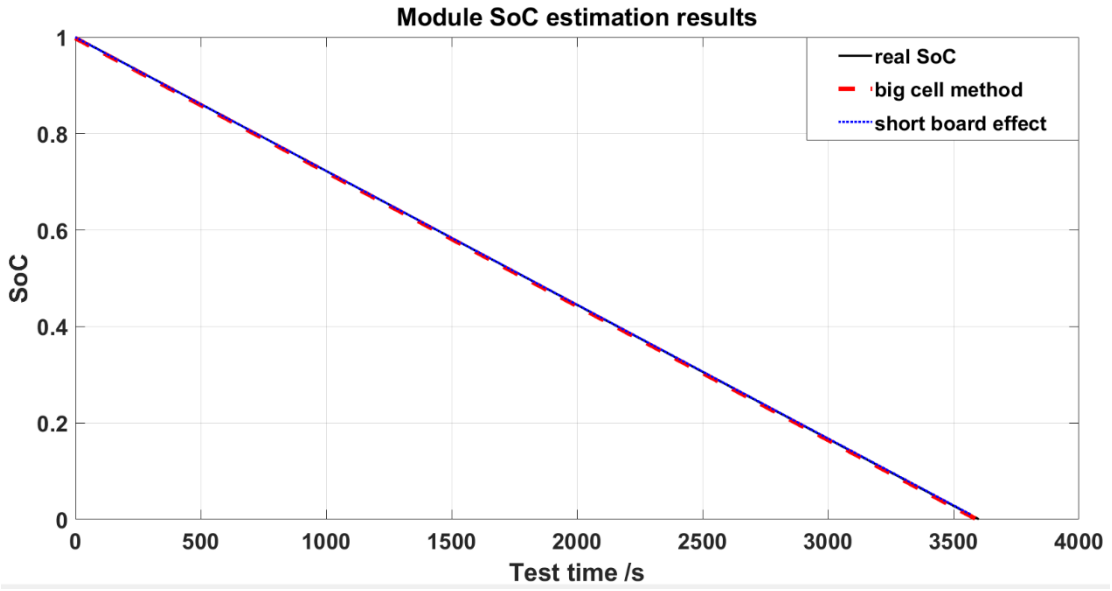

Figure 5- 14: Module SoC estimation results

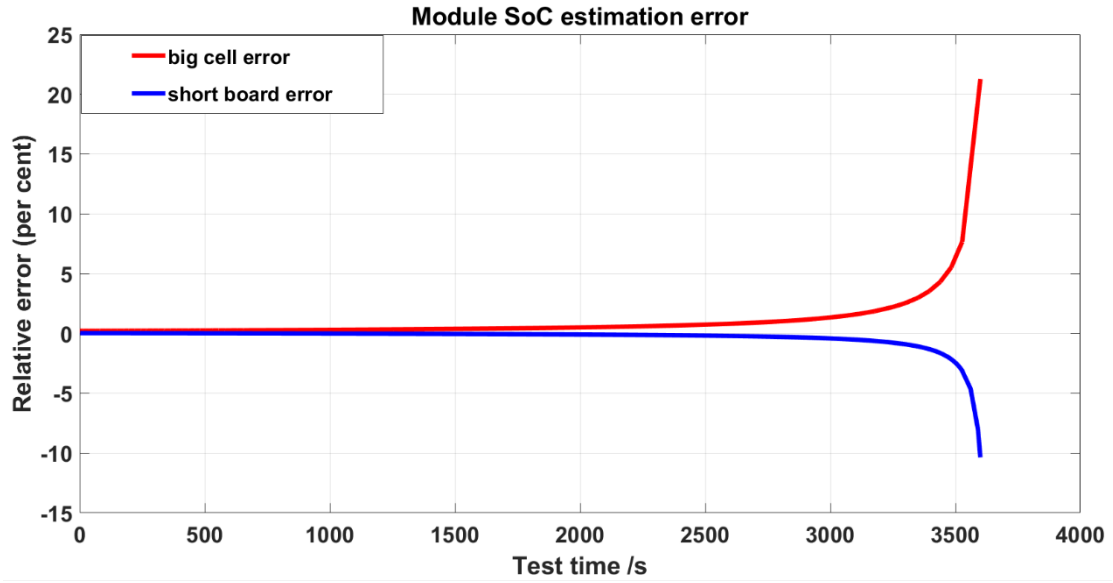

Figure 5- 15: Module SoC estimation errors

- Pack SoC & error:

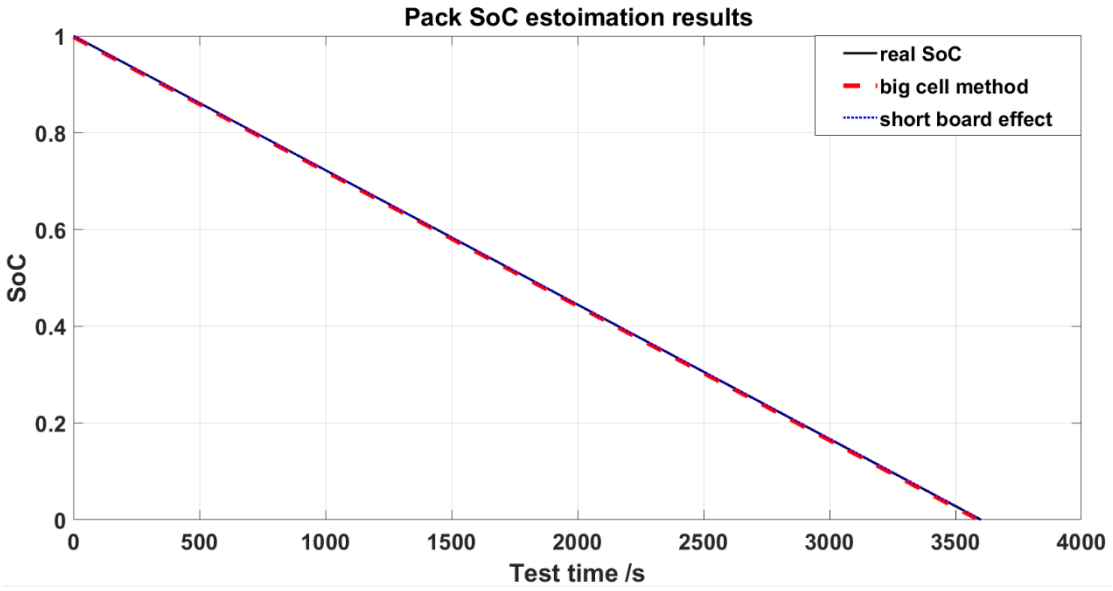

Figure 5- 16: Pack SoC estimation results

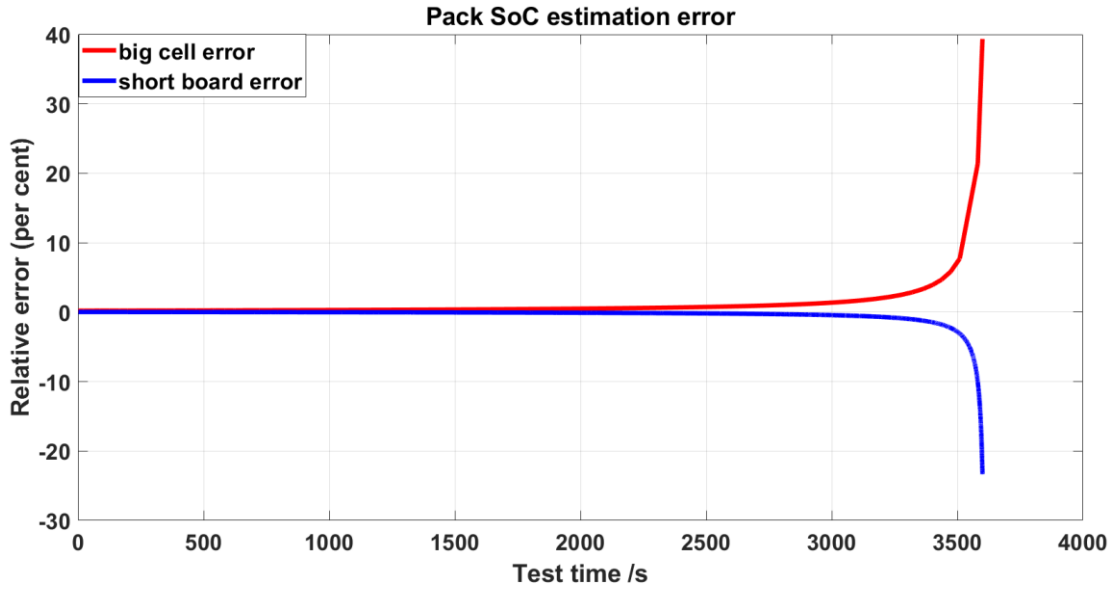

Figure 5- 17: Pack SoC estimation errors

Table 5- 2: Pack SoC estimation error

Peak error (%)	'Big cell'	'Short board'
String	8.854	-4.333
Module	21.27	-10.36
Pack	39.35	-23.26

Several conclusions can be drawn from the six figures and one table:

1. Error accumulates as the battery group size grows from string to pack. It is not difficult to understand since a large error usually consists of many minor errors. Cell inconsistency also increases as the battery group grows, leading to a more significant peak error.

2. The final pack error is relatively large via both methods, which is unsatisfactory. It is a problem worth investigating since EKF is proven to perform well in cell SoC estimation. It indicates that the battery pack is not simply established by aggregating cells. Many other factors need to be considered, like cell balancing and additional resistance [48].

3. The 'Short board effect' SoC estimation value is always smaller than the reference. It could result from not involving the cell-to-cell balancing part in the pack. The extreme cell would be refined after cell balancing.

4. The 'Big cell' SoC estimation value is always larger than the reference. It might arise from the ignorance of the additional impedance when the parameters are directly merged.

6 Conclusions and Future Work

6.1 Conclusions

In general, this project has made good progress, and the results align with the initial expectations. Aiming at the three primary goals: battery modeling, parameter identification, and SoC estimation, this report gives the corresponding solutions one by one and applies them all. The final results are compared and verified with the real values respectively. They all turn out to be satisfactory, except the fly in the ointment is that the error in pack SoC estimation is relatively large.

In terms of battery modeling, this report proceeds from simple to complex, modeling single cell, string, module, and pack in turn. After a relevant literature review, the second-order Thevenin model is selected in this project and implemented in Simulink. Double exponential fitting is used to identify the cell's polarization resistance and capacitance due to the already performed preliminary experiments. The validation results turn out to be great, with the relative error less than 2 per cent.

Regarding the cell SoC estimation, this report adopts a variety of estimation methods and applies them all. Through comparative analysis, their errors are obtained respectively. In this project, the Coulomb counting method shows clear advantages over other methods due to the accurate initial SoC value and precise experiment data recording. The open circuit voltage (OCV) method shows the least accuracy since the OCV value needed is not recorded. It can only be obtained via approximation. The extended Kalman filter (EKF) method performs well and meets the requirements. Moreover, it shows great robustness towards noisy input and different initial preset conditions.

However, when it comes to the battery pack SoC estimation, the results are not so good. The battery pack is successfully established by the 'Aggregating' and 'Scaling' methods. Subsequently, the 'Short board effect' and the 'Big cell' methods were used for pack SoC estimation, respectively. The string SoC estimation error is still acceptable (8.8%), but the module and pack SoC estimation error is relatively large (nearly 40% for the pack). The error may come from the ignorance of the following factors: cell inconsistency and additional impedance. Better methods like screening process based methods and bias correction based methods can also be applied to reduce the error if more battery pack data is provided.

6.2 Limitations

Speaking of limitations, it is a pity that I could not do the charge/discharge experiment of the Li-ion battery in the laboratory myself. It means I have no access to first-hand experiment data. In addition, I cannot actively obtain the data I need, like connecting data in series to get a string for testing. I could only search for the existing battery data online.

In addition, even though the cell SoC estimation results are good, the final outcome of the battery pack SoC estimation result is not good enough. It may result from the method I use in the project. Some critical factors like cell balancing and additional resistance are ignored in the model.

6.3 Future work

Here lists some future work that can be further done based on the current results:

1. Try more cell SoC estimation methods to improve the accuracy. Although the EKF SoC estimation results are proven to be passable (3.7%~8.5%), a more precise SoC result can be obtained with more battery data and more complicated estimation methods. For instance, unscented Kalman filter (UKF) and data-driven models like artificial neural network (ANN) could possibly be applied to minimize the cell SoC estimation error.

2. Improve the battery pack modeling and pack SoC estimation. In this project, the final battery pack SoC estimation results turn out to be unsatisfactory (nearly 40%). After comparative analysis, the results are related to the following three factors: cell inconsistency, additional impedance, and pack SoC estimation methods. In the future, a cell balancing strategy should be applied, and additional connection impedance is supposed to be considered. Furthermore, better pack SoC estimation methods need to be applied in order to reduce the error.

3. Do more research on the battery pack and expand it into a battery management system (BMS). In order to enable the battery pack to be put into use in the microgrid, it is not enough to estimate the pack SoC simply. More functions of the battery pack must be implemented, such as state of health (SoH) estimation, state of power (SoP) estimation, and state of energy (SoE) estimation. In addition, more factors need to be taken into account, like working temperature, battery cycle life, etc.

Bibliography

[1] Ministry of the Environment and Energy. (2017). Sweden's Draft Integrated National Energy and Climate Plan.

[2] S. Shukla and M. Pandit, "Renewable Microgrids with Economic and Environmental Benefits: A Review," 2021 IEEE 2nd International Conference On Electrical Power and Energy Systems (ICEPES), Bhopal, India, 2021, pp. 1-6, doi: 10.1109/ICEPES52894.2021.9699589.

[3] Y. Jiao and D. Månsson, "Analysis of Two Hybrid Energy Storage Systems in an Off-Grid Photovoltaic Microgrid: A Case Study," 2020 IEEE PES Innovative Smart Grid Technologies Europe (ISGT-Europe), The Hague, Netherlands, 2020, pp. 554-558, doi: 10.1109/ISGT-Europe47291.2020.9248913.

[4] X. Liu, T. Zhao, H. Deng, P. Wang, J. Liu and F. Blaabjerg, "Microgrid Energy Management with Energy Storage Systems: A Review," in CSEE Journal of Power and Energy Systems, vol. 9, no. 2, pp. 483-504, March 2023, doi: 10.17775/CSEEJPES.2022.04290.

[5] M. Banerjee and H. Kaur, "A Comparison Among Lithium-Ion, Nickel-Cadmium & Nickel-Metal-Hydride Batteries for Charging and Discharging in Electric Vehicle by Bidirectional Dc-Dc Converter," 2022 IEEE IAS Global Conference on Emerging Technologies (GlobConET), Arad, Romania, 2022, pp. 361-368, doi: 10.1109/GlobConET53749.2022.9872335.

[6] S. Podder and M. Z. R. Khan, "Comparison of lead acid and Li-ion battery in solar home system of Bangladesh," 2016 5th International Conference on Informatics, Electronics and Vision (ICIEV), Dhaka, Bangladesh, 2016, pp. 434-438, doi: 10.1109/ICIEV.2016.7760041.

[7] J. P. Aditya and M. Ferdowsi, "Comparison of NiMH and Li-ion batteries in automotive applications," 2008 IEEE Vehicle Power and Propulsion Conference, Harbin, China, 2008, pp. 1-6, doi: 10.1109/VPPC.2008.4677500.

[8] G. Marin-Garcia, G. Vazquez-Guzman, J. M. Sosa, A. R. Lopez, P. R. Martinez-Rodriguez and D. Langarica, "Battery Types and Electrical Models: A Review," 2020 IEEE International Autumn Meeting on Power, Electronics and Computing (ROPEC), Ixtapa, Mexico, 2020, pp. 1-6, doi: 10.1109/ROPEC50909.2020.9258711.

[9] K. V. Raj, K. Rayudu and G. Battapothula, "Critical Review on Battery Management Systems," 2022 International Conference on Applied Artificial Intelligence and Computing (ICAAIC), Salem, India, 2022, pp. 1676-1680, doi: 10.1109/ICAAIC53929.2022.9793001.

[10] Meng, Jinhao, et al. "Overview of lithium-ion battery modeling methods for state-of-charge estimation in electrical vehicles." Applied sciences 8.5 (2018): 659.

[11] Tamilselvi, S., Gunasundari, S., KaruppiAh, N., Razak RK, A., Madhusudan, S., Nagarajan, V. M., ... & Afzal, A. (2021). A review on battery modelling techniques. Sustainability, 13(18), 10042.

[12] Plett, Gregory L. Battery management systems, Volume I: Battery modeling. Vol. 1. Artech House, 2015.

[13] N. Jantharamin, "Battery Modeling Based on Artificial Neural Network for Battery Control and Management," 2018 21st International Conference on Electrical Machines and Systems (ICEMS), Jeju, Korea (South), 2018, pp. 2111-2114, doi: 10.23919/ICEMS.2018.8549015.

[14] J. Meng, G. Luo and F. Gao, "Lithium Polymer Battery State-of-Charge Estimation Based on Adaptive Unscented Kalman Filter and Support Vector Machine," in IEEE Transactions on Power Electronics, vol. 31, no. 3, pp. 2226-2238, March 2016, doi: 10.1109/TPEL.2015.2439578.

[15] Plett, Gregory L. Battery management systems, Volume II: Equivalent-circuit methods. Artech House, 2015.

[16] R. R. Thakkar, Y. S. Rao and R. R.Sawant, "Performance Analysis of Electrical Equivalent Circuit Models of Lithium-ion Battery," 2020 IEEE Pune Section International Conference (PuneCon), Pune, India, 2020, pp. 103-107, doi: 10.1109/PuneCon50868.2020.9362386.

[17] I. López-Granados, J. M. Sosa, G. Vázquez, A. R. López and D. Langarica, "A Brief Review of Battery Model Parameter Identification Methods," 2021 IEEE International Autumn Meeting on Power, Electronics and Computing (ROPEC), Ixtapa, Mexico, 2021, pp. 1-6, doi: 10.1109/ROPEC53248.2021.9667980.

[18] Z. Cen, P. Kubiak and I. Belharouak, "Online parameter estimation/tracking for Lithium-ion battery RC model," 2016 International Renewable and Sustainable Energy Conference (IRSEC), Marrakech, Morocco, 2016, pp. 936-940, doi: 10.1109/IRSEC.2016.7983979.

[19] Xia, Bizhong, et al. "Online parameter identification of lithium-ion batteries using a novel multiple forgetting factor recursive least square algorithm." Energies 11.11 (2018): 3180.

[20] Y. Wu, H. Chen, L. Cao, J. Duan, X. Chen and J. Zhai, "Research on Online Identification of Lithium-ion Battery Equivalent Circuit Model Parameters," 2022 9th International Forum on Electrical Engineering and Automation (IFEEA), Zhuhai, China, 2022, pp. 130-136, doi: 10.1109/IFEEA57288.2022.10038123.

[21] J. M. L. Fonseca, G. Sambandam Kulothungan, K. Raj and K. Rajashekara, "A Novel State of Charge Dependent Equivalent Circuit Model Parameter Offline Estimation for Lithium-ion Batteries in Grid Energy Storage Applications," 2020 IEEE Industry Applications Society Annual Meeting, Detroit, MI, USA, 2020, pp. 1-8, doi: 10.1109/IAS44978.2020.9334862.

[22] R. Ahmed, S. RAhimifard and S. Habibi, "Offline Parameter Identification and SoC Estimation for New and Aged Electric Vehicles Batteries," 2019 IEEE Transportation Electrification Conference and Expo (ITEC), Detroit, MI, USA, 2019, pp. 1-6, doi: 10.1109/ITEC.2019.8790474.

[23] R. Xiong, J. Cao, Q. Yu, H. He and F. Sun, "Critical Review on the Battery State of Charge Estimation Methods for Electric Vehicles," in IEEE Access, vol. 6, pp. 1832-1843, 2018, doi: 10.1109/ACCESS.2017.2780258.

[24] Rivera-Barrera, Juan Pablo, Nicolás Muñoz-Galeano, and Henry Omar Sarmiento-Maldonado. "SoC estimation for lithium-ion batteries: Review and future challenges." Electronics 6.4 (2017): 102.

[25] J. Meng et al., "An overview of online implementable SoC estimation methods for Lithium-ion batteries," 2017 International Conference on Optimization of Electrical and Electronic Equipment (OPTIM) & 2017 Intl Aegean Conference on Electrical Machines and Power Electronics (ACEMP), Brasov, Romania, 2017, pp. 573-580, doi: 10.1109/OPTIM.2017.7975030.

[26] S. Shete, P. Jog, R. K. Kumawat and D. K. Palwalia, "Battery Management System for SoC Estimation of Lithium-Ion Battery in Electric Vehicle: A Review," 2021 6th IEEE International Conference on Recent Advances and Innovations in Engineering (ICRAIE), KedAh, Malaysia, 2021, pp. 1-4, doi: 10.1109/ICRAIE52900.2021.9703752.

[27] C. R. Lashway and O. A. Mohammed, "Adaptive Battery Management and Parameter Estimation Through Physics-Based Modeling and Experimental Verification," in IEEE Transactions on Transportation Electrification, vol. 2, no. 4, pp. 454-464, Dec. 2016, doi: 10.1109/TTE.2016.2558843.

[28] Zhang, Ruifeng, et al. "A study on the open circuit voltage and state of charge characterization of high capacity lithium-ion battery under different temperature." Energies 11.9 (2018): 2408.

[29] Charkhgard, Mohammad, and Mohammad Haddad Zarif. "Design of adaptive H∞ filter for implementing on state - of - charge estimation based on battery state - of - charge - varying modelling." IET Power Electronics 8.10 (2015): 1825-1833.

[30] J. Xu, C. C. Mi, B. Cao, J. Deng, Z. Chen and S. Li, "The State of Charge Estimation of Lithium-Ion Batteries Based on a Proportional-Integral Observer," in IEEE Transactions on Vehicular Technology, vol. 63, no. 4, pp. 1614-1621, May 2014, doi: 10.1109/TVT.2013.2287375.

[31] X. Shu, Z. Chen, J. Shen, F. Guo, Y. Zhang and Y. Liu, "State of Charge Estimation for Lithium-Ion Battery Based on Hybrid Compensation Modeling and Adaptive H-Infinity Filter," in IEEE Transactions on Transportation Electrification, vol. 9, no. 1, pp. 945-957, March 2023, doi: 10.1109/TTE.2022.3180077.

[32] C. Chen, R. Xiong and W. Shen, "A Lithium-Ion Battery-in-the-Loop Approach to Test and Validate Multiscale Dual H Infinity Filters for State-of-Charge and Capacity Estimation," in IEEE Transactions on Power Electronics, vol. 33, no. 1, pp. 332-342, Jan. 2018, doi: 10.1109/TPEL.2017.2670081.

[33] Y. He, Z. Hong, Z. Zhang and S. Huang, "Particle Filter Based Robust State and Parameter Estimation for Estimating SoC and Discharge Current of Lithium Batteries," 2022 IEEE 11th Data Driven Control and Learning Systems Conference (DDCLS), Chengdu, China, 2022, pp. 244-249, doi: 10.1109/DDCLS55054.2022.9858503.

[34] Z. Zou, M. Zhou and J. Cao, "An improved SoC estimation method based on noise-adaptive particle filter for intelligent connected vehicle battery," 2021 33rd Chinese Control and Decision Conference (CCDC), Kunming, China, 2021, pp. 1223-1228, doi: 10.1109/CCDC52312.2021.9602226.

[35] S. Nejad, D. T. Gladwin and D. A. Stone, "On-chip implementation of Extended Kalman Filter for adaptive battery states monitoring," IECON 2016 - 42nd Annual Conference of the IEEE Industrial Electronics Society, Florence, Italy, 2016, pp. 5513-5518, doi: 10.1109/IECON.2016.7793527.

[36] Sepasi, Saeed, Reza Ghorbani, and Bor Yann Liaw. "Improved extended Kalman filter for state of charge estimation of battery pack." Journal of Power Sources 255 (2014): 368-376.

[37] H. He, R. Xiong, X. Zhang, F. Sun and J. Fan, "State-of-Charge Estimation of the Lithium-Ion Battery Using an Adaptive Extended Kalman Filter Based on an Improved Thevenin Model," in IEEE Transactions on Vehicular Technology, vol. 60, no. 4, pp. 1461-1469, May 2011, doi: 10.1109/TVT.2011.2132812.

[38] Aung, Htet, and Kay Soon Low. "Temperature dependent state - of - charge estimation of lithium ion battery using dual spherical unscented Kalman filter." IET Power Electronics 8.10 (2015): 2026-2033.

[39] Changhao Piao, Xiaoyong Yang, Cong Teng and HuiQian Yang, "An improved model based on artificial neural networks and Thevenin model for nickel metal hydride power battery," 2010 International Conference on Optics, Photonics and Energy Engineering (OPEE), Wuhan, 2010, pp. 115-118, doi: 10.1109/OPEE.2010.5508184.

[40] P. Leninpugalhanthi et al., "Lithium-Ion Battery Life Estimation Using Machine Learning Algorithm," 2022 8th International Conference on Advanced Computing and Communication Systems (ICACCS), Coimbatore, India, 2022, pp. 573-576, doi: 10.1109/ICACCS54159.2022.9785066.

[41] Chang, Zhiguo, et al. "Review of SoC estimation methods for lithium battery based on EKF." 2021 IEEE 4th Advanced Information Management, Communicates, Electronic and Automation Control Conference (IMCEC). Vol. 4. IEEE, 2021.

[42] Stern, Milton, and Al L. Geary. "Electrochemical polarization: I. A theoretical analysis of the shape of polarization curves." Journal of the electrochemical Society 104.1 (1957): 56.

[43] Q. Yu, Y. Huang, A. Tang, C. Wang and W. Shen, "OCV-SoC-Temperature Relationship Construction and State of Charge Estimation for a Series– Parallel Lithium-Ion Battery Pack," in IEEE Transactions on Intelligent Transportation Systems, doi: 10.1109/TITS.2023.3252164.

[44] CALCE Battery Team, School of engineering, University of Maryland, digital image, viewed 12th September 2022, <https://web.calce.umd.edu/batteries/data/low_ocv.png>.

[45] Doughty, Daniel Harvey, and Chris C. Crafts. FreedomCAR: electrical energy storage system abuse test manual for electric and hybrid electric vehicle applications. No. SAND2005-3123. Sandia National Laboratories (SNL), Albuquerque, NM, and Livermore, CA (United States), 2006.

[46] Nemes, Raul Octavian, et al. "Parameters identification using experimental measurements for equivalent circuit Lithium-Ion cell models." 2019 11th International Symposium on Advanced Topics in Electrical Engineering (ATEE). IEEE, 2019.

[47] C. Sen and N. C. Kar, "Battery pack modeling for the analysis of battery management system of a hybrid electric vehicle," 2009 IEEE Vehicle Power and Propulsion Conference, Dearborn, MI, USA, 2009, pp. 207-212, doi: 10.1109/VPPC.2009.5289848.

[48] Li, Jianwei, and Michael S. Mazzola. "Accurate battery pack modeling for automotive applications." Journal of Power Sources 237 (2013): 215-228.

[49] F. Baronti, R. Di Rienzo, N. Papazafiropulos, R. Roncella and R. Saletti, "Investigation of series-parallel connections of multi-module batteries for electrified vehicles," 2014 IEEE International Electric Vehicle Conference (IEVC), Florence, Italy, 2014, pp. 1-7, doi: 10.1109/IEVC.2014.7056173.

[50] N. Watrin, D. Bouquain, B. Blunier and A. Miraoui, "Multiphysical lithium-based battery pack modeling for simulation purposes," 2011 IEEE Vehicle Power and Propulsion Conference, Chicago, IL, USA, 2011, pp. 1-5, doi: 10.1109/VPPC.2011.6043098.

[51] R. Carter, A. Cruden, P. J. Hall and A. S. Zaher, "An Improved Lead–Acid Battery Pack Model for Use in Power Simulations of Electric Vehicles," in IEEE Transactions on Energy Conversion, vol. 27, no. 1, pp. 21-28, March 2012, doi: 10.1109/TEC.2011.2170574.

[52] C. Sen and N. C. Kar, "Battery pack modeling for the analysis of battery management system of a hybrid electric vehicle," 2009 IEEE Vehicle Power and Propulsion Conference, Dearborn, MI, USA, 2009, pp. 207-212, doi: 10.1109/VPPC.2009.5289848.

[53] R. C. Kroeze and P. T. Krein, "Electrical battery model for use in dynamic electric vehicle simulations," 2008 IEEE Power Electronics Specialists Conference, Rhodes, Greece, 2008, pp. 1336-1342, doi: 10.1109/PESC.2008.4592119.

[54] J. Kim, J. Shin, C. Chun and B. H. Cho, "Stable Configuration of a Li-Ion Series Battery Pack Based on a Screening Process for Improved Voltage/SOC Balancing," in IEEE Transactions on Power Electronics, vol. 27, no. 1, pp. 411-424, Jan. 2012, doi: 10.1109/TPEL.2011.2158553.

[55] Dubarry, Matthieu, Nicolas Vuillaume, and Bor Yann Liaw. "From single cell model to battery pack simulation for Li-ion batteries." Journal of Power Sources 186.2 (2009): 500-507.

[56] Xiang, Lihong, et al. "Review on development and application of SoC key technologies for electric vehicle battery packs." 2021 IEEE Sustainable Power and Energy Conference (iSPEC). IEEE, 2021.

[57] Huang, Cong-Sheng, Bharat Balagopal, and Mo-Yuen Chow. "Estimating battery pack SoC using a cell-to-pack gain updating algorithm." IECON 2018-44th Annual Conference of the IEEE Industrial Electronics Society. IEEE, 2018.

[58] Dubarry, Matthieu, Nicolas Vuillaume, and Bor Yann Liaw. "From single cell model to battery pack simulation for Li-ion batteries." Journal of Power Sources 186.2 (2009): 500-507.

[59] Hu, Xiaosong, Fengchun Sun, and Yuan Zou. "Estimation of state of charge of a lithium-ion battery pack for electric vehicles using an adaptive Luenberger observer." Energies 3.9 (2010): 1586-1603.

[60] Li, Junfu, et al. "State of charge estimation based on a simplified electrochemical model for a single LiCoO2 battery and battery pack." Energy 133 (2017): 572-583.

[61] ShAhrooei, A. "Comparison of Open Datasets for Lithium-Ion Battery Testing." BatteryBits (2020).

[62] CALCE Battery Team, School of engineering, University of Maryland, Battery Data, accessed 12th September 2022, < https://web.calce.umd.edu/batteries/data.htm>.

[63] CALCE Battery Team, School of engineering, University of Maryland, digital image, viewed 12th September 2022, < https://calce.umd.edu/sites/calce.umd.edu/files/INR_18650.png>.

[64] Patel, Chirag. "Developing Battery Management System using Simulink." MATLAB EXPO (2019).

[65] R. C. Kroeze and P. T. Krein, "Electrical battery model for use in dynamic electric vehicle simulations," 2008 IEEE Power Electronics Specialists Conference, Rhodes, Greece, 2008, pp. 1336-1342, doi: 10.1109/PESC.2008.4592119.

[66] X. Wei, B. Zhu and W. Xu, "Internal Resistance Identification in Vehicle Power Lithium-Ion Battery and Application in Lifetime Evaluation," 2009 International Conference on Measuring Technology and Mechatronics Automation, Zhangjiajie, China, 2009, pp. 388-392, doi: 10.1109/ICMTMA.2009.468.

[67] Huria, Tarun, et al. "Simplified extended kalman filter observer for SoC estimation of commercial power-oriented lfp lithium battery cells." SAE Int (2013).

[68] Plett, Gregory L. "Extended Kalman filtering for battery management systems of LiPB-based HEV battery packs: Part 3. State and parameter estimation." Journal of Power sources 134.2 (2004): 277-292.

[69] G. D. Meena and S. Janardhanan, "Discretization of Linear Time-Varying Systems," 2020 International Conference on Emerging Frontiers in Electrical and Electronic Technologies (ICEFEET), Patna, India, 2020, pp. 1-6, doi: 10.1109/ICEFEET49149.2020.9186982.

[70] J. Lee, J. -H. Ahn and B. K. Lee, "A novel li-ion battery pack modeling considerging single cell information and capacity variation," 2017 IEEE Energy Conversion Congress and Exposition (ECCE), Cincinnati, OH, USA, 2017, pp. 5242-5247, doi: 10.1109/ECCE.2017.8096880.

TRITA-EECS-EX-2023:679